Development of a kHz optical remote sensing system for *in situ* insect monitoring

By

Alem Kindeya Gebru

Dissertation for the degree of Doctorate of Philosophy in Physics in the Faculty of Science at Stellenbosch University

Laser research institute, Department of Physics

Stellenbosch University

Private Bag X1, Matieland 7602, South Africa

Promoters

Prof. Erich. G. Rohwer
Department of Physics
Stellenbosch University

Dr. Pieter. H. Neethling
Department of Physics
Stellenbosch University

Dr. Mikkel. B. Sørensen
Department of Physics
Lund University

March 2016

Declaration

By submitting this dissertation electronically, I declare that the entirety of the work contained therein is my own, original work, that I am the sole author thereof, that reproduction and publication thereof by Stellenbosch University will not infringe any third party rights and I have not previously in its entirety or in part submitted it for obtaining my qualification.

To mam, sh and stota

Abstract

Development of a kHz optical remote sensing system for *in situ* insect monitoring

Department of Physics

Stellenbosch University

Private Bag X1, Matieland 7602, South Africa

Dissertation: PhD

March 2016

In this work we have developed a kHz optical remote sensing system for *in situ* insect monitoring applications. This is an active and passive remote sensing system based on laser and sunlight. This system showed potential for monitoring pollinators in agricultural fields. It enables the implementation of improved vector control mechanisms and pest management. The passive remote sensing setup called dark field spectroscopy uses sunlight as an illumination source. Considering the passive remote sensing techniques, it is shown that one can determine flight direction, retrieve spectral information, and resolve wing-beat frequency (and harmonics) and iridescence features of fast insect events. With regards to active remotes sensing technique, a number important range resolved quantitative assessments of insects such as size, speed and wing-beat frequency can be performed. It is shown that the CW-LIDAR based on the Scheimpflug principle improves the range resolution beyond the diffraction limit. The reason for this is because of the fact that the sampling frequency is in the order of kHz and insects behave like blinking particles similar to super resolution microscopy called stochastic optical reconstruction microscopy (STORM) where molecules blinks between bright and dark states. Generally, this dissertation highlights the potential of applied optical remote sensing techniques to remotely identify insects and understand their impact onan ecosystem.

Ontwikkeling van 'n kHz optiese afstandswaarneming stelsel vir die in situ monitering van insekte

Departement Fisika
Universiteit Stellenbosch
Privaatsak X1 , Matieland 7602 , Suid-Afrika
Verhandeling: PhD
Maart 2016

In hierdie werk het ons ’n kHz sisteem ontwikkel waarmee insekte oor ’n afstand *in situ* gemonitor kan word. Die sisteem is beide aktief en passief, gebaseer op laser- en sonlig. Die sisteem het potensiaal getoon om bestuiwers in ’n landbou omgewing te monitor. Dit stel in staat die implementering van verbeterde vektor beheer meganismes en pes bestuur. Die passiewe opstelling, genoem donker veld spektroskopie, gebruik sonlig as ligbron. Met die opstelling kan die bewegings rigting, spektrale inligting, die frekwensie (en hoër harmonieke) waarteen die vlerke beweeg en glans kenmerke bepaal word van vinnige insek gebeurtenisse. Deur gebruik te maak van die aktiewe opstelling kan ’n aantal belangrike posisie afhanklike kwantitatiewe bepalings gemaak word soos insek grootte, spoed en vlerkfrekwensie. Dit word verder getoon dat CW-LIDAR, gebaseer op die Scheimpflug beginsel, die afstand resolusie verbeter verby die diffraksie limiet. Die rede hiervoor is die feit dat die meet frekwensie in die orde van ’n kHz is, en insekte hulle soos flikkerende deeltjies gedra, soortgelyk aan wat waargeneem word in die super resolusie mikroskopie tegniek, genaamd “stochastic optical reconstruction microscopy” of te wel STORM, waar molekules flikker tussen helder en donker toestande. In die breë gesien, beklemtoon die proefskrif die potensiaal van toegepaste optiese afstand meet tegnieke om oor ’n afstand insekte te identifiseer en hulle impak op ’n ekosisteem te verstaan.

Table of contents

List of acronyms

- **OCS-** optical cross section
- **CW-LIDAR-** continues wave light detection and ranging
- **UV-** Ultraviolet
- **VIS-** visible
- **NIR-** near infrared
- **SWIR-**Shortwave infrared
- **STORM-** stochastic optical reconstruction microscopy
- **PALM** - photo activation localization microscopy
- **DIAL** - differential absorption LIDAR
- **Si-** silicon
- **InGaAs** - indium gallium arsenide
- **FOV-** field of view
- **FWHM –** full width at half maximum
- **TOF-LIDAR –** time of flightLIDAR
- **DOF** – depth of field
- **RGB** – red green blue colours
- **FFT-** fast Fourier transform
- **DFT** – fast computational algorism for discrete Fourier transform
- **PSD** - Power spectral density
- **LUMBO** – Lund university mobile biosphere observatory
- **AFSIN -** African spectral imaging network

Chapter I

1. Introduction

1.1 Background

The issue of climate change has been a very hot topic of the last decade due to the vulnerability of our environment. The main causes could be natural changes or industrialization due to human activities[1-5]. Although natural phenomena also have an impact, human related influence is significant.An improved quantitative and *in-situ* surveillance techniques could support decision making and proper management of the environment. The study of insect activities could help in the process of understanding the bigger picture as they are part of the environment. It is known that insectscomprise 80% of the terrestrial animal population on earth, which makes them very important classes[6]. They can be used as delicate indicators for the minute changes in the environment. They can be helpful to determine age of dead body in forensic entomology [7-10]. Insects such as bees are responsible for pollinating about 80% of flowering plants[11, 12]. They are excellent biomarkers of flowing water purity, pesticide abuse, and are climatic change indicators [13]. Generally, insects play a crucial role in maintaining the natural balance of the earth. On the other hand, insects can have a negative impact on agricultural productivity [14] and disperse forestry and agricultural pests [15]. They can also transfer disease to livestock and humans [16]. Various species of mosquitoes can transfer diseases to human beings [17].

The studies of insects have been done for many years to understand their nature, to use insects as an indicator of natural phenomena and to control their influence on the environment. Such studies have been mainly based on manual counting, which off course has made an important contribution to the field. Some of the examples of those techniques are: water pan trap, light traps, sweep nets, flight intercept traps, pitfall traps, and beating trays [18-22], Fig.1.

Figure 1: *Types of traps commonly used in the field of entomology.* ***Left****: Water pan trap, which uses water to attract insects [23].* ***Middle****: Light traps: this is based on light as source to attract insects [24].* ***Right****: This is used by experts to catch insects while flying by moving the net from side to side [25].*

In addition to manual counting, the prospect of automatic insect classification has been presented by Batista et.al [26]. It is understood that the above mentioned techniques have made

significant contributions towards understanding the nature of insects and to use them as indicators; however it remains challenging to investigate fast insect-insect interaction mechanisms or a vast number of insects using conventional techniques *in situ*. To address those issues, it is important to implement more efficient and accurate insect monitoring techniques, which enables one to have a detailed understanding of insect activity. A comprehensive description of insect activity could shed light on the wellbeing of the environment.

The quantitative assessment of an insect's interaction strengthand their biodiversity in respect to topography, weather and type of vegetation is a formidable challenge to entomologists and environmental ecologists. This is because insect interactions happen on the milliseconds time scale, which demands a fast detection scheme. A wide range of applied optical remote sensing techniques have been used since 1970's. Insect monitoring using a fluorescence LIDAR (Light Detection And Ranging) technique was demonstrated by Brydegaard *et al*[27]. This was a feasibility study used to study the properties of damselfly species *Calopteryx splendens and Calopteryx virgo,*and their laboratory studies showed that this species exhibited entangled reflectance and fluorescence properties, which indicates that gender can be determined remotely. A similar technique has been implemented *in situ* by the same group in Lund University where the abundance of one gender of the damselflies could be associated with certain vegetation. The group has demonstrated the potential of fluorescence LIDAR *in vivo* andestimated the distance to the two species of damselfly (*Calopteryx splendens and Calopteryx virgo*) from a vegetation and water [28]. Some of the pioneering work that have been done in the area of elastic LIDAR by the group in Montana State University are the study of honeybees for sniffing land mines. They have shown that flying honey bees trained to locate landmines through odour can be detected using scanning polarization LIDAR and they are also able to show that the bee density shows good correlation with maps of the chemical plume [29]. The subsequent work by the same group indicates that the use of modulated return signal scattered from flying honey bee, which can be used to differentiate if the object is actually a honey bee or vegetation. The backscattered light from a honey bee showed a characteristic wingbeat frequency (170-270Hz) [30,31].

RADAR (Radio Detection And Ranging) has been used for almost half a century. It is one of the optical techniques, which is used for the study of insect diversities and bird migration. It isalso widely used for civilian and military airplane tracking [32-37]. RADAR based applications in entomology and communication mainly uses frequencies below10GHz since attenuation due to air is insignificant at higher frequencies[38]. The atmosphere is opaque at around 22GHz and 60 GHz. This is because of strong absorption by water vapour and oxygen respectively.However, it is transparent to radio waves at around 35GHz and 90GHz. [38]. Generally, radio wave observable from earth operates within the atmospheric window (9cm and 10m wavelength) [39], see *Figure 2*. Apart from the visible, there are a few more atmospheric windows around 1µm and 10µm.

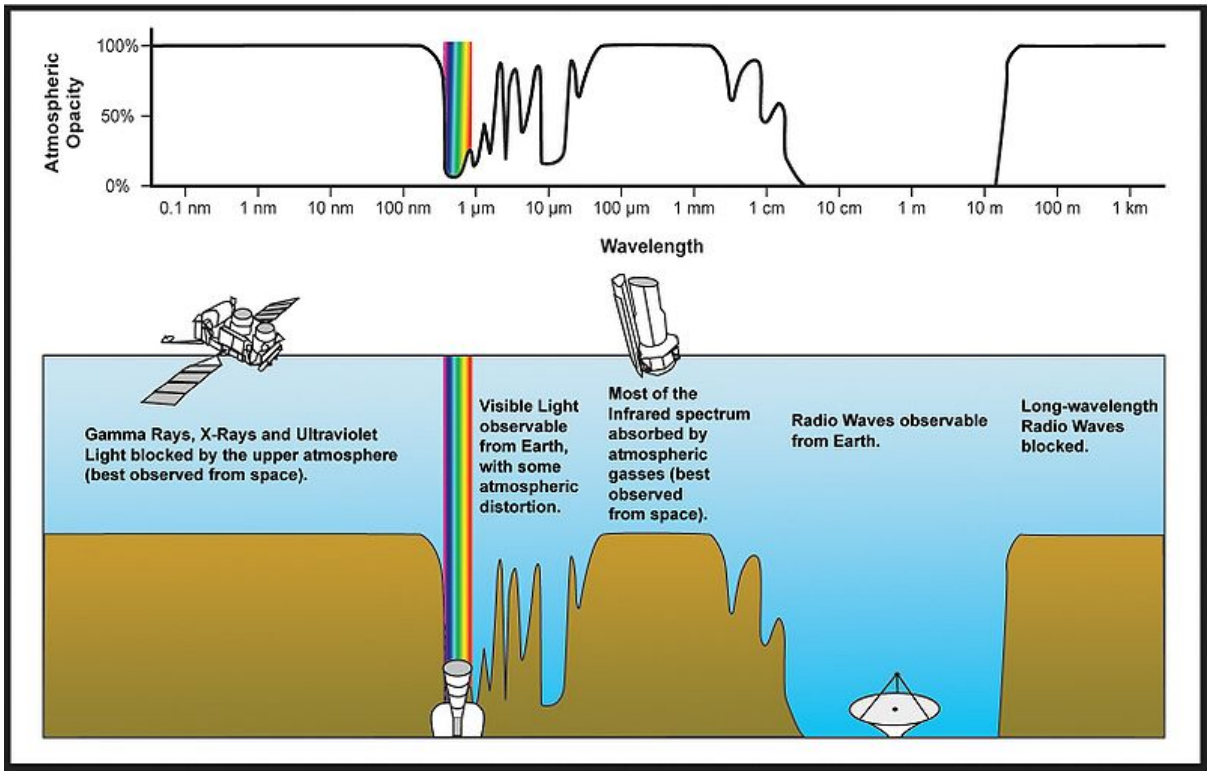

Figure 2*:*Atmospheric opacity: *The atmosphere is opaque in the range between 0.1nm to around 300nm and 10µm to around 9cm, which indicates that it is best to perform atmospheric studies from space using satellites in these wavelength rages. However, it is possible to use radar from earth within the transparent window (9cm and 10m).It becomes opaque again at wavelength greater than 10m. Adopted from [39]*

Attenuation of ballistic light in LIDAR is the sum of both scattering losses as well as absorption due to vibrational transitions in atmospheric molecules. The signal also decreases with distance due to the invers square law of intensity with distance. In this kind of experiments, a train of pulse is sent by the radar and the receiver detects echo from the interacting object, see Fig.3.

The range is calculated from the round trip time of the radio wave, where the speed of the radar signal is considered to be equivalent to the speed of light in vacuum ($c = 2.997 * 10^8 ms^{-1}$). This means that the sampling frequency is constrained by the round trip time of the pulse. Example: if the pulse duration is 2µs, the range resolution will be 300m, which is too big for the purpose of radar entomology, but it could work for aircraft radar applications, see Eq.1.1 [39].

$$\Delta r_{max} = \frac{c\tau}{2} \quad \text{..... (1.1)}$$

Where:Δr_{max} is the maximum range resolution, τ is the full width at half-maximum (FWHM) of the pulse (t_FWHM); and c is speed of light in vacuum($c = 2.997 * 10^8 ms^{-1}$)

The radar entomology systems usually operate in the range between 100ns to 50nspulse length in order to achieve range resolution from 15m to 7.5m respectively [38]. One of the challenges to improve the range resolution in this technique is because of the fact that some techniques such as q-switching are not applicable in RADAR. The record detection range so far in entomological LIDAR is 2km for insects and 4km for birds [38]. Some of the challenges in the

field of RADAR entomology are: interpretation of the data, contrast between the object of interest as compared to background, especially when the insect is around vegetation, and the strength of the amount of radiation reaching the receiver for detection [38]. However, the vegetation and clouds are a major issue in LIDAR as compared to RADAR. Harmonic RADAR can detect tagged insects inside vegetation and can penetrate clouds [40-43]. The optical remote sensing developed in this project is capable of improving the range resolution as well as the temporal resolution of the radar entomology. The CW-LIDAR used in this project is not limited by the round trip time of the laser pulse and we have achieved angular resolution beyond the diffraction limit [44]. The detail of this method is discussed in chapter III.

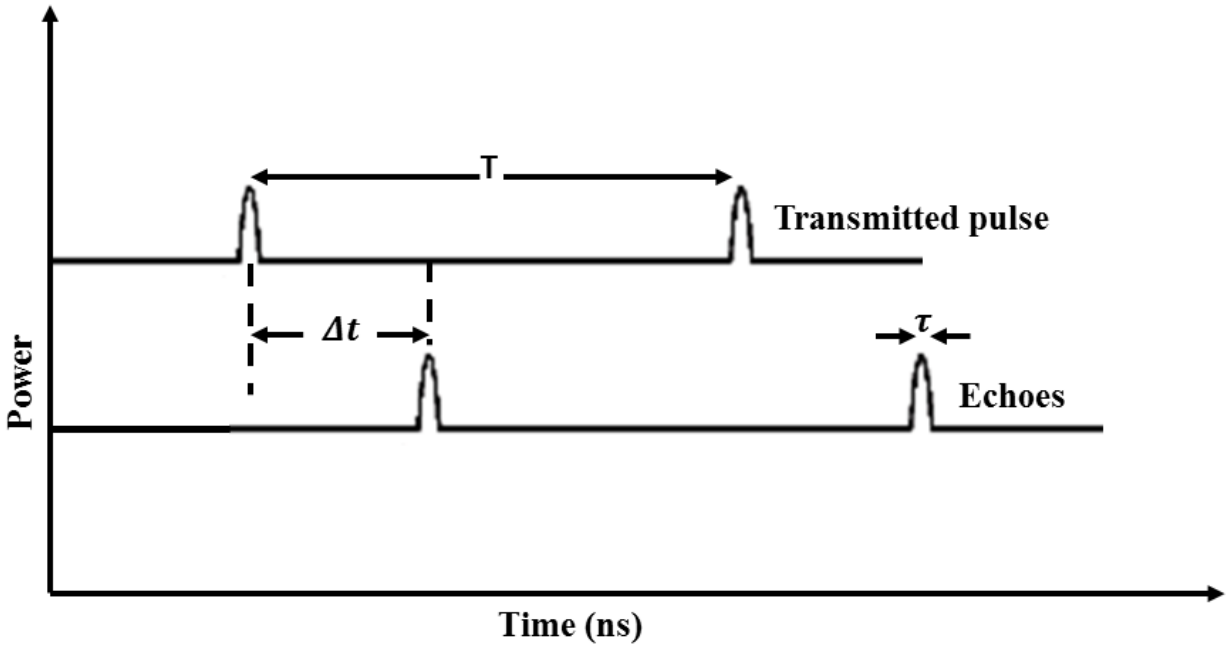

Figure 3: *Working principle of RADAR entomology: The top signal shows the transmitted laser pulse train where T is the interval between pulses. The bottom signal is the back scattered echo of the transmitted pulse from the object. The round trip time of the transmitted laser pulse returned from a scatterer is denoted by Δt. This is used to calculate the range information of the scatterer.*

1.2 Entomological aspects

1.2.1 Forestry pest

Forests play an important role in attaining the natural balance of our ecosystem and supporting life on earth in general [45-49]. Forests are natural absorbers (carbon sink) of CO_2 emission, are essential for growing food and medicine, it maintaining water and air quality, and they regulate moisture and prevent erosion and floods. The importance of forests for the existence of life is significant and one can say that the role of forests for the human existence is vital. This resource could be affected by forestry pests such as beetles, which could compromisethe wellbeing of the environment. Beetles attack the forest by lying eggs on the growl and introduce a blue strain fungus, which makes the plant defenceless [50-54]. This forces the tree to die

within few weeks of successful attack, see Fig.4. The effect could be minimized or alleviated if one can monitor the activity of such pests using optical remote sensing techniques [55], which could give some clue how to address the issue by either introducing natural predators or using pesticides at an appropriate life stage of the pest. We have performed an experiment to investigate the activity of bark beetles at Nyteboda, Sweden. Bark beetles mainly attack dead trunks [56,57].

Figure 4**:** *Comparison of the effect of forestry pest.* ***Left:*** *Healthy pine tree [58].* ***Middle and right:*** *infested pine tree by beetles [59].*

1.2.2 Pollination

Insects are natural service providers of the ecosystem. The ecosystem service given by pollinators has huge economic benefits in terms of attaining biodiversity of plant species, nutrient recycling, waste decomposition etc. According to the millennium ecosystem services (MA) report 2005[60], ecosystem services are defined as the benefits that human get from the ecosystem and can be divided into four main branches: Supporting services, provisional services, regulation services and cultural services [60-62]. These services are usually taken for granted, which compromises the sustainability of the ecosystem. Considering statistics from USA, the economic value of these services given by insect reaches at least $57 billion [63]. It is also estimated that 15% to 30% of the USA diet comes directly or indirectly through animal mediated pollination, which indicates the amount of money that could be lost if pollinators are not functioning properly[63]. The diversity of beautiful flowering plant species, which are observed in the environment are indeed due to pollination by insects such as honey bees and bumble bees, see Fig 5. One of the main entomological investigations we are interested in is basically to assess temporal and spatial distribution of pollinators over different agricultural landscapes. We found that there is a variation in terms of size distribution and activity over km range in an agricultural filed. This is discussed in chapter III.

Figure 5*: *Flowering plants pollinated by insects. Honey bees and bumble bees are some of the main pollinators of flowering plant species.

1.2.3 Disease vectors

Disease causing vectors are having a significant impact on productivity. It is know that malaria is one of the main killer diseases in the tropical regions, especially in Africa and one of the main reasons affecting the growth of the continent by affecting the youth. It is responsible for around 300 million infections and 2 million deaths per year [64]. A lot of studies have shown that the economic impact of malaria is huge in terms of agricultural productivity, pharmaceutical and medical expenses and over all infrastructures, which is built to prevent and cure malaria epidemic [65-67].

Eukaryotic microorganism, which belongs to the family of plasmodium, is the cause of malaria. Specifically, the protozoan parasite called plasmodium falciparum is the one transmitted by the female anopheles mosquito, which is responsible for the malaria infection [68-70]. The life cycle of the parasite mainly involve three stages, see Fig.6: **Human liver stage**:this involves Ex-oerythrocytic cycle. In this cycle the liver cell with replicates parasite (Schizont) gets matured and will then raptured and releases Merozoites in to the blood stream[71,72].**Human blood stage:**involveserythrocytic cycle. In this cycle the Merozotes replicates in the red blood cell (RBC) [73, 74]**. Mosquito stage**: involves sporogonic cycle, in which fertilization occurs in the mosquito stomach to release the spores (sporoziotes) [75, 76]. A number of advanced optical techniques have been developed over the years for early malaria diagnostics [77-81]. Another malaria diagnostic technique, which is based on imaging scattering spectroscopy showed the potential for instant evaluation of unstained thin blood smears [82, 83]. Studies have indicated that in order to tackle the issue of a malaria epidemic, we need to see it as an ecological problem [84]. This study indicated that the population of different species of mosquito varies seasonally depending on wet and dry seasons and mosquitos spend the dry season in a dormant state. Example: The population of *Anophelescoluzzi* peaks in September and October in Mali, West Africa while it drops and stays at low levels in most of the dry season [84]. The method they used was manual counting of different species ofmosquitos for

5 consecutive years. From this, one can see that the prospect of deploying optical techniques such as the one discussed in this dissertation could improve the outcome of the evaluation.

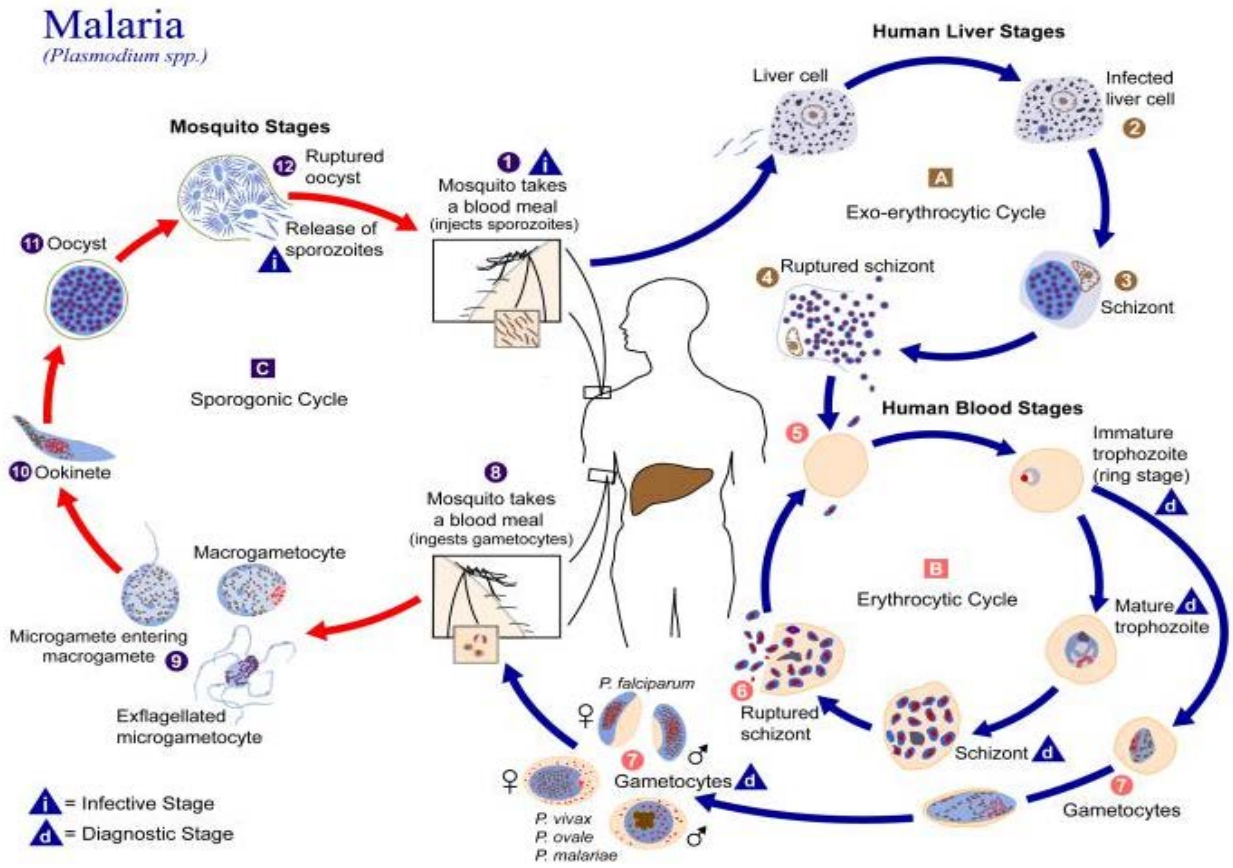

Figure 6: *Plasmodium life Cycle: The life cycle of the parasite is extremely complicated. The three different stages indicates that the human body is used as source of food for the mosquito while the mosquito itself is used as place of fertilization for the parasite and in the process it releases the spores (Sporozoites). The first two cycle (*Exo-*erythrocytic and erythrocytic) happens in human or animal body. The third cycle (Sporogenic cycle) happened in the body of the mosquito. Public domain image, obtained from centre of the disease control (CDC).*

1.3 Remote sensing and standoff detection

Remote sensing is a way of investigating an object of interest without making physical contact. Remote sensing mainly encompasses satellite and arial imaging [85, 86]. Active remote sensing techniques such as LIDAR and SAR (Synthetic Aperture RADAR) cover a very small fraction of the total field as compared to satellites and arial imaging [87,88]. LIDAR involves the investigation of topography and tree canopy[89, 90], atmospheric monitoring, aerosol, wind sensing, and temperature sensing. A molecular ranging technique, which is called DIAL (differential absorption LIDAR) [91,92] is another example of active remote sensing. Remote sensing can also be done using a standoff detection system, which typically covers a range of around 100m. Such techniques involve remote Raman spectroscopy, remote life time measurement [93] and dark filed spectroscopy [94, 95], which is one of the techniques used in this project. Those remote sensing techniques are all non-intrusive techniques, which enables *in situ* measurement. In principle, all laser based techniques are remotes sensing. One of the differences between different remote sensing techniques is the area it covers. They could also

be differentiated based on the distance between the object under investigation and the receiver. This distance could be centimetres for microscopic application while it is in the order of kilometres for LIDAR experiments. The CW-LIDAR and dark field spectroscopy techniques implemented in this project are discussed in section (1.3.1) and (1.3.2) respectively.

1.3.1 Active remote sensing

Active remote sensing can be defined as a method of retrieving information by illuminating a certain light source to an object of interest. In our case, we have used a 3W and 808nm wavelength multimode laser diode source as an illumination source. The laser source emits near infrared (NIR) continuous wave (CW) light, which is transmitted by ø90mm F/5 refractor telescope. The laser light is transmitted over several km ranges and terminated at distance of 250m (building termination) and 11km (cliff wall termination of Helderberg ridge), see Fig.7.

Figure 7:*FOV CW-LIDAR experimental setup. Upper panel: image of the FOV from the department to Helderberg ridge. Lower panel: map showing the range we have monitored. These two positions were chosen just because of convenience as they were the closest and the farthest location we could find in the field of view (FOV) from an experimental position (the third floor of the Physics department (Merensky building) respectively). The location of the transmitting and receiving telescope is 33^{0}55'55.53" S 18^{0}51'54.61"E, at an altitude of 130 meter above sea level and cliff wall termination at 11km distance is located at 34^{0}02'07.32" S 18^{0}52'13.06"E, at an altitude of 770 meter above sea level.*

The purpose of the refractor telescope is to expand the laser beam so that insects crossing the ø90mm laser beam would be detected. This enables us to resolve the wing-beat frequency, and size. In other words, the insect will have enough time to stay in the FOV as compared to when the beam width is smaller. The separation distance between the refractor and receiving telescope is 120cm, which is equal to the focal length of the reflecting telescope, see Fig.8. The

whole system is placed on a horizontal metal mount and the telescopes are parallel to each other. The vertical and horizontal movement of the whole system is motorized and computer controlled.

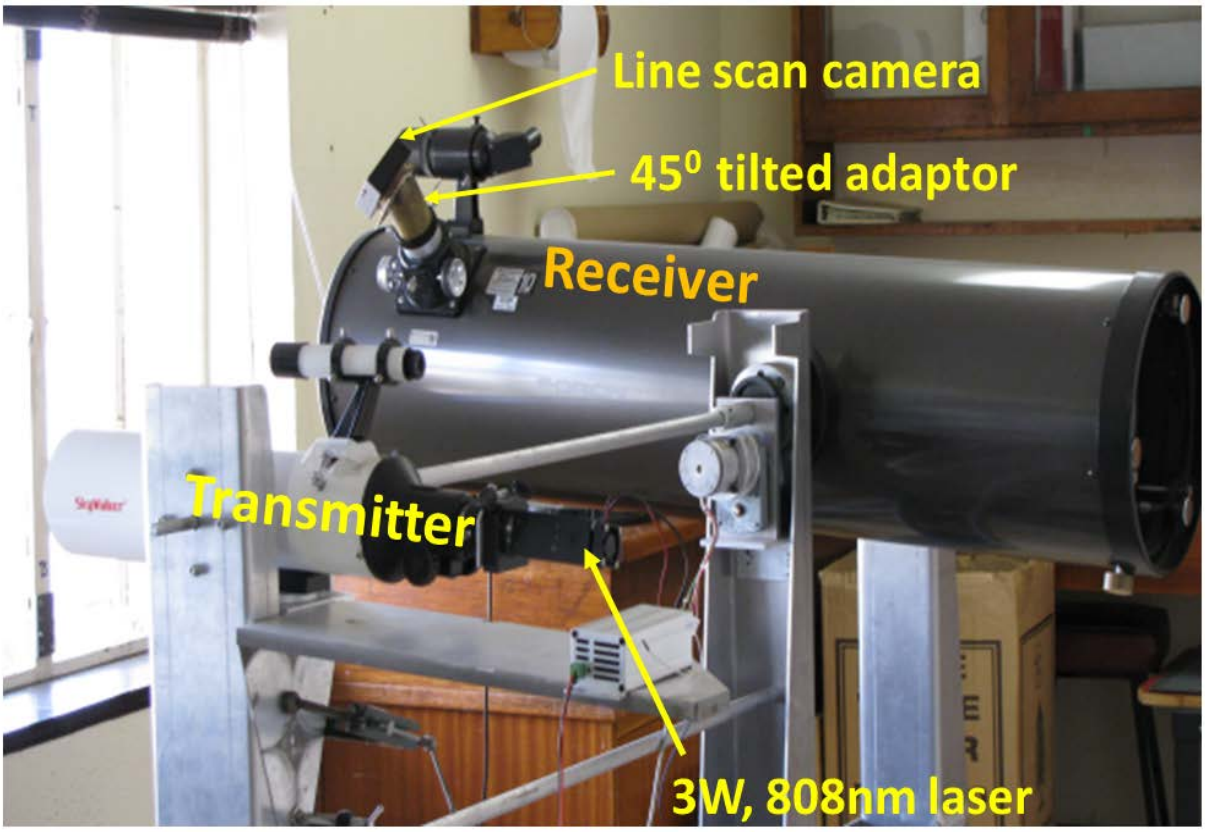

Figure 8: *Transmitter and receiver alignment geometry: The transmitter Ø90mmF/5refractor telescope. The receiver is Ø254mm, F/4 reflecting telescope with 1024pixel line scan camera.*

The line scan camera is aligned at a skewed angle based on the triangulation principle and using trigonometric relations [96, 97]. Triangulation is a way of measuring the distance between two points using the angle instead of directly measuring the distance between the points. In our setup, the line scan camera was attached to a45^0 tilted metallic adaptors, see Fig.9. The surface of the pixel array will then be at 45^0 tilt angles since it is directly attached to the adapter. This fulfils the Scheimpflug condition and the Hinge rule[98, 99], which is a very effective imaging technique to achieve infinite depth of field. The details of Scheimpflug condition and Hinge ruleare discussed in Chapter III.

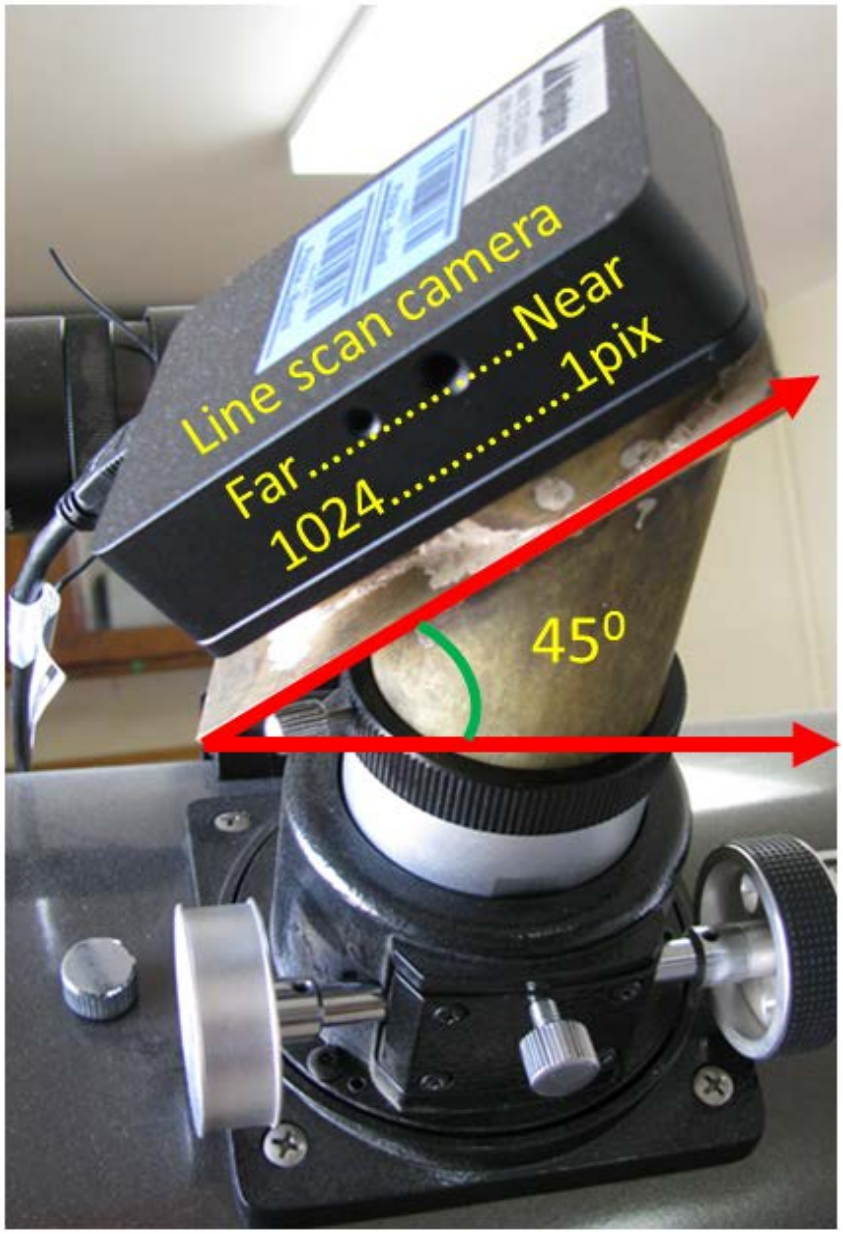

Figure 9: *Closer look of the detector alignment geometry in the receiving telescope. The pixels are 45^0 tilted with respect to the horizontal.*

1.3.2 Passive remote sensing

Passive remote sensing uses sun light as an illumination source. Unlike active remote sensing systems, the passive remote sensing instruments collect radiation from the object being detected without transmitting light. In other words, this kind of instrument senses light reflected by the object from another source other than the instrument. Examples of passive remote sensing detectors are: radiometers, which is used to quantify an electromagnetic (EM) radiation in some wavelength band[100,101] , spectrometers to detect the spectral content of EM radiation, imaging radiometers to generate two dimensional matrix of pixels and produce images[102,103] and spectroradiometers to measure the intensity of radiation in multispectral

bands[104,105]. In this dissertation, we have used sun light as illumination source. The detectors are silicon (Si) and indium gallium arsenide (InGaAs) photodiodes and spectrometer. This experiment is based on dark field spectroscopy [94, 95], were dark termination cavity was used to lower the background signal, see Fig.10. We have used the same Newtonian telescope as the receiving telescope that was used in the active remotes sensing experiment shown in the previous section. The main difference in this case is that the sun was used asanillumination source.Thedetectors are photodiodes and spectrometers instead of the line scan camera.The experimental setup and details of dark filed spectroscopy is discussed in chapter III.

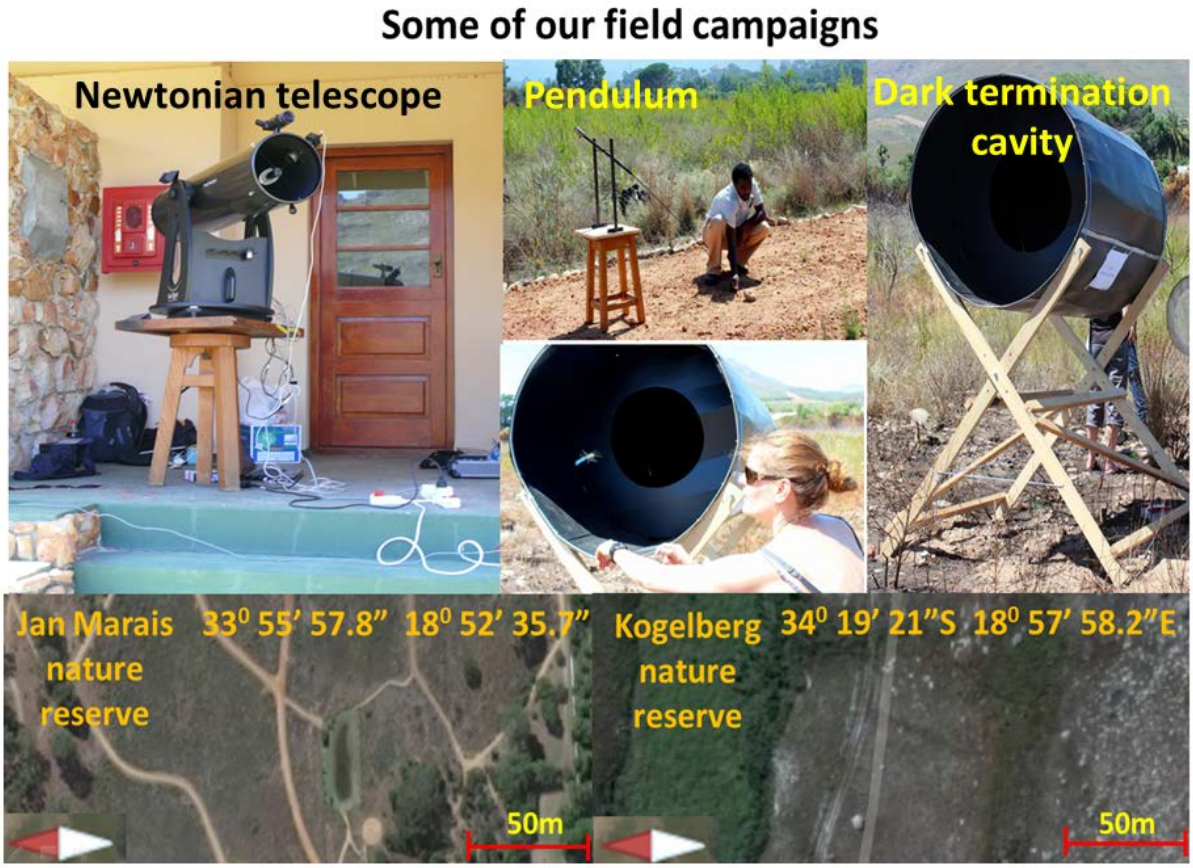

Figure 10:Newtonian telescope*:to collect backscattered signal from insect crossing the FOV. This telescope is the same as the receiving telescope showed in section (1.3.1).* ***Pendulum****: we use to calibrate flight direction of insects.* ***Dark termination cavity****: we use to lower the back ground.*

Chapter II

2. Light tissue interaction

2.1 Interaction process

The interaction of light with the body and wing of insect can be considered as light-tissue interaction. This process involves backscatter, side scatter, forward scatter and ballistic scatter. Forward scattered and side scattered light refers to the light along the same axis of the incident light and orthogonal to the incident light respectively [106,107]. While ballistic scatteringrefers to photons, whichare capable of penetrating straight through a turbid medium or tissue for a short distance before it gets refracted or absorbed. Our passive and active system is designed to collect backscattering signal from atmospheric fauna. This arrangement enables us to achieve improved signal strength as compared to forward scattering. Insects, like other objects produce a backscattering signal when they interact with light and one can be able to measure backscatter and extinction using LIDAR. Thebackscattered signal contains qualitative and quantitative information about the insect, such as: size, wing-beat frequency, flight direction and colour information as it was mentioned in the previous section. One can exploit this feature in order to identify insects remotely. The scattering process involves direct and more or less collimated illumination from the sun and omnidirectional sub-illumination from below (vegetation), see Fig 11.

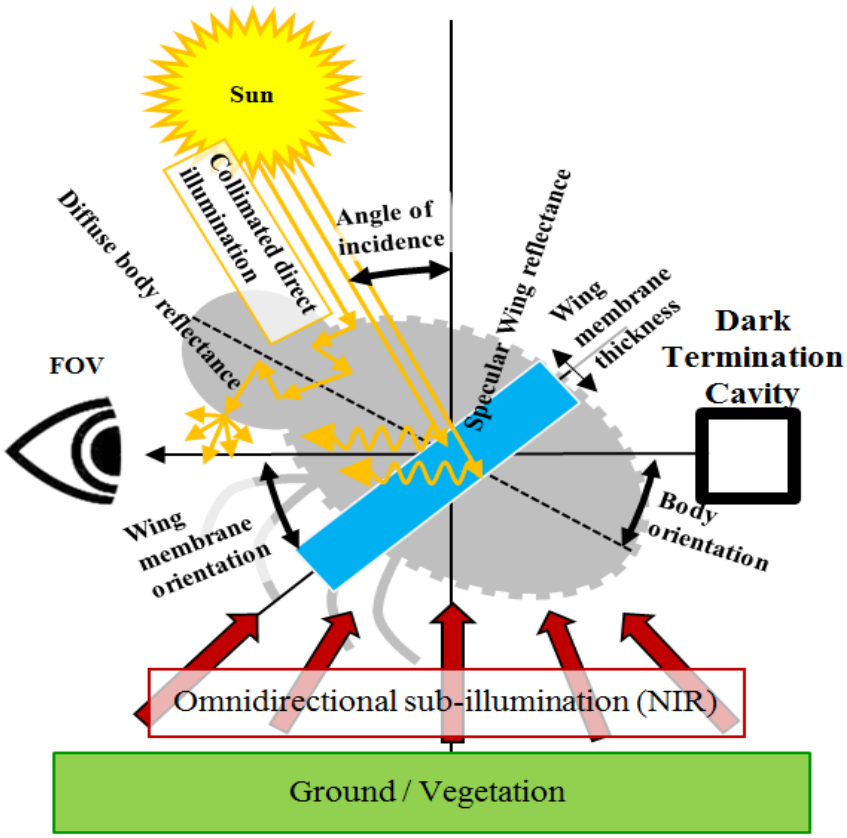

Figure 11: *Insect scattering processes. The passive remote sensing involves three light-tissue interaction processes: Melanin absorption in the visible (VIS), Vegetation sub- illumination in the near-infrared (NIR), and thin-film iridescence (interfering waves) due to specular reflection.*

These two contributions (collimated direct illumination from the sun and omnidirectional sub-illumination from vegetation) are basically the illumination source in a passive remote sensing experiment, see Fig.11. One illumination source is used in the active setup, which is an 808nm wavelength laser as discussed previously, but the scattering process has some similarity. In the dark field experiment, the specular reflection would appear at different phase in the wingbeat cycle. In the LIDAR, it appears when wing-surface normal coincides with the laser beam direction.

2.2 Absorption

Absorption can be referred to the probability per unit length of a photon being absorbed by a certain medium. The characteristics of absorption widely vary depending on the wavelength of light and the type or nature of the object interacting with the light. Considering the photon energy in the visible regime, absorption makes electronic transitions of valence electrons. Typical examples of such phenomena are the sharp absorption lines of gases [108,109]. The photon energy in the ultraviolet (UV) and X-tray regime causes ionization and inner shell excitation respectively. The most common example from daily life is the use of microwave oven. In this case, water molecules absorb light in the microwave wavelength region. The rotational and vibrational energy of the molecule will then be converted to heat energy, which leads to heating of the food. Photons in the infrared are less energetic as compared to Visible, UV and x-ray. Infrared photons are responsible for the transitions related to rotation and vibration process. The linear absorbance of a certain medium can described using Beer-lambert law. This law describes the exponential decay of intensity of light when passing through absorbing medium, see figure 12.

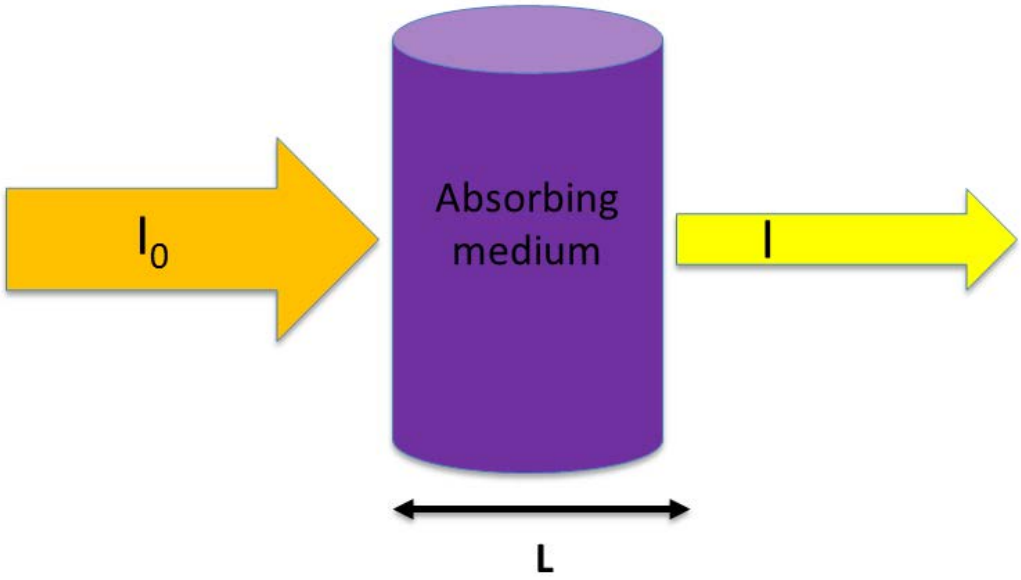

***Figure 12**: Beer-Lambert law describing the decrease in intensity of light when propagating through absorbing medium. L represents the path length of the light through the medium.*

The absorbance can be described as the logarithmic ratio of the transmitted and impinging intensities of the light, see Eq.2.1. This expression is commonly used to investigate the concentration of absorbing medium using absorption spectroscopy techniques.

$$A = \log_{10} \frac{I}{I_0} \quad \text{(2.1)}$$

Where, A is absorbance of the absorbing medium, I and I_0 the transmitted and incident intensities respectively. Biological samples like insects reflect more in the near infrared (NIR) where the absorption is low. Absorption increases towards the visible and the tissue becomes opaque in the UV [64].

2.3 Scattering

Scattering is process referred to change of photon propagation direction when it interacts with matter. Using Snell's law, one can describe the angle of incident and refraction of light passing through different medium. The fraction of reflected and refracted or transmitted light can then be described using Fresnel equations. The origin of scattering could be due to elastic or inelastic process. In terms of the strength of the effect, elastic scattering process is significant. This includes Rayleigh scattering from dipole such as molecules, Mie scattering due to cylindrical and spherical refracting particles. An example of inelastic scattering process are Raman scattering [110-114], which is due to rotational and vibrational transitions of molecules and Compton scattering [115,116], which is scattering process from a charged particle, usually an electron. Elastic scattering processes such as Mie scattering [117,118] and Rayleigh scattering [119-121] have higher scattering probabilities. Mie scattering can happen due interaction of light with Aerosol particle [122-124]. Rayleigh scattering is caused by small radiating dipoles (molecules), which are significantly smaller than the scattering wavelength. The intensity of Rayleigh scattered light is inversely proportional to the fourth power of the wavelength (λ^{-4}), see Eq.2.2. This explains why the sky is blue during the day since blue has a higher scattering probability compared to red. If the earth would have ten times thicker atmosphere the air would still have Rayleigh scattering, but the sky would be white. In principle, violet has a higher scattering probability, but the intensity of the sun spectrum falls off in the ultraviolet range (below 310nm) because of absorbing atmospheric molecules in that wavelength. The remaining UV light from 310-400nm is removed due to scattering. The strongest attenuator of UV light is scattering process, which extinguishes the UV light, but it doesn't absorb it. Rayleigh scattering also causes the orange colour of the sky during sunrise and sunset since the light from the sun has to pass through a thicker atmosphere (higher atmospheric volume) as compared to zenith observation where the atmospheric volume is smaller. These processes remove the blue light from the direct path to the observer and only red light is observed see Fig 13.

$$I = I_0 \frac{8\pi^4\sigma^2}{\lambda^4 R^2}(1 + \cos^2\theta) \quad \text{(2.2)}$$

Where σ is scattering cross-section, λ wavelength of the laser and R is distance. Rayleigh scattering is the most dominant scattering process in a situation where the scatterer size is

significantly smaller that the scattering wavelength. Raman scattering is less likely compared to the elastic processes.

***Figure 13: Left**: Blue sky due to Rayleigh scattering from atmospheric gases (Example: Nitrogen and oxygen molecules) since light travels through small atmospheric volume. **Right:** During sunset, only unpolarised red light is seen since the light travels through higher atmospheric volume.*

2.3.1 Coherent and incoherent scattering

The backscattering signal from the insect comes from two contributions: diffuse reflectance (incoherent scattering) from the body and wing of the insect and specular reflectance (coherent scattering) from the wing of the insect, See Fig 14.

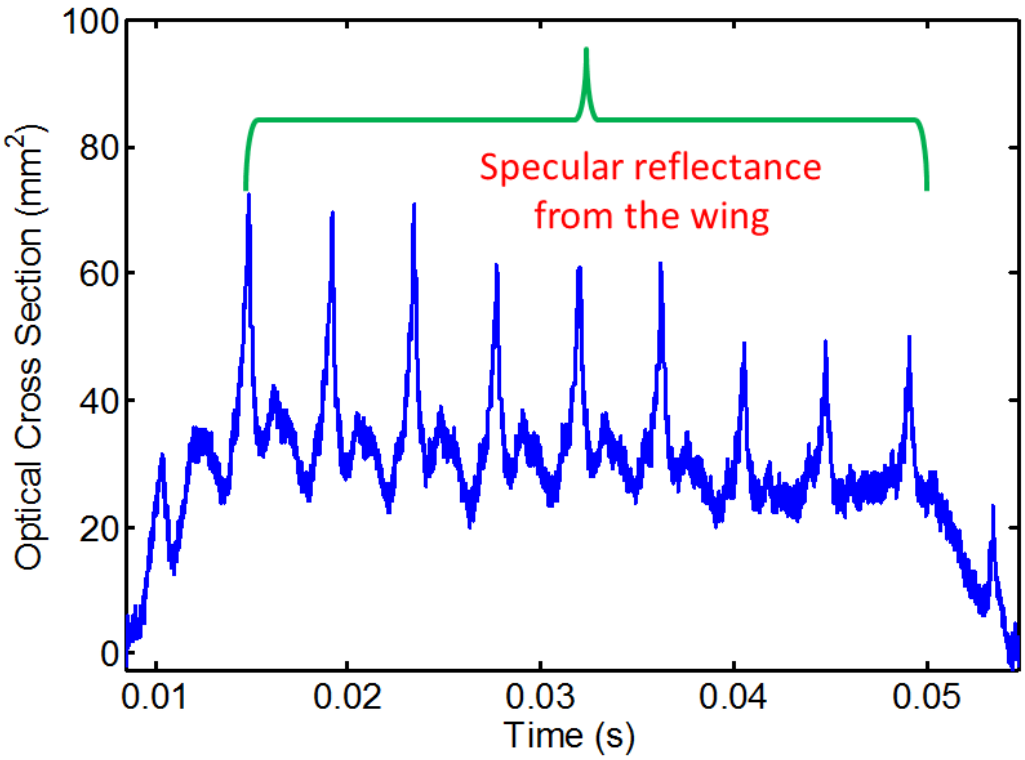

Figure 14: *Specular reflectance from the wing, which is responsible for the generation of higher harmonics.This effect is more pronounced if the observed insect has glittering wings.*

The specular reflectance is more significant when observing an insect with glittering wings, where the wing behaves like a mirror. The specular wing reflectance in the Short wave infrared (SWIR) provides information about the thin film interference from the spectral fringes of the wing membrane, which can be seen as rapid spikes in the temporal signal. Thin film interference occurs when two light waves reflected from the upper and lower surface of the film interferes, where the refractive index of the upper medium is smaller than the lower ($n_1 < n_2$) [125-127]. The interference could be constructive or destructive depending on the effective refractive index of the medium, thickness of the film and angle of incidence of the original wave.

In order to understand the condition of the interfering wave, one has to calculate the optical path difference (OPD) of a light reflected from both the upper and lower boundaries of the thin film. The OPD is just a difference between optical path lengths of two waves, which enables one to determine if the interference between the two waves is constructive or destructive. Considering a light wave incident at an angle θ on the thin film surface with thickness L, some of the incident light can be reflected from the upper surface and a certain portion of the transmitted wave could also be reflected back from the lower boundary of the film. The interference between two waves produce a new wave, which can reveal information about the property of the medium such as effective refractive index of the medium and thickness of the thin film. We can describe this phenomenon by showing a simplistic ray diagram with two different refractive indexes (n_1 *and* n_2), see Fig.15. The OPD of this specific example can be given by the difference between the path length of the two rays ($\bar{B}$ and $\bar{C}$), see Eq.2.2.

$$OPD = n_2(\overline{PQ} + \overline{QR}) - n_1(\overline{PS}) \quad \text{(2.3)}$$

Applying trigonometric relations, one can see that $\overline{PQ} = \overline{QR} = L/\cos\theta_2$ and $\overline{PS} = 2L(\sin\theta_2 \cos\theta_1)/\sin\theta_2$(law of reflection). From Snell's law, it is known that ratio of the sine's of the angleofincidence and refraction are equal to the reciprocal of the ratio of the refractive indices, see Eq.2.4.

$$\frac{\sin\theta_1}{\sin\theta_2} = \frac{n_2}{n_1} \quad \text{(2.4)}$$

By combining the above two equations (Eq. 2.3 and Eq. 2.4) and assuming that the light is incident from the air ($n_1 = 1$), we can formulate the OPD of light in a thin film situation, see Eq.2.5.

$$OPD = 2n_2 L\cos\theta_2 \quad \text{(2.5)}$$

Where$L$-is thickness of the film, n_2- is refractive index of the medium and θ_2- is the angle of incidence in the lower boundary of the film.The interference will be constructive if the OPD is an integer multiple of the wavelength and it will be destructive interference if it is half integer. When we reformulate Eq.2.5, we can see that OPD is proportional to the wavelength of the light for constructive interference, see Eq.2.6.

$$2n_2 L\cos\theta = m\lambda \quad \text{(2.6)}$$

Where m is integer and λ-is wavelength of the light.

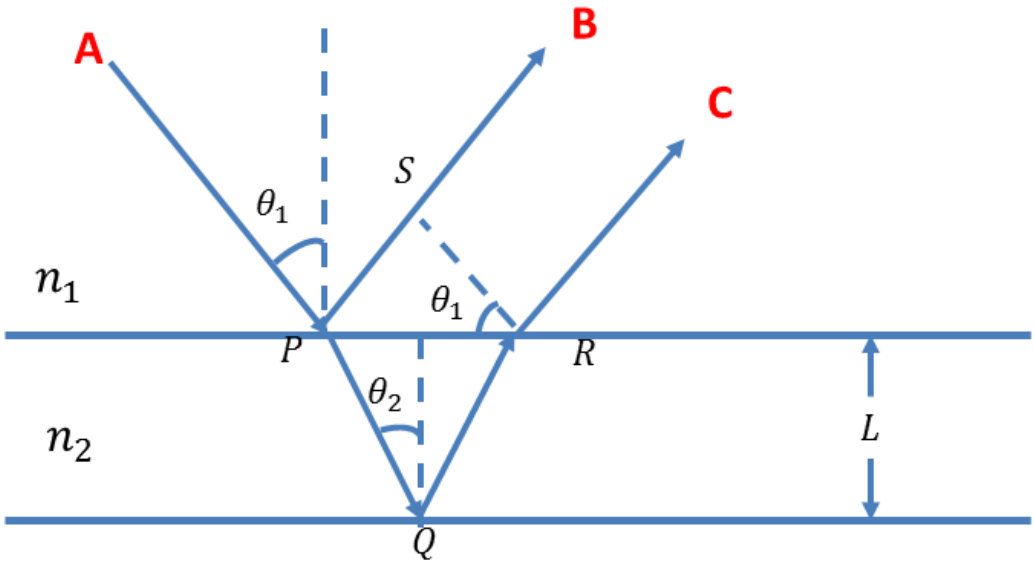

Figure 15: *Schematic diagram of thin film interference. The incident light (A) reflected from the upper and lower boundary of the thin film producing two waves (B and C respectively).*

The concept of thin film interference has huge commercial applications for antireflection coating of mirrors and optical filters [128-133]. Soap bubbles, oil films have also tremendous commercial application. Some other examples, which involves thin film interference phenomenon such as blue wing-patches of butterflies and different insect species, see Fig 16. In this context, the insect wing acts like a thin film and one could in principle use Fresnel equations to quantify the specular reflectance with respect to the polarization, angle and refractive index. Equations from Fabry-perot cavity can then explain wing membrane thickness and fringes. Such equations provide quantitative description of the amount of light reflected and transmitted at the interface. However, it is a bit difficult to apply this remotely to flying insect unless the self-scanning nature of insect wing is exploited. This needs to be investigated further in order to implement realistic ways of measuring wing-membrane thickness of insects *in situ*.

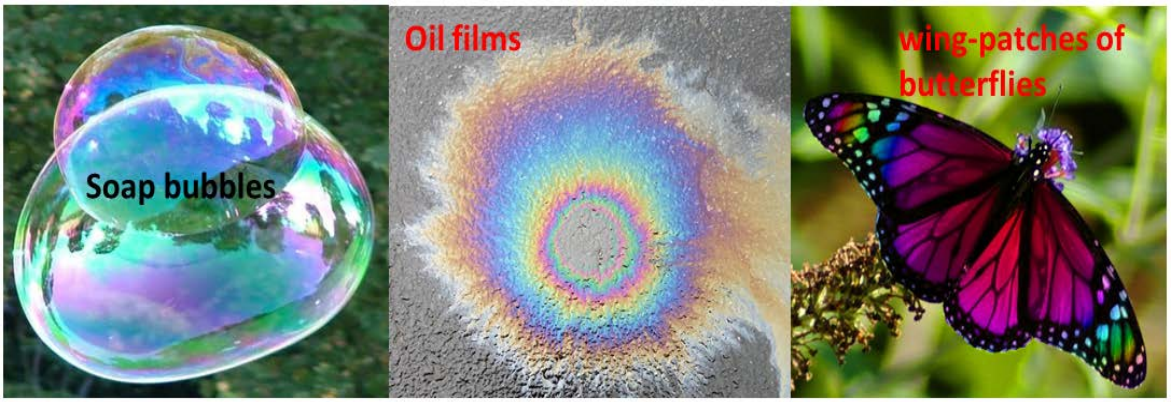

Figure 16: *Example of thin film interference phenomena [134]:* ***Left****: Soap bubbles.* ***Middle****: oil films, where the refractive index of the oil is bigger than air on top and the water below [135].* ***Right****: different colour wing-patches of butterfly [136].*

2.3.2 Insect scattering in temporal domain

The back scattering time series from an insect provides information about the duration the insect stays in the probe volume of the field of view (FOV), body and wing size and wing-beat frequency, see Fig.17. It should be noted that size determination using dark field spectroscopy technique is only accurate close to object plane and the termination where the calibration and controlled release was made. This is because limited range information could be retrieved from the flank rise and fall times associated with event distance. However, the CW-LIDAR technique employed in this thesis enables to achieve range resolved measurements. The highest peak corresponds to a specific orientation of the insect when the optical cross section (OCS) is the largest. Similarly, the lowest peak corresponds to the lowest OCS. This means that every peak corresponds to one orientation depending on the different phases of the wing-beat. The OCS oscillates in time depending on the orientation of the insect in the FOV. For instance, if the insect is detected from the front, it will appear larger once during the wing-beat cycle (1ω). On the other hand, the insect will appear larger twice when detected from the side (2ω). This shows that the accuracy of OCS not only depends on the range resolved intensity calibration, but also on the phase of the wing-beat cycle and physiological orientation of the insect inflight. This oscillating behaviour of the OCS of insects in LIDAR experiments can be parametrized by a discrete set of harmonics. The equation that describes the oscillating OCS behaviour involves the non-oscillating body contribution and the oscillating wing-beat contribution.

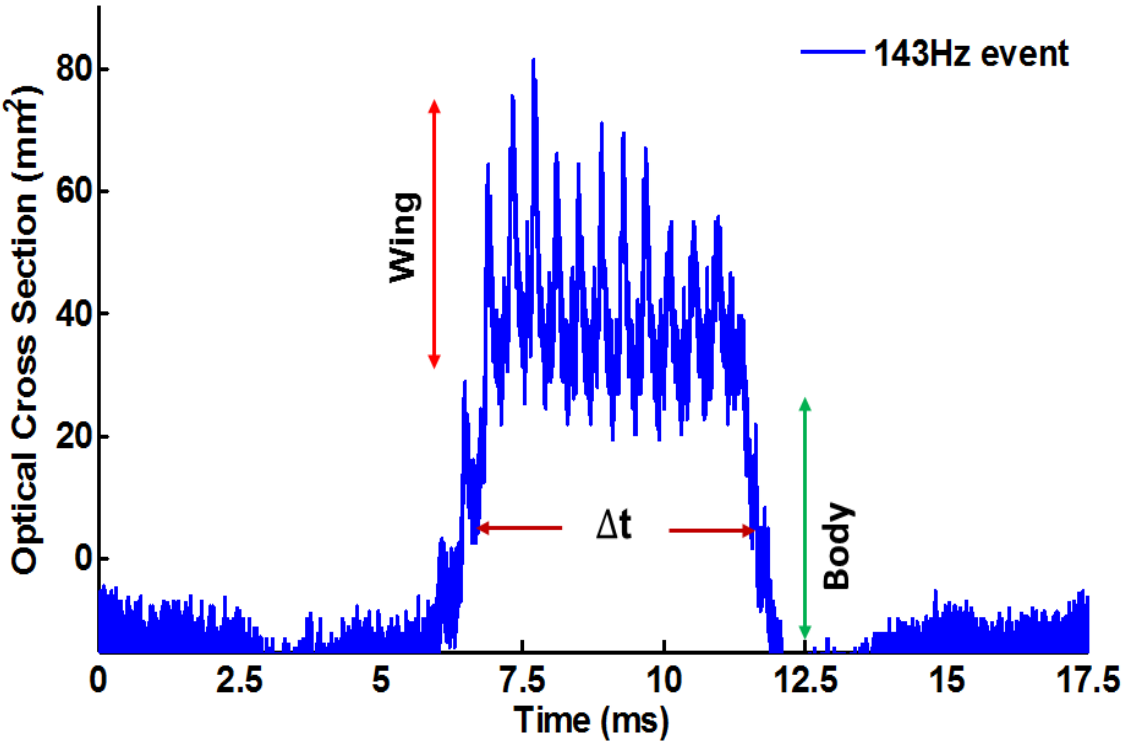

Figure 17: *Insectback scattered time series: The oscillating part (red arrow) indicates wing size; the non-oscillating part (green arrow) indicates body size. The time in which the insect stays in the FOV is denoted by* $\boldsymbol{\Delta t}$*. The y-axis is optical cross-section (OCS) in* mm^2 *and x-axis is time in ms.*

The detailed discussion of these phenomena is given in Chapter V and one can see that this aspect could introduce some uncertainties in the analysis of OCS, see Eq.2.8 [137].

$$OCS(t) = \beta(t) \sum_{h=0}^{h<1/2 f_s} \left(C_{1,h} \sin(2\pi f_0 h t) + 2\, C_{2,h} \cos(2\pi f_0 h t) \right) \ldots\ldots\ldots \text{(2.8)}$$

Where: t is time, β is the time series of the non-oscillating scattering contribution, which is obtained by using low pass filter to remove the oscillatory contribution (due to wing-beat), $f_S$is the sampling frequency, C is the optical cross-section coefficient, h is running integer index of harmonics and $f_0$is fundamental frequency[137]. The reason why $h < {}^1/_2\, f_s$ is because of the Nyquist criterion that the maximum frequency that can be resolved in the time domain is half of the sampling frequency.

The diffuse reflection from the body and wing is responsible for the fundamental and lower harmonics. The higher harmonics are due to specular reflection from the wing. The reason why the specular reflection is coherent is because of the fact that phase of light is preserved after scattering. The specular reflection (rapid spikes in the temporal waveform) means high frequency in spectral domain. To reproduce such rapid spikes, it is required to have high frequency; otherwise the temporal waveform would have looked smooth. In other words, the rapid spike will disappear if one reconstructed the temporal waveform using only the lower harmonics. This indicates that the specular reflection is coherent and the rapid spikes in time domain is responsible for the higher harmonics in the frequency domain, see Fig.18. This figure shows an insect event with a 143Hz fundamental frequency and its 2nd, 3rd and 4thharmonics

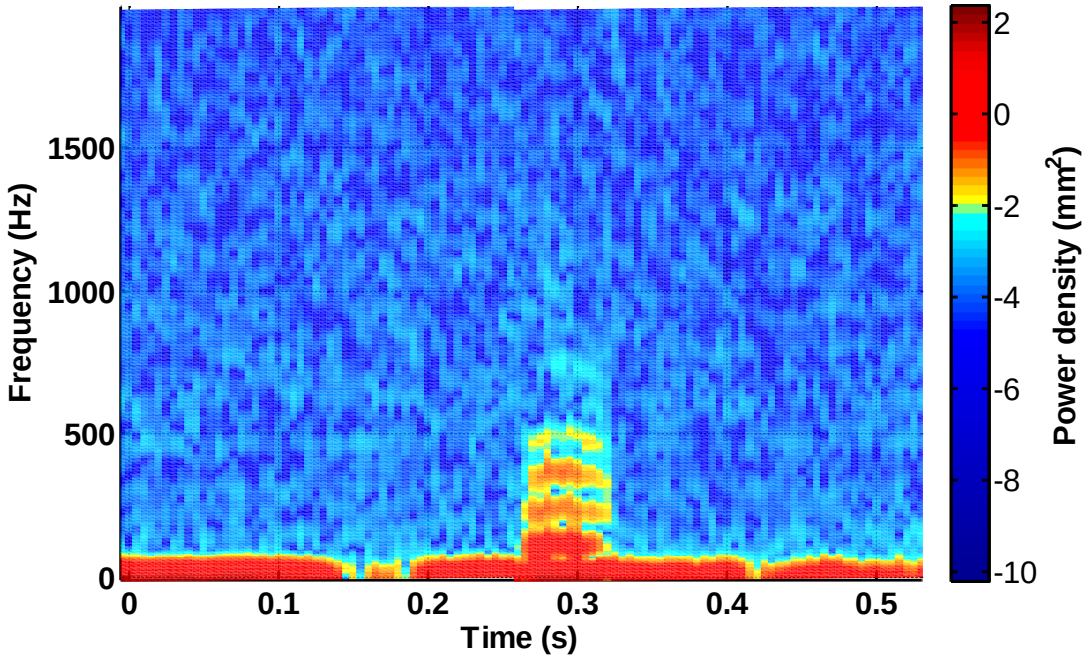

Figure 18: *Spectrogram showing body size, fundamental frequency, and harmonic overtones of the same insect event. The direct current (DC) level or zero frequency shows the body size. The fundamental frequency at 143Hz and the higher order harmonics are shown.*

2.3.3 Insect Scattering in spectral domain

Reflectance from insect varies in different bands; such has VIS, NIR, and SWIR. In the VIS and NIR the scattering from an insect is highly influenced by the colours of the insect due to the body and wing melanization of the insect while the SWIR is insensitive to the colour, see Fig.19. The quantitative analysis of the absolute OCS is therefore more accurate in the SWIR and the signal is 10-20% higher due to higher reflectance of insects in that range [137]. Estimation of an OCS in the NIR is affected by melanization due to the fact that the insect melanin may vary from anterior to posterior or from ventral to dorsal [137]. This means it is unlikely to expect symmetry in the frontal- and transverse plane in the NIR, which shows that the OCS in SWIR is the same as the true cross-section of all insect regardless of their colours. This minimizes the uncertainty that could occur due to colour differences of insects. In other words, if onedetected white and black butterfly at the same range their size should be the same in the SWIR, but not necessarily in the NIR. The same is true with other insect species, which is a huge advantage in the accuracy of determining OCS in the SWIR.

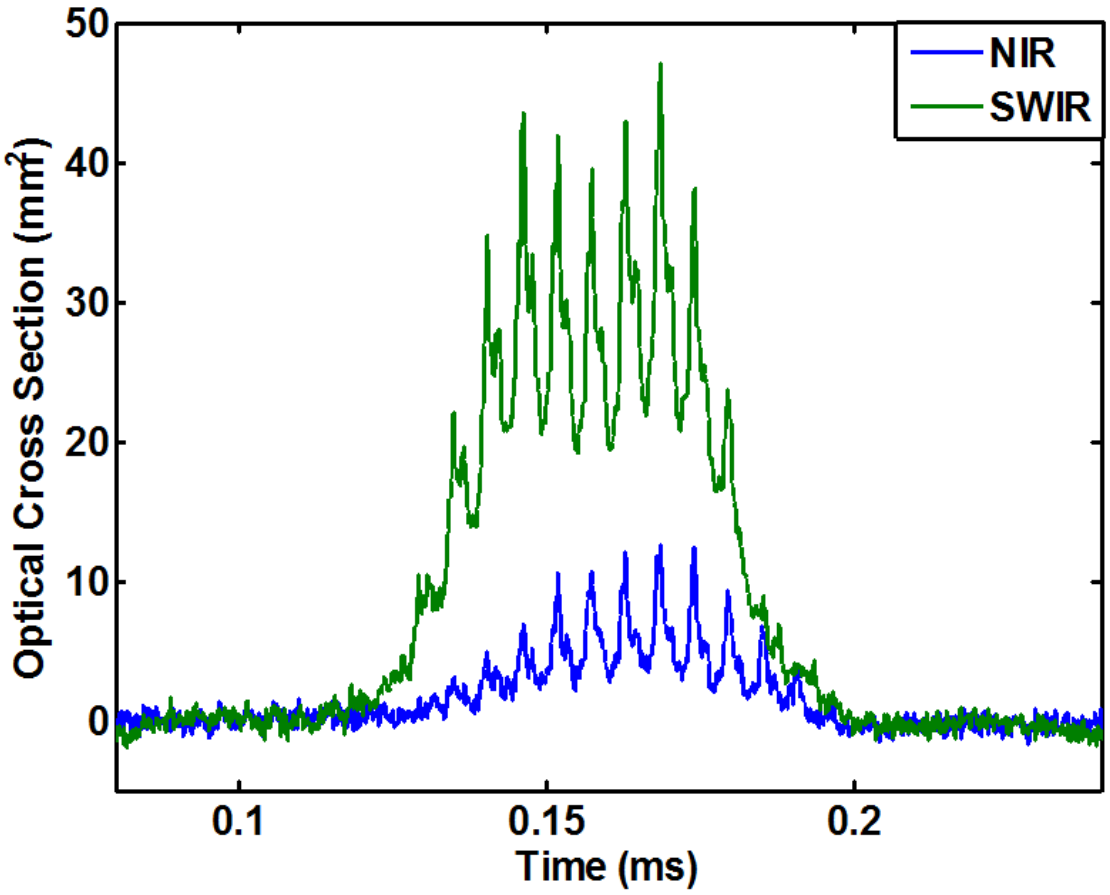

Figure 19: *Relative size of insect event in the NIR as compared with SWIR. The size of the insect is bigger in SWIR, which is in accordance with earlier findings. This OCS difference in this specific example is higher than 20%.*

Chapter III

3. Instrumentation

3.1 Light source

3.1.1 Sun light

The Sun is a crucial light source for the existence of lifeon earth. The solar radiation from the sunreaching the earth ranges from the ultraviolet (UV) to infrared (IR), with intensity of about $1kW/m^2$. The sun is a black body radiator, where the radiation peaks in the visible range around 550nm. This corresponds to a surface temperature of the sun, which is around 5600K. The spectrum has several opaque regions caused by atmospheric absorption and pollutant molecules such as H_2O, CO_2, O_3, and CH_4 [138]. Those absorption lines created by the absorbing molecule are called Fraunhofer lines[139,140]. This kind of techniques, which uses sun light as an illumination source is called passive remote sensing. In this dissertation, sun light was mainly exploited in papers (I, II, III). Wing-beat frequency, iridescences features, flight direction and colour information were investigated using sun light. The main challenge of using solar based radiation as a light source is the fact that the radiation from the sun is not stable and it keeps changing with the atmospheric conditions. For instance, the amount of light reaching the ground varies when there is cloud covering the sun as compared to the clear skies situation, see Fig.20. Additionally, the angle of on incidence impinging in to the field of view varies as sun moves during the day. This necessitates regular calibration of the instrumentsince the amount of light impinging in the FOV varies depending on the atmospheric conditions. To minimize uncertainties, most of the experiments were done in clear sky conditions where the solar irradiance is very stable and reference data were recorded every 30 minutes throughout the measurement period. A pendulum was also used to estimate the amount of light impinging the field of view. Detail of the calibration process discussed in section 4.3.

Figure 20: *Sun illumination during cloudy conditions. The illumination intensity varies depending how dense the cloud is, which demands frequent calibration of the system.*

3.1.2 Lasers

Laser is an acronym for the term light amplification by stimulated emission of radiation. The physics behind all types of lasersis basically the same. They all require gain medium and one has to achieveelectronic population inversion to produce laser light [141,142]. The type of laser varies from the smallest,like vertical cavity surface-emitting lasers(VCSEL)[143,144] to the largest in size such as the lasers in the ignition facilities of fusion experiments [145,146]. In terms of wavelength, there are wide ranges of commercial lasers are available. This includes the shortest wavelength of free electron lasers [147] to the longerwavelength of microwave range lasers called microwave amplification by stimulated emission of radiation (maser) [148,149]. The type of lasers to use varies depending on the application such as welding and cutting purposes[150,151], data communication and storage[152,153] or spectroscopic experimental applicationssuch as non-linear and relativistic optics [154-157] . In this dissertation, 808*nm*, 3*W* infrared laser was used. This is a continuous wave diode laser, which can be modulated in the order of kilohertz. This laser was employed in the active remote sensing experiment presented in this dissertation.

3.2 Dark field spectroscopy

3.2.1 Experimental setup

Passive remote sensing system was developed based on dark field spectroscopy. The aim of this experiment is to be able collect the backscattered signal from an insect crossing the field of view (FOV). Dark field spectroscopy is a way of lowering the background signal where signal rises from 0%, rather than decreases from 100%as in transmission experiments. Ideally, one can achieve a high signal to background ratio using this technique by employing an infinitely dark termination cavity. However, practically, this is difficult to achieve since there will still be scattering from the atmosphere itself and Rayleigh scattering even from pure air.In this setup, Newtonian telescope (Focal length (F) 1200mm and ø254mm aperture), dark termination box (ø100cm, 150cm long) was used. In this dissertation, different kind of setup was used in Sweden and South Africa. The setup used in South Africa is given in Fig. 21. A similar but more advanced system was built in Lund, Sweden by Dr. Mikkel Brydegaard. This set up is a new research development platform for the assessment of insect activities and migrating birds. This facility is called Lund Mobile Biosphere Observatory (LUMBO), See fig 22. LUMBO is a new mobile observatory setup, which can be placed anywhere for experiments.

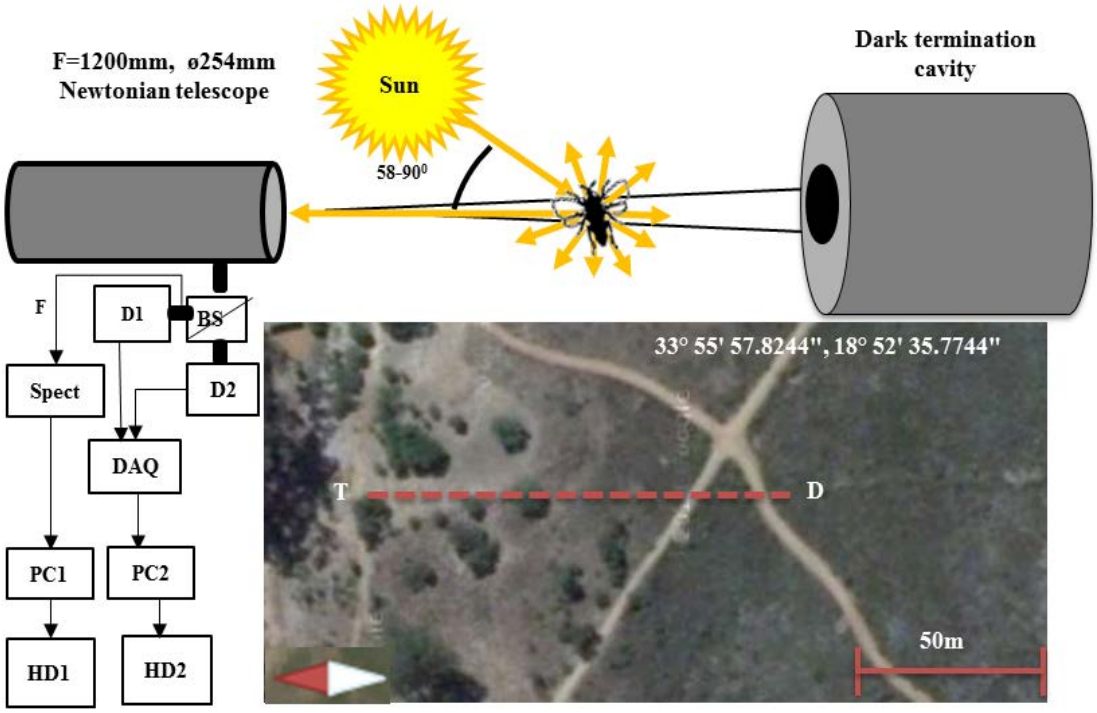

***Figure 21**: Experimental setup. D1: detector 1 (silicon (Si) quadrant and spectrometer in D2: Si/InGaAs sensors. F: fiber patch cable. Spect: spectrometer. DAQ: data acquisition device. BS:beam splitter; T: telescope; D: dark termination; PC1 and PC2: laptops for data collection, HD1and HD2: data storing external hard drive. The map shows the location of one measurement campaign in the Jan marais nature reserve, Stellenbosch, South Africa. The distance between the telescope and dark termination is200m southwards.*

***Figure 22**: LUMBO: It has two main parts the blue container in the left is a control room. The white dome is where the five telescopes and detectors are placed. The dome is motorized and can rotate $360^{0.}$ The field of view opens 90^{0}*

LUMBO has two main sections: the white dome, where the telescope and all detectors are placed and the control room where the data storage and control computers are placed, see Fig.23.

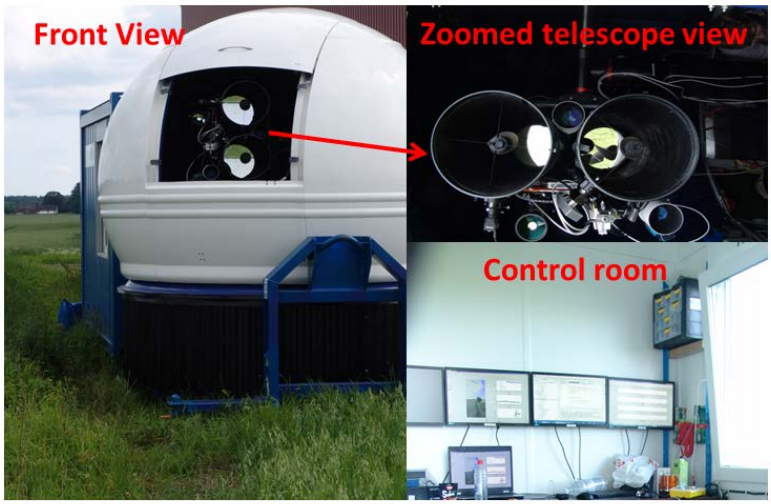

***Figure 23**: LUMBO: Front view, zoomed telescope image and image of control room. We have used five different telescopes (two Newtonian reflecting telescopes, F=120cm, two refractor telescope, F=50cm, and one Maksutov telescope, F=130cm)*

During various field campaigns in Sweden a variety of detectors and instruments were used for the study of insect diversity, forestry pests, interaction strength and overall activity. In June-July 2013, we had a field campaign in Brunslov, Stensoffa, and in June-July 2014 at Brunslov and Nytboda, Sweden. The aims of the experiments were to investigate biodiversity of insects across various agricultural landscapes, investigate the efficiency of traps of forestry pests (Example: beetles), and assess the influence of fences between fields on the biodiversity of insects, see Fig 24.

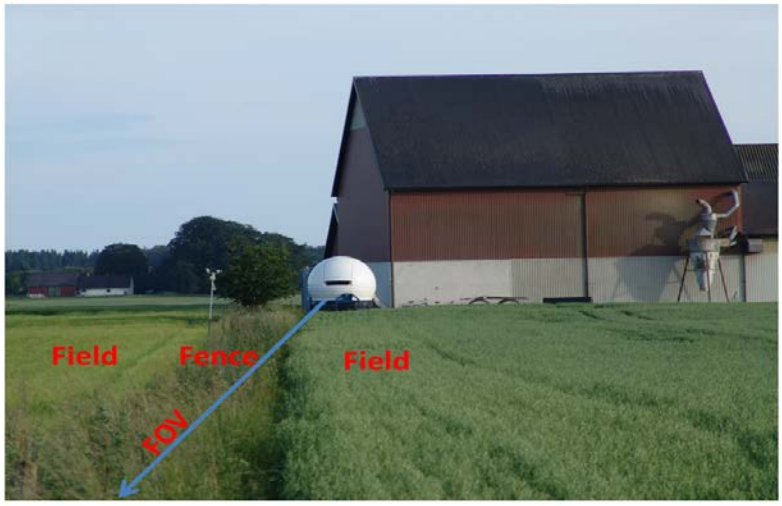

***Figure 24**:Biodiversity between two fields. In the middle of the two farms there is a about half a meter wide fence where a lot of plant species has grown on. This fence is believed to increase the biodiversity of insects, which could have significance environmental impact in terms attracting pollinating insect.*

3.2.2 Detector setup and spectral band

The setup covers three discrete spectral bands: Visible (VIS, 0.32 to 0.68µm), near infrared (NIR, 0.66 to 1µm) and short wave infrared (SWIR, 1 to 2.4µm). This is a triple band setup, which is developed to investigate the absolute optical cross-section (OCS), wing-beat frequencyand iridescencefeatures [158].This setupinvolved two parts:In the first partsilicon (Si) quadrant photodiode was used to detect the visible signal and a dual detector (Si photodiode and InGaAs photodiode, integrated into a layered package) to collect infrared signal. A spectrometer was used to collect thespectrum of insect event, which allows for the collection of spectral information and wing-beat information from the dual detector concurrently, see Fig. 25.A beam splitter (cold mirror) was employed to transmit the infrared and reflect the visible.

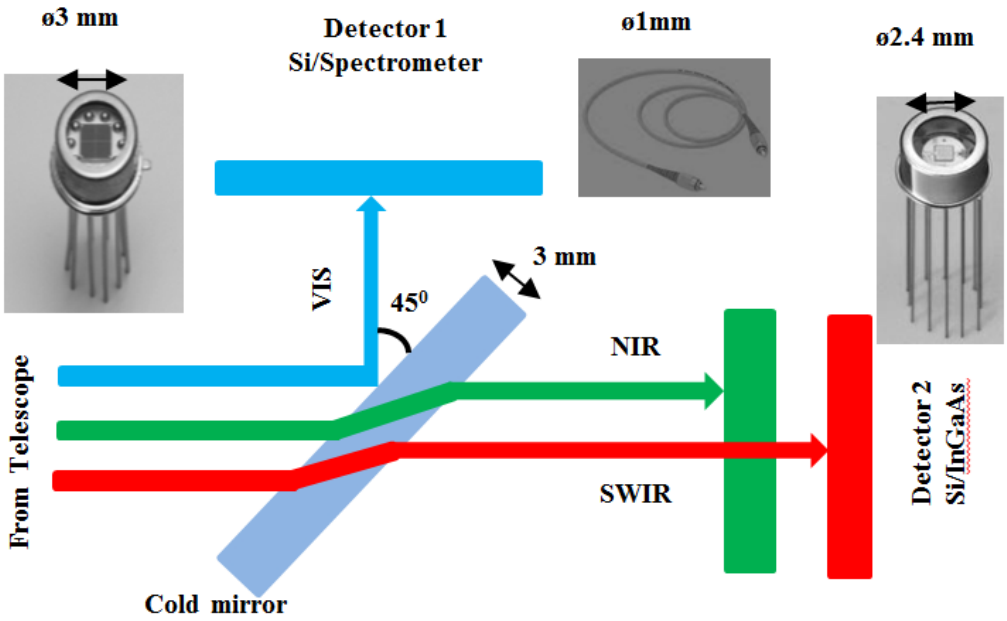

Figure 25: *Schematic plot of detector alignment of the setup.The three discrete bands are: Visible (VIS), near infrared (NIR), short wave infrared (SWIR).*

The bandwidth of the detector is determined by the full width at half maximum (FWHM) of each spectral band.This crude spectral discrimination offers three bands with bandwidths from 0.3 to 1µm FWHM (0.4 µm for the VIS, 0.3 µm for the NIR, and 1µm for the SWIR), see Fig.26.

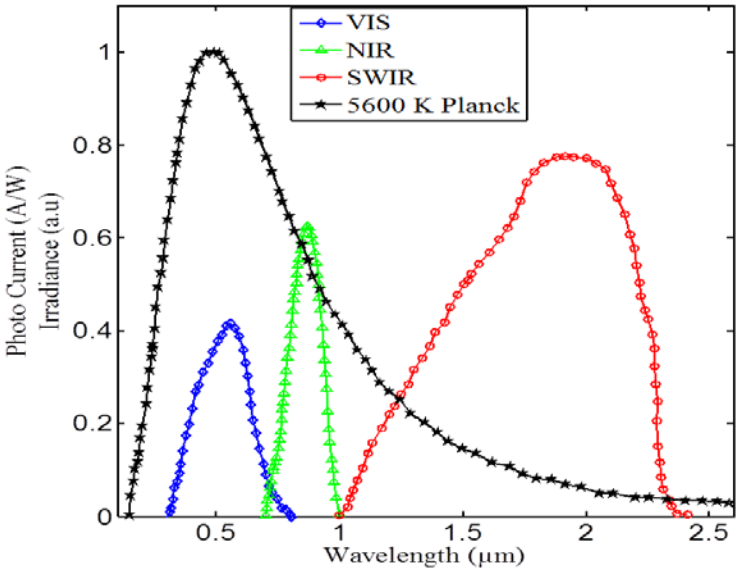

Figure 26:*Plot of sensitivity versus wavelength for the three detectors. VIS-Si(D1-Quadrant detector): VIS scattering, NIR-Si (D2): vegetation sub-illumination, and SWIR InGaAs (D2): thin-film iridescence.*
Another detector setup we have implemented in Sweden and South Africa involves VIS (Si) and SWIR (InGaAs) quadrant photodiodes. A similar beam splitter (cold mirror)was used to reflect the visible and transmit the infrared, see Fig.27. The NIR quadrant covers 0.19 to 1µm and SWIR quadrant 0.9 to 1.7µm.The aim of this experiment was to determine flight direction of insects from the time sequence of the quadrant signal and estimate interaction kinetics of insects.

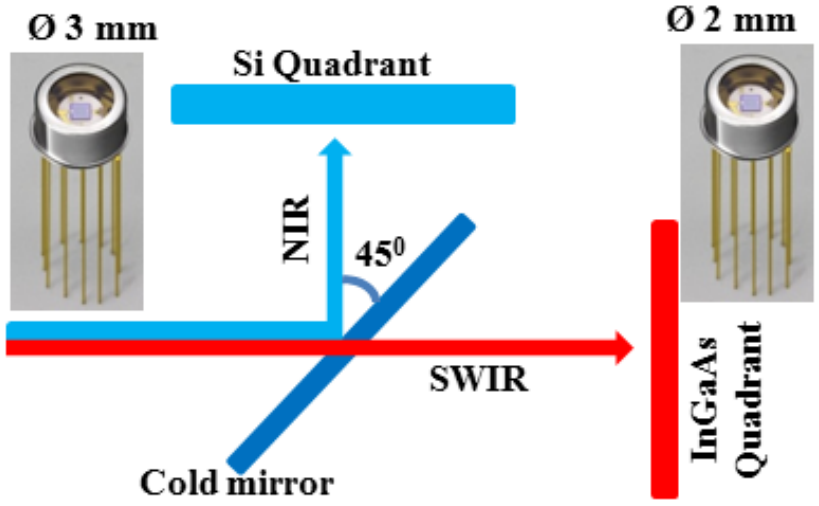

Figure 27*: Schematic detector setup of dark field experiment of LUMBO.*

3.2.3 Experimental capability

The passive remote sensing setup is capable of achieving a wide range of benefits in terms of investigating activities of insects*in-situ.*The most obvious advantage is the fact that it uses sunlight as an illumination source, which isone of the abundant broadband light sources. It is also cheaper compared to other passive remote sensing techniques that can a do similar job. This system is capable of providing both qualitative and quantitative information:

A.Determinationof flight direction:

Flight direction can be determined using the Si and InGaAs quadrant photo diodes. The time sequence of the signal in each section of the quadrant provides the direction in which the insect event enters and leaves the FOV, see Fig.28. Adetailed calibration procedure of flight direction trajectories is discussed in chapter IV.

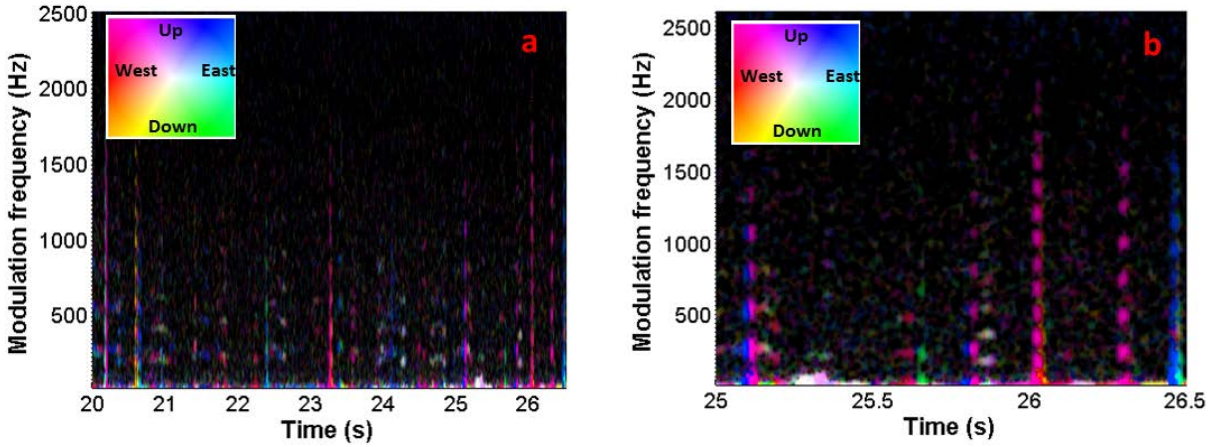

Figure 28:*(a): Flight direction of honey bees in to and out of the beehives at agricultural research council (ARC) in Stellenbosch, South Africa. (b): zoomed on the time between 25-26.5 seconds. The color changes from blue topink for the bee event at 25.1seconds. This indicates that the beewas flying from east to the west (in to the beehive). The two bees at 26 and around 26.4second seem to be leaving their hive, but they left the hive without being detected by the other quadrant.*

B.Absolute Optical Cross-Section (OCS)

Absolute OCSis the size of the insect multiplied by the effective reflectance of a given spectral band and its accuracy depends on proper calibration. The quantitative OCS comes from the calibration using white diffuse spheres of different sizes. The detailed OCS calibration process is discussed in chapter IV. The estimation of absolute OCS in the dark field experiment is only accurate close to the object plane where the calibrations were performed. This is because of the fact that we couldn't retrieve range information so fare and it is difficult to introduce the range-dependent sensitivity or the form factor in this technique[159]. The accuracy of absolute OCS could be improved by considering the steepness of the signal, flight direction and body orientation. The absolute OCS has contribution from the body and wing of the insect, see Fig.29. In this figure, one can see that there are two contributions to the total absolute OCS of the insect: the oscillating part comes from the wing contribution and the non-oscillating part from the body contribution.

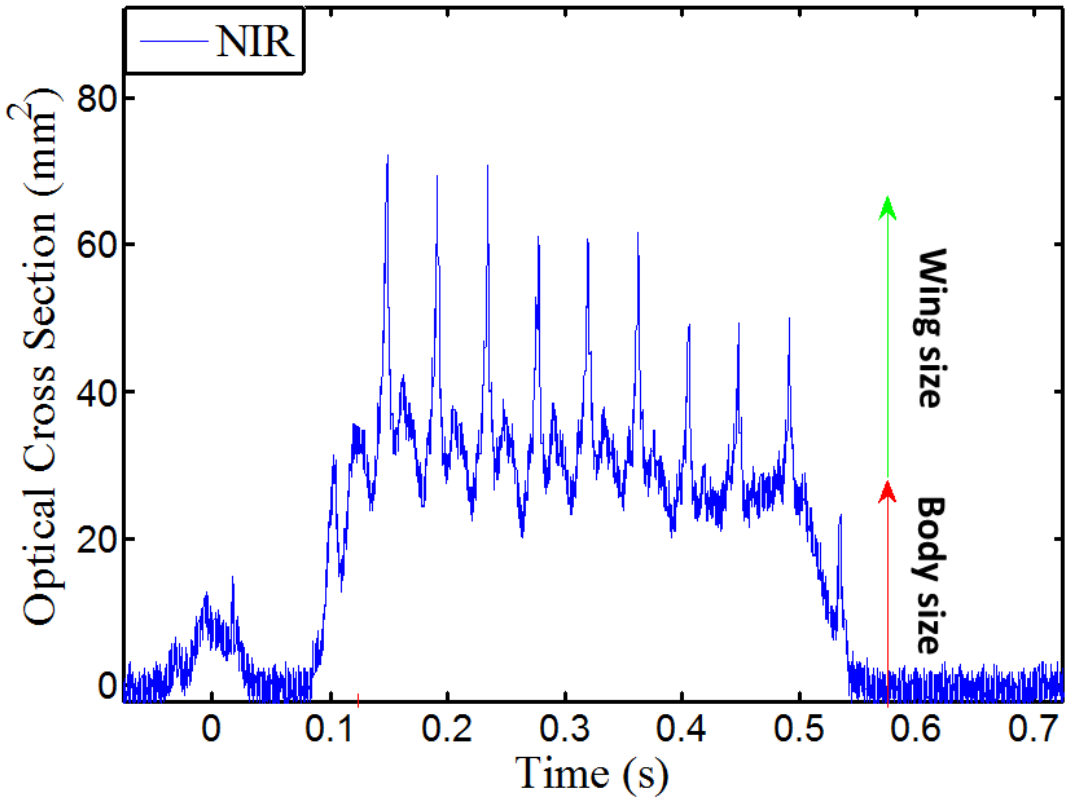

Figure 29: *Absolute OCS of insect event in the near infrared (NIR). The red arrow indicates the body contribution and the green arrow indicates the wing contribution to the total absolute OCS. In principle, the signal is not expected to correspond to the actual size especially when the specular reflection occurs.*

C.Iridescence features

Thisis a characteristic property of a certain a surfaces where the reflected colour changes withangle of illumination or observation. This phenomenon happens due to the interference of light reflected from the microstructures of a surface. Example: From soap bubbles or films [160], and the wings of a butterfly [161]. Iridescence feature have been used to study structural colouration of different biological samples such as the neck feathers of pigeons, which shows that cyan feathers change colour to magenta at large viewingangles [162-164] and the stable microstructural patterns in the wings of different insect species [165-169]. In our context, we have investigated iridescence features of insects using two bands of the twodetectors (Si Quadrant photodiode and the Si part in the dual detector, which monitors the NIR range). The Si band is used to collect the VIS signal and the other Siband from the dual detectormonitors the NIR, see Fig 30. We use these two bands to compare how the shape of the temporal waveform of the two signals changes. In this case, two concepts were assessed: The first is to investigate the effect of melanin, which is the most common chromophorefound in all insects, mainly responsible for dull black and brownish colours[170].The second is to investigate the contribution of vegetation sub-illumination on the slow part of the wing-beat. Hence, we can see that the shape of the temporal waveform varies, see Fig.31. This could be due tothe two reasons we mentioned above.

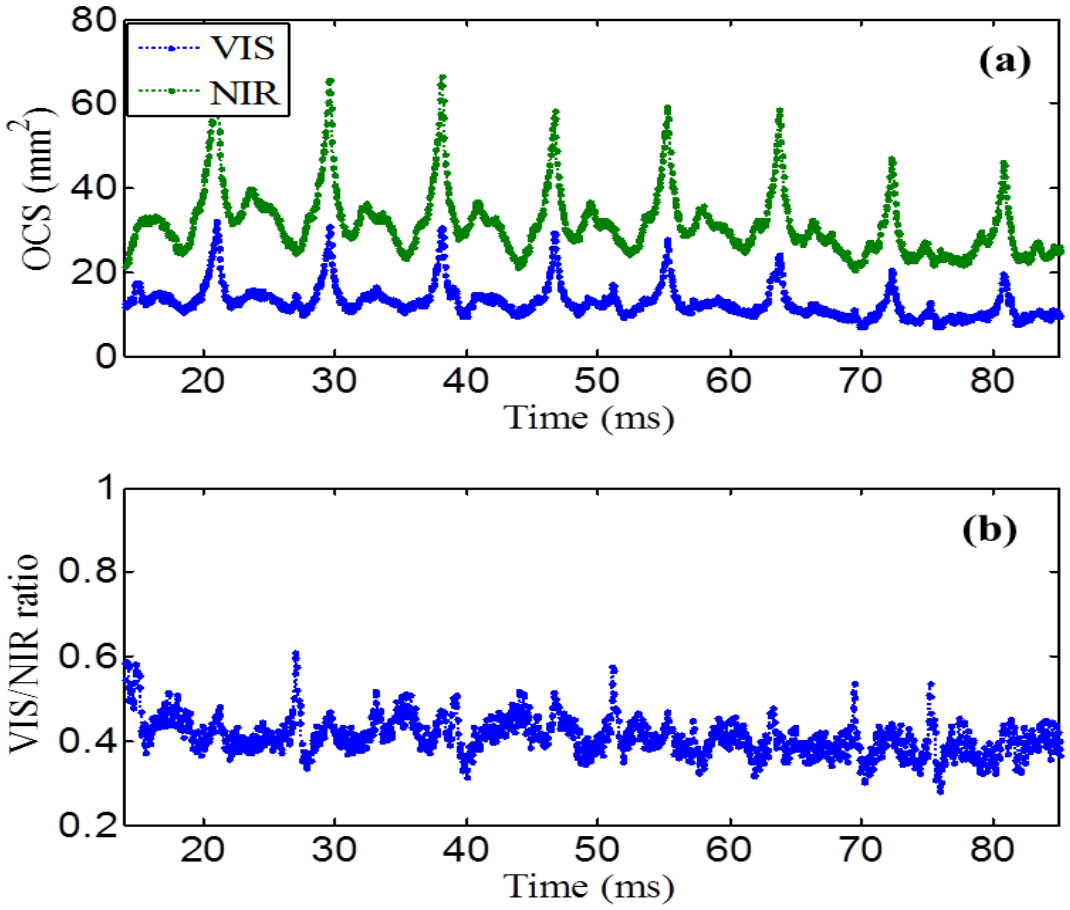

***Figure 30**: Iridescent properties: (a) spectral difference in the VIS and NIR ranges. (b) Ratio of VIS and NIR signal.*

D. Wing-beat frequency and harmonics

Wing-beat frequency is a measure of the number of times an insect beats its wings per second. The wing-beat frequency of insects varies depending on species, ambient temperature, speedand other aerodynamic constraints [171-173]. In this dissertation, wing-beat frequencies of different insects were resolved, from the slower damselfly, to the fasterhoney bee, which are about 60Hz and 240Hz respectively. In addition to the fundamental wing-beat frequency, higher harmonics was also resolved, see Fig31. The harmonics frequencies are caused by specular reflectionas it was discussed in chapter II.

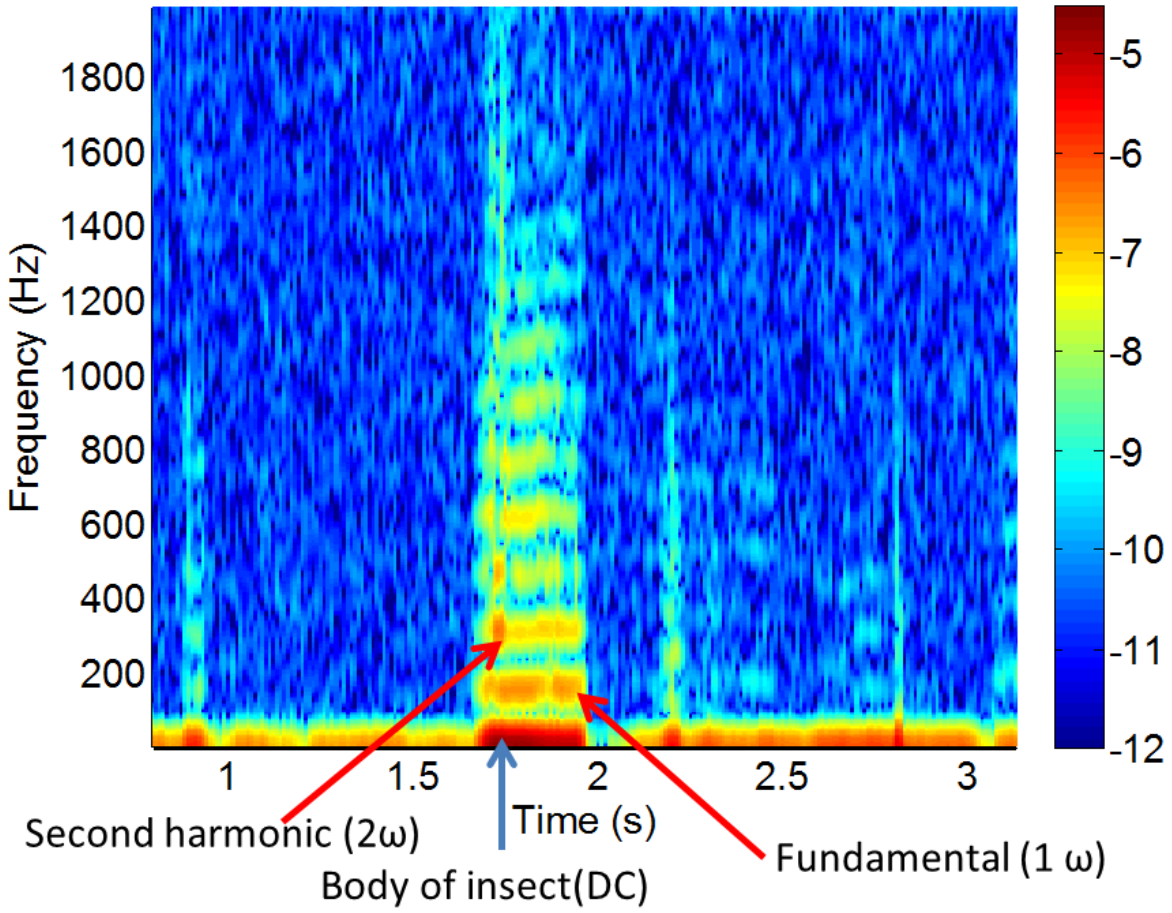

***Figure 31**: Spectrogram of an insect event with a 200Hz, fundamental frequency and its harmonics*

E. Spectral information

Insect color difference beyond human vision can be determined using spectrometer. The so called Spectral information is another important aspect of our experiment, which allows us to collect colour informationfor remote insect classification. A quantitative measure of temporal variation of a certain insect species in relation to temperature and wind speed can be done [94]. We have done controlled release of colour marked insects to test the instrument and we have detected the green powder marked dragon fly, see Fig.32. We have confirmed this event from the recoded time when the insect was released and wing-beat frequency of the dragonfly detected by the dual detector at the exact same time.

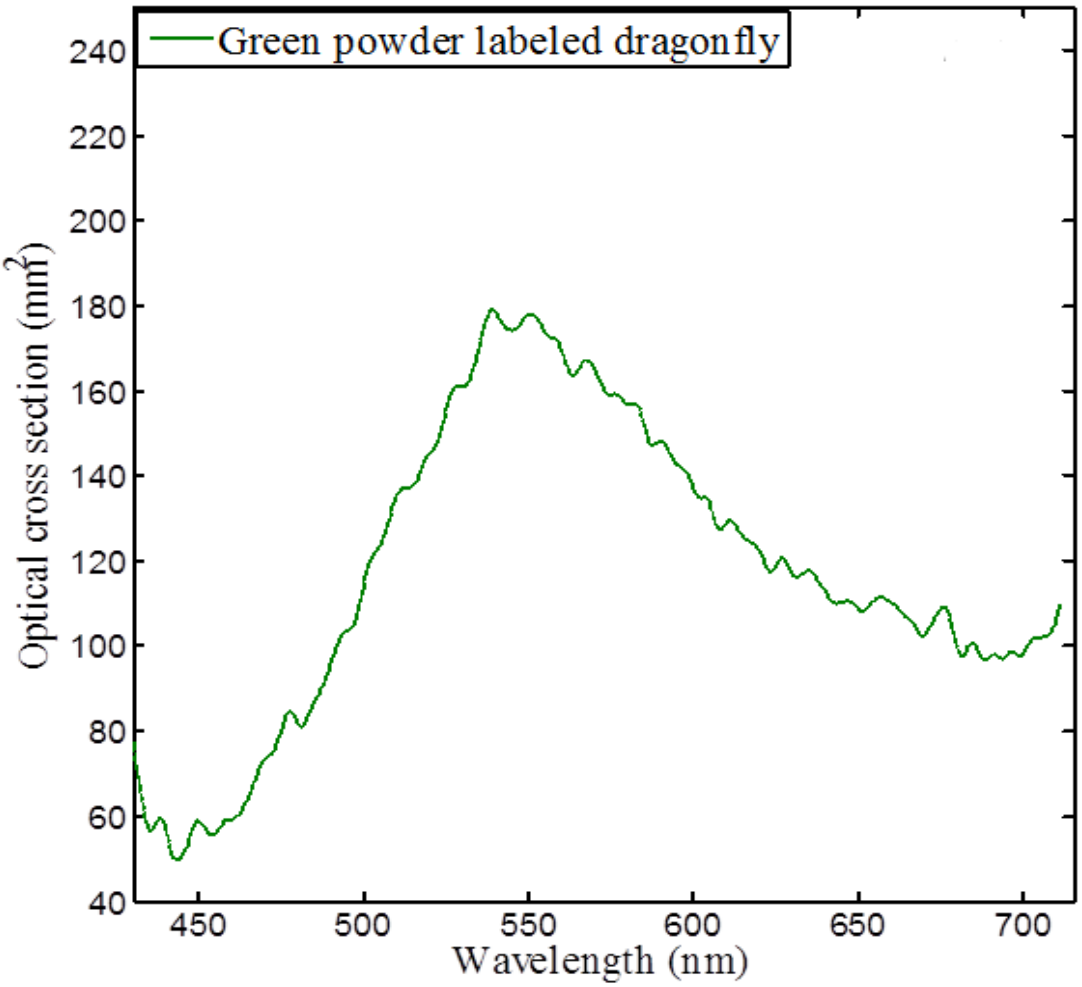

***Figure 32**: Spectral signature of a green powder marked dragonfly measured using a spectrometer. The spectrum has predominantly green features around 550nm due to the powder*

3.3 Continuous wave light detection and ranging (CW-LIDAR)

3.3.1 Time of flight LIDAR (TOF-LIDAR)

We have developed continuous wave light detection and ranging (CW-LIDAR) for environmental monitoring applications based onthe Scheimpflug principle [98]. This method enables us to achieve fast sampling, which is not limited by the round trip time of the laser light. The importance of implementing a high sample frequency is to be able to resolve wing-beat frequencies and its harmonics. Arange resolution beyond the diffractionlimit was presentedusing this techniqueunlike the conventional LIDAR techniques, which is limited by pulse duration[44].

The main advantages of the Scheimpflug setup as compared with the conventional LIDAR systemare the following [44]:

- The continuous radiation poses less-eye-safety concern
- It does not require high damage threshold transmitting optics[174,175].
- It is less costly
- Pulse LIDAR monitoring is limited to spectral range 0.2-1.7µm since it uses cascaded detectors such as PMTs and avalanche-photo-diodes (APDs)
- CW –LIDAR can be accomplished with Si, InGaAs or HgCdTe linear array within the range 0.2-12µm
- The sampling frequency can reach 20kHz, which enables resolution of wing-beat frequency and its harmonics

By employing this method, one can investigate temporal and spatial distribution of pollinators on a landscape scale andestimate thefluxes of disease transmitting insect. In this dissertation, measurement was performed using three different laser radar systems: Stellenbosch Scheimpflug LIDAR, which is developedat the laser research institute (LRI), Physics department, Stellenbosch University, Lund University mobile biosphere observatory (LUMBO) Scheimpflug LIDAR in Lund, Sweden and Norway electro optics (NEO) Scheimpflug LIDAR inLørenskog, Oslo, Norway, both of which were developed by Dr. Mikkel Brydegaard, See Fig.33. Dr. Brydegaard has advanced the topic of entomological LIDAR and published numerous methods and applications.

The working principle of the three setups is essentially the same. However, they have a few differences in terms of the detectors used, alignment geometry of the camera and separation distance between the transmitting and detecting telescopes, see Fig 33.The purpose and capability of the setups also differ in certain aspects.

Figure 33**: Scheimpflug LIDAR Setup: **Left**: Stellenbosch kHz remote sensing setup. This works both in active and passive mode using laser and sunlight as illumination source respectively. **Middle:Norway electro-optics (NEO) *continues wave laser radar* setup. *This was designedfor the active mode using 808nm IR laser light source. **Right**: Lund university mobile biosphere observatory (LUMBO) setup, which is multipurpose mobile system capable of insect monitoring and bird tracking.*

Table 1:*Instrumentation of Stellenbosch LIDAR, LUMBO LIDAR and NEO LIDAR*

LIDAR setups	**Stellenbosch LIDAR**	**LUMBO LIDAR**	**NEO LIDAR**
Receiver	Ø254 mm F/4 Newtonian reflector telescope	ø100mm F/4 Newtonian reflector telescope	ø203 mm F/4 Newtonian reflector telescope
Transmitter	Ø90 mm with an F/5 refractor	Ø102 mm with an F/5 refractor	ø152 mm with an F/4 refractor
Laser source	3W, 808nm infrared GaAlAs diode laser	3W, 808nm infrared GaAlAs diode laser	1W 408nm, 5W, 808nmGaAlAs diode laser, 3W 1550nm.
Detector	Si-CCD array with 1024 pixels and a pixel size of 14x14 µm. The detector is tilted 45˚	Si-CCD array with 1024 pixels (2048 pixel if binned) and a pixels size of 14x14 µm. The detector is tilted 40˚	Si-CCD array with 3648pixels and a pixel size of 8x200 µm, CMOS sensor 2048pix, InGaAs camera.

			The detector is tilted 45˚
Receiver-Transmitter Separation distance	120cm	60cm	80cm
Filters	Long pass filter, Laser line filter (interference band pass filter)	Long pass filter, Laser line filter (interference band pass filter)	Long pass filter, Laser line filter (interference band pass filter)

3.3.2 Scheimpflug Principle

The Scheimpflug principle is a way of imaging anobject while achieving infinite focal depth, without closing the aperture [44, 98]. Before having detailed discussion of Scheimpflug principle, it is important to know how imaging works in a normal photography where the depth of field (DOF) varies depending on the size of the aperture. DOF is the front to back zone of an image, which determines the range in which an image can be in focus.A larger aperture has smaller focal ratio(f/number) which results in a shallow DOF and the opposite is true for a smaller aperture. With a bigger aperture, the image can be in focus at a certain position and out of focus on the other end. On the other hand, one can achieve deeperDOF by using a smaller aperture, See Fig. 34 and Fig.35. This constraint comes from the fact that the image plane, the lens plane and the plane of sharp focus are parallel. However, those three planes can cross at a certain point by implementingthe Scheimpflug principle. This situation is calledthe Scheimpflug condition. Fulfilling this condition enables to achieve infinite focal depth with an open aperture.

Figure 34:*Left: deeper depth of field with closed aperture makes the whole image in focus. **Right**: the shallow depth of field with open an aperture makes only the one flower at the bottom to be in focus. Adopted from [176].*

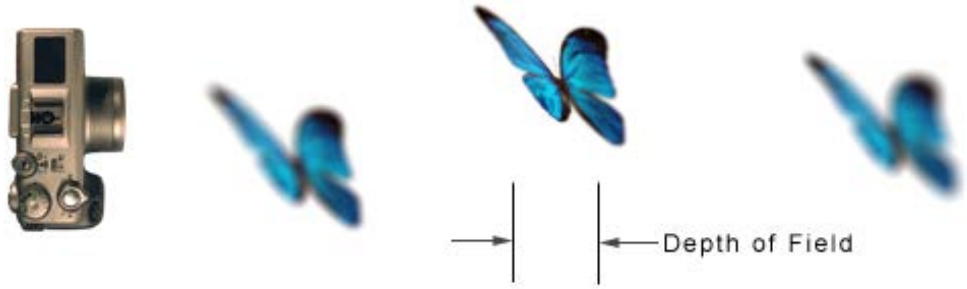

***Figure 35**: Image of a butterfly with a larger aperture and smaller focal ratio resulting in a shallow DOF[177].*

In the context of CW-LIDAR, the laser beam is imaged in to line scan camera with 1024 pixel. To fulfil the Scheimpflugcondition, we impose three conditions [44]: 1) the plane of the CCD, the receiving lens and the transmitting beam should coincide at the same point. 2) The distance between the receiving telescope and transmitting telescope should be equal to the focal length of the receiving telescope if the CCD tilt angle is 45^0. 3) The ray impinging on the outermost pixel, representing infinity, through the centre of the receiving lens is parallel to the transmitted beam, see Fig.36. Each pixel images a specific range of the beam and the constraint of range resolution is mainly the diffraction limit of the receiver and beam width. However, the blinking property of atmospheric faunaenables us to achieve arange resolution beyond the diffraction limit [44].It has to be noted that the Newtonian receiving telescope is replaced by refractor for the sake of simplification.

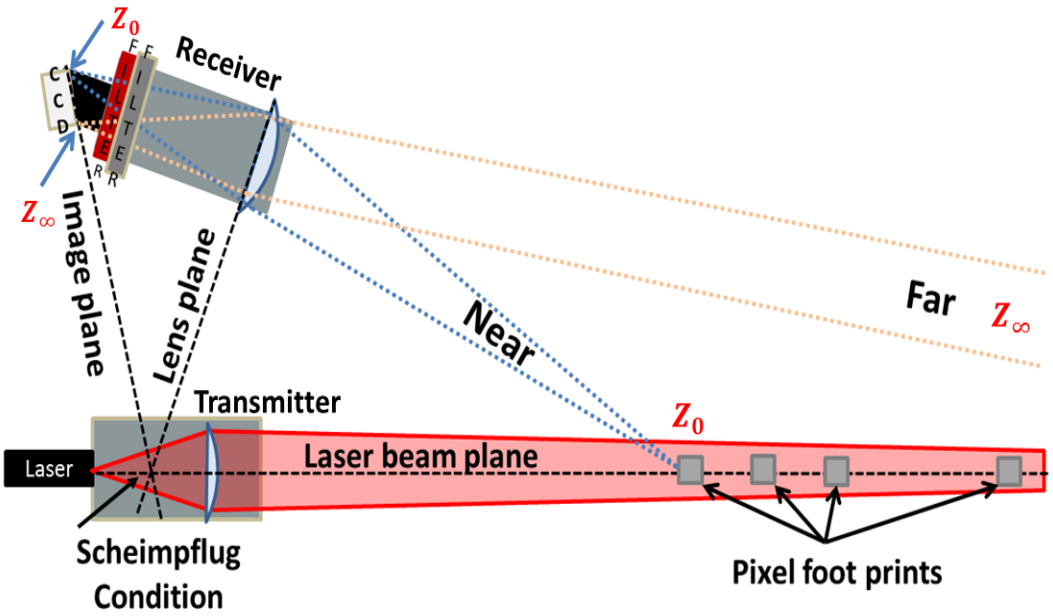

***Figure 36**: CW-LIDAR is based on theScheimpflug principle: the image plane, lens plane and object plane (beam plane) meets at a point, which fulfils the Scheimpflug condition.This allows us to achieve infinite focal depth without closing the aperture. It has to be noted that the Newtonian receiving telescope is replaced by refractor for the sake of simplification.*

The challenge of using only Scheimpflug line is the fact that it is difficult to find the actual focus since this line can move up and down. This means thatone would need two distinct points in order to precisely determine the position and slope of the Scheimpflug line [99]. This iswhere the importance of Hinge line comes in to play, see Fig.37. The Scheimpflug line is the intersection of focal plane (yellow line), lens plan (Purple) and plane of sharp focus (red). The Hinge line is the intersection of the parallel to focal plane lens plane (green), the frontal plane (blue) and the plane of sharp focus (red). The front focal plane is that plane parallel to the lens plane, but exactly one focal length distance away from the lens plane towards the subject.If we change the tilt angle, the Scheimpflug and Hinge linewould move up and down whilethe plane of sharp focus remains the same. On the other hand, the focus makes the Hinge line to move horizontally and the Scheimpflug line moves up/down while the Hinge line distance (J) remains the same [99].

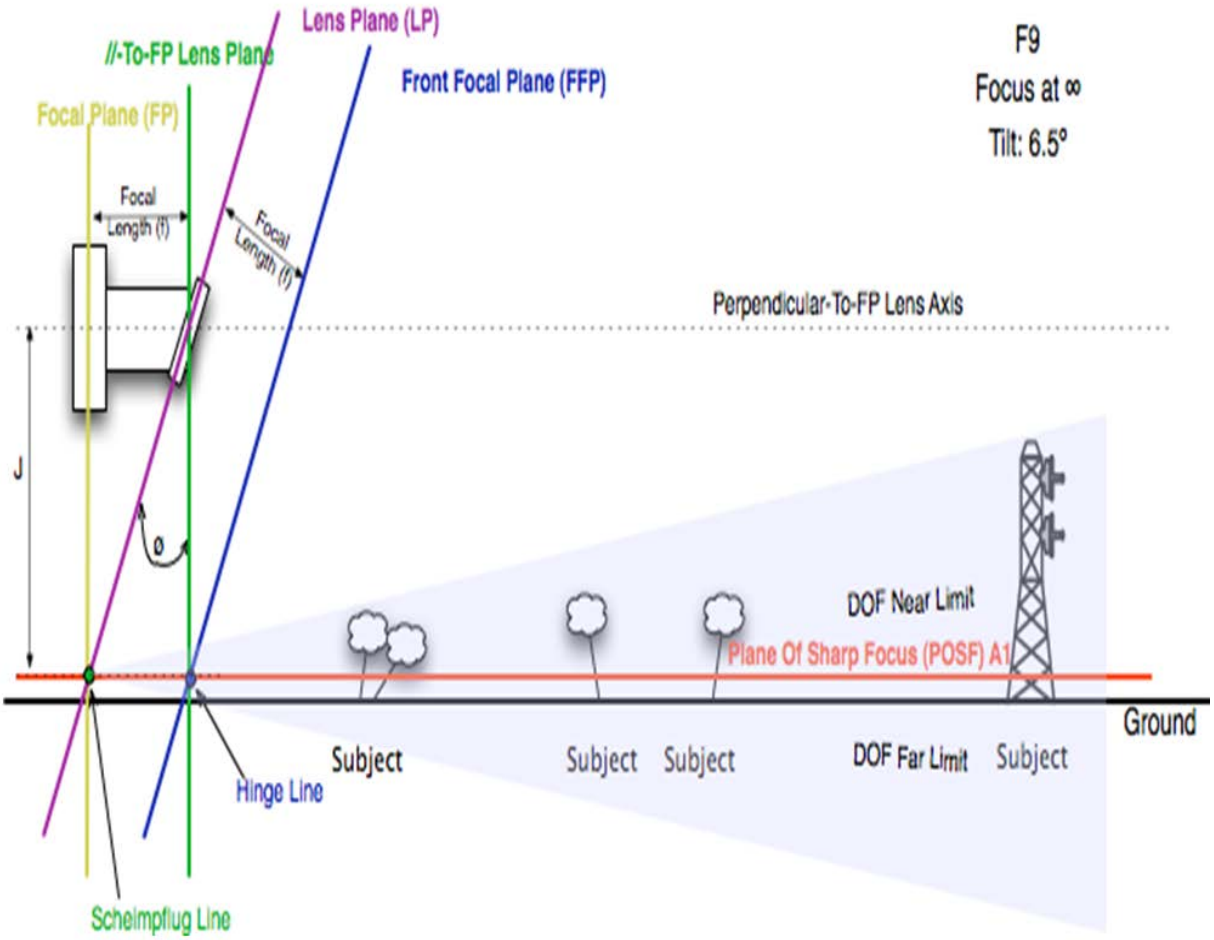

Figure 37: Scheimpflug and Hinge lines. Hinge line is defined to be the intersection of the parallel-to-focal-plane lens plane (green), the front focal plane (blue) and the plane of sharp focus (red). J is the Hinge line distance, which is the vertical distance between the nodal point of the lens axis and the nodal point of the lens. (Adopted from[99])

3.3.3 Experimental capability

The CW-LIDARtechnique has advantages as compared to the dark field experiments when it comes to retrieving range information and the accuracy of OCS. It iscapable of assessing range resolved biodiversity of pollinators like honey bees, the impact of diseases transmitting biting vectors, and overall insect activity*in-situ.* Using this technique, one can be able to determine absolute OCS, wing-beat frequency and harmonics and thetemporal and spatial distribution of atmospheric fauna over a several kilometres range. Assessment ofspatialdistribution of insects on different agricultural environments and geographic land scales was done in Brunslov, Sweden using this technique, see Fig.38.The distribution curve shows the variation of insect population throughout the whole range.From an entomological point of view,this could have implications considering biodiversity in respect to topography and vegetation. From a Physics point of view, one can see that a range resolved assessment of insect distribution can be performed over a several kilometre range. A detailed result of biodiversity assessment is discussed in paperIV related to the absolute OCS detection limit. In this case, the different in

air volume monitored and the detection limit at different range has to be compensated for when comparing between different ranges.

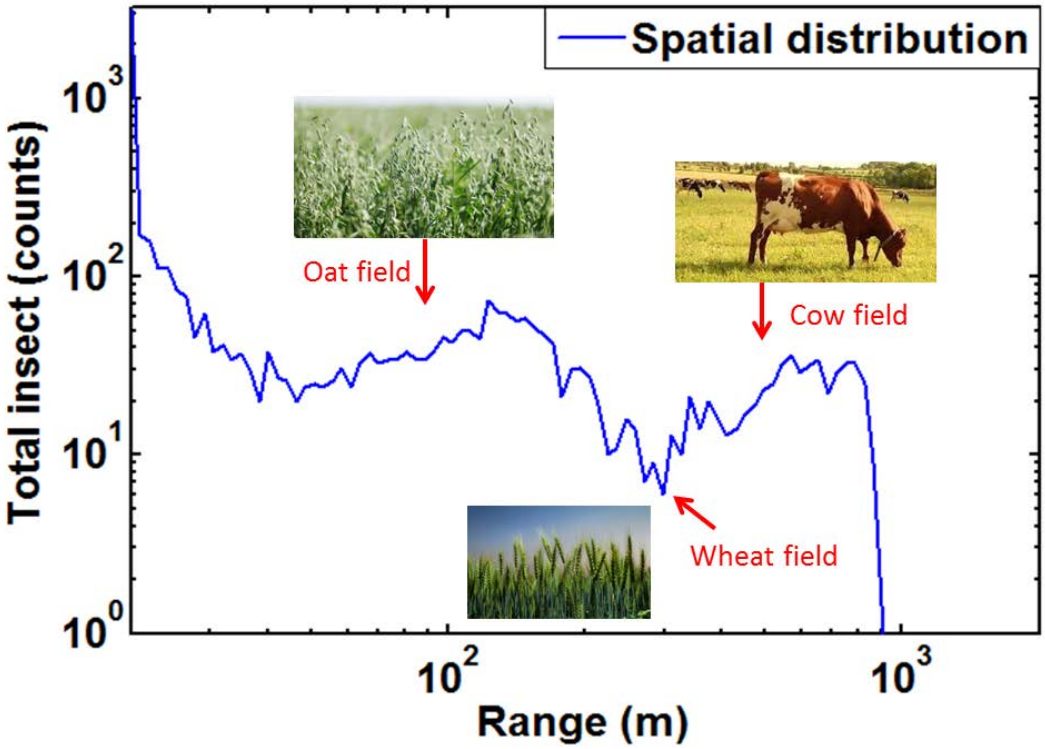

***Figure 38**: Spatial distribution of insects over a km landscape scale in Brunslov, Sweden. The number of insects increases around 128 meters and drops off around 300m and then increases around 655m. Those regions are where the oat farm, wheat farm, and cow field are situated respectively. This experiment was done during night (00:30 to 04:30am local time).The variation in the number of insect over different agricultural landscapes show the preference of insect to a certain plant species or type of animal, which could be of interest to entomologists.*

The range resolution of this technique is constrained by the diffraction limit [179] of the receiver and the beam width, but we have recently shown that range resolution beyond the diffraction limit can be achieved because of the sparse nature of atmospheric fauna. In this case, we consider insects as blinking particles. This technique is related to the concept of stochastic optical reconstruction microscopy (STORM)[180-182], where sparsely dye molecule switching between dark and fluorescing states are imaged over time to be able to narrow the point spread function beyond the limit Abbe's criterion would allow[183,184]. It is also similar to some other super resolution microscopy technique called photo activation localization microscopy (PALM) [185-187]. In our context, we exploited this concept of STORM, where sparse insects behaving like blinking particles are imaged over time by implementing a kHz sampling frequency. In paper II, we have shown that the angular resolution can exceed the diffraction limit in a situation where sparsely distributed blinking particles appear.

In addition to spatial distribution, one can monitor the temporal distribution of insects during a period of time. This helps to get a complete picture of the activities of insects in time and

space. Temporal distribution of the spatial distribution of the insect shown in Fig.38 was also analysed to evaluate the dynamics in time. From the temporal distribution histogram, one can see that the lowest total insect count is found around 03:30am local time, see Fig.39. The two figures (Fig.38 and Fig.39) are examples of the capability of the technique to retrieve temporal and spatial distribution information of insects over a km range.

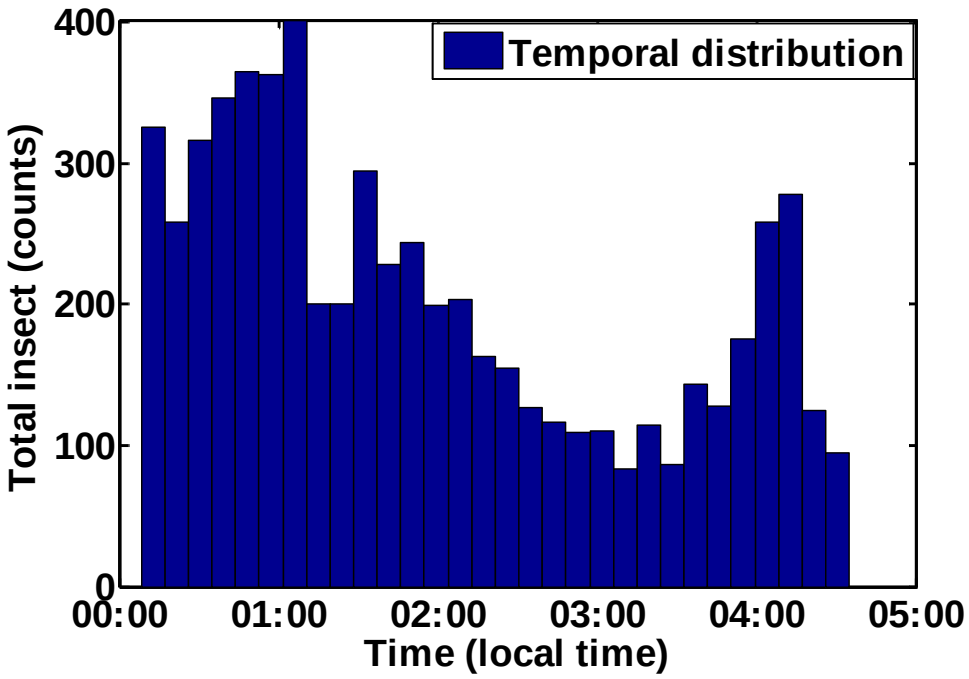

Figure 39: *Temporal distribution of insects during night time, in Brunslov, Sweden. This experiment was done for 4 hours in total (00:30 -04:30, local time). The numbers of insect increases around 1am local time. This could be when night time insectsstart to appear. The population drops around 3am and then increases around 4am. This could be because of the night time insect started to disappear and day time insect started to populate respectively.*

Chapter IV

4. Calibration

4.1 Range calibration- CW-LIDAR

Range calibration is one of the most important aspects of the active remote sensing experiment. Itallows us to determine the exact position of atmospheric fauna in space. From an entomological point view it is important to know which insect species prefers a certain agricultural landscapeor which parasite affects livestock orhumans. There are different ways in whichone can calibrate the CW-LIDAR. In this dissertation, the range calibration was done by calculating the angular position of each pixel footprint. The thin lens equation was used to determine the distance between the CCD termination pixel and the lens. This involves object distance (S_0), image distance (S_i) and Focal length (f), see Eq. 4.1.

$$\frac{1}{S_o} + \frac{1}{S_i} = \frac{1}{F} \quad \text{..... (4.1)}$$

In this context,the object distance is the distance to the termination position (termination range) and image distance refers to the distance between the termination pixel and lens.The angular position of each pixel footprint will then be determined from a known distance to a remote target and this enables to back calculate the range. Generally, we implemented a trigonometric back calculation from the known distance to the termination, pixel size and the separation of the transmitter and receiver systems to determine the position of each pixel footprint in space. The detail of the range calibration is discussed in[44,188]. A simplified expression of the range calibration is given by the product of separation distance and the tangent of the angle of pixel footprint, see Eq.4.2.

$$Range(r) = D_{Sep} \times tan(90^0 - \theta\_Pixel\ ) \quad (4.2)$$

Where D_{Sep} is separation distance between the transmitter and the receiver telescopes. The angles of each pixel footprint (θ_{Pixel}) iscalculated from theCCD tilt (β), focal length of the receiving telescope, termination range and pixel pitch, see Eq.4.3.

$$\theta_{Pixel} = \alpha + tan(\gamma) \quad (4.3)$$

Where: γ is the relative angular tilt of each pixel and α is the angle between the laser beam and receiver optical axis.The above equations allow us to image different range on to different positions of the detector array. It is important to achieve an overlap between the pixel footprints of the line scan camera and the laser beam. Ideally, the pixel footprint has to be in a perfect overlap with the laser beam. This is to make sure that the pixel footprints in space are aligned with the laser beam. This means that the detector will be in focus for the whole range of distance while the resolution varies with range, see Fig.40. The range scale in this case is not linear due to the nature of the Scheimpflug method [44]. The pixel footprints close to the receiver closer to each other than those pixels looking farther in the distance.

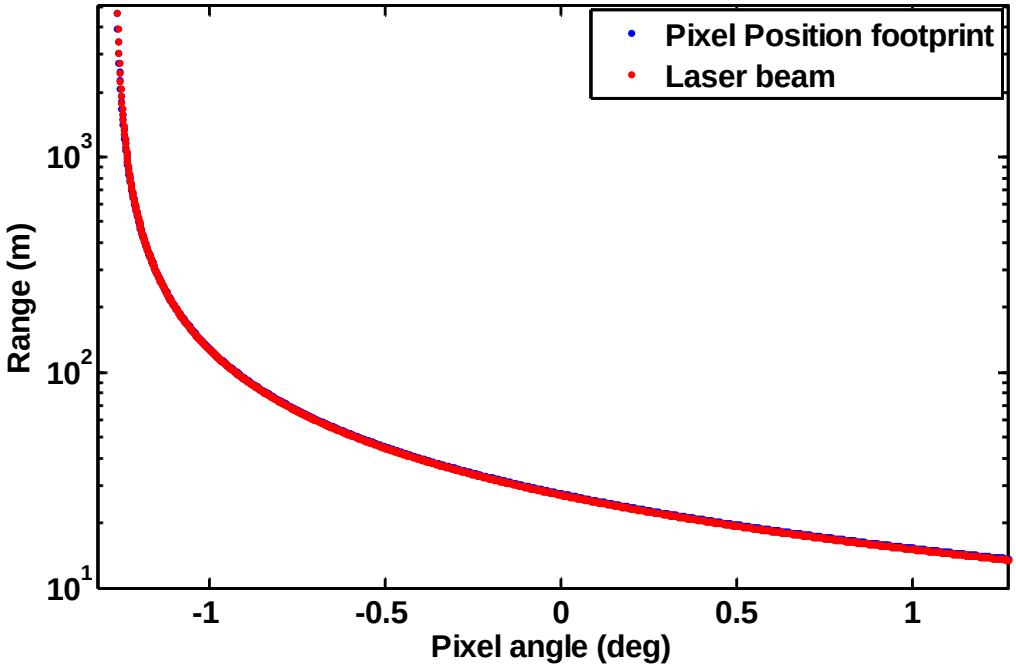

Figure 40: *Analytical description of focus range versus observed angle. Ideally, the pixel footprints (blue) perfectly overlap on top of the beam (red). The non-linear range scale is due to the nature of the Scheimpflug method.*

4.2 OCS calibration

4.2.1 OCS Calibration from termination reflectance – CW-LIDAR

Calibration of OCS in the CW-LIDAR experiment can be done in different ways, such as from the termination reflectance or using white diffuse sphere with 100% reflectance. In our laser radar experiment, we used the termination reflectance to calibrate the absolute OCS. The procedure we implemented in this case is as follows: First we calculated the optical OCS of the termination echo from the known parameters of interest: receiver telescope field FOV at termination (area of the termination echo) and termination reflectance.Termination OCS is basically the product of the illuminated area and reflectance, see Eq.4.4. The beam is elliptical shape at termination.

$$OCS_{term} = (W_{tb} \times H_{tb}) \times R_{term} \quad \text{(4.4)}$$

- W_{tb}: Beam width at termination
- H_{tb}: Beam height at termination
- R_{term}: Scattering from atmospheric fauna.

From the OCS at termination, sensitivity is extrapolated back to words the LIDAR using the static molecular return with homogenous atmosphere assumption. This enablesoneto determine OCS of atmospheric fauna from the known termination OCS value. Ideally, the intensity difference between the termination reflectance with and without an insect event crossing the FOV could give the OCS of the insect, but the fact that the reflectance from the termination may not be stableenough; due to the dynamic atmospheric conditionsintroduce uncertainties. Due to this reason, this analysis is based on termination reflectance and we implement aform factor to recalibrate the echo intensity into an optical cross-section with a standard unit (Example: mm^2, cm^2 etc.). The form factor is a range dependent function, which describes the relation between signal intensity and range in a LIDAR experiment, see Fig.41. This is a fundamental function in the remote sensing field, which relate the received photon count to a distance. It can also be considered as an overlap function between the laser beam and telescope FOV. The determining factor of geometric form factor is the distance at which the initial overlap between the laser beam and telescope FOV begin, to the point at which the overlap is considered to be complete. There are different ways to experimentally measure the form factor: inserting a known OCS object at different positions in the field of view and the detection of nitrogen Raman signal and by measuring water vapour and aerosols in the earth's atmosphere [189]. It can also be described analytically using Eq.4.5[190,191].

$$\boldsymbol{I(r) = \frac{I_0\left(1+tanh\left(\frac{r-r_0}{R}\right)\right)}{r^2}} \quad \text{(4.5)}$$

Where:$\boldsymbol{I_0, r, r_0,}$ and $\boldsymbol{R}$ are constant signal, distance from the LIDAR location, overlap area and an intermediate point of the overlap region respectively.

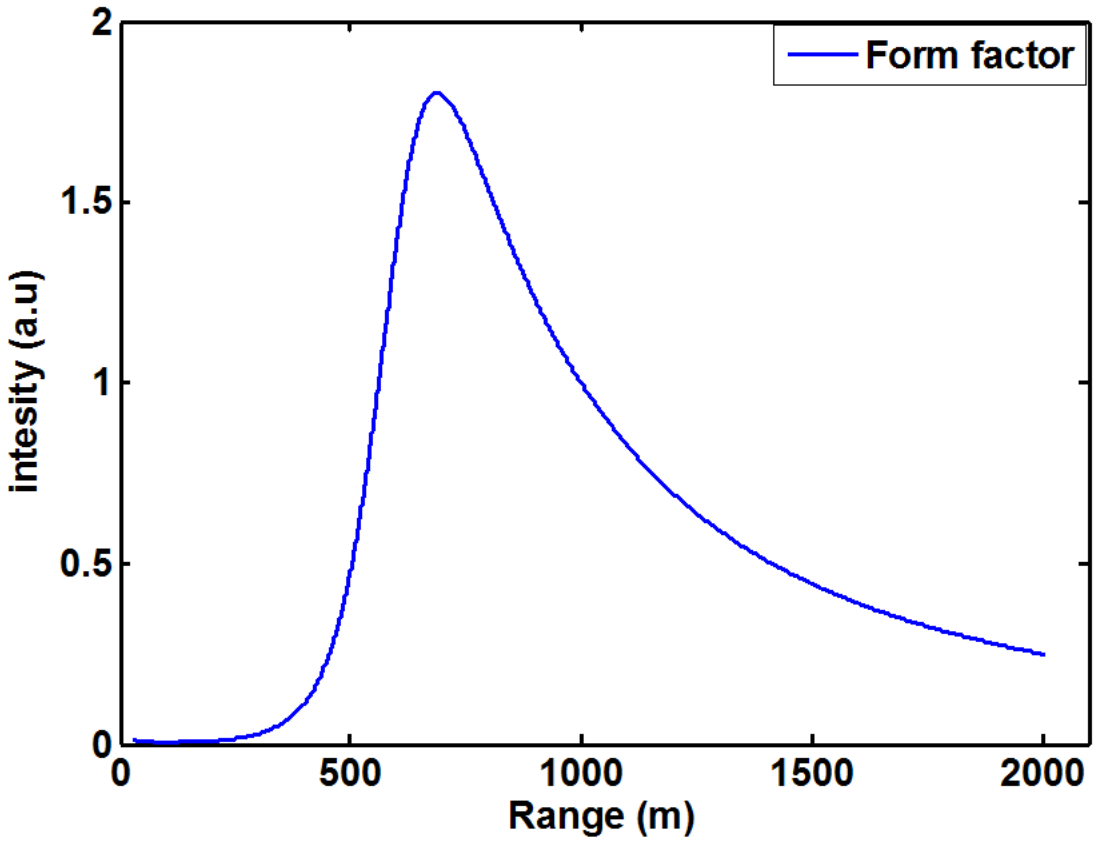

Figure 41:*Numerical estimate of Geometric form factor for Newtonian telescopeover 2km range.*

Based on the numerical estimate, we can see that the intensity of each event depends on the range where the event is detected, which highlights the importance of introducing the form factor. In this work, the form factor was rescaled through the known OCS, σ_{term}, for the termination; see Eq.4.6[55].The OCS calibration can be verifiedby relating the value to the apparent size and estimating the reflectance of atmospheric fauna at 808nm wavelength [55].

$$\boldsymbol{\sigma_{event}} = \frac{\boldsymbol{\sigma_{term} r^2_{event} \left(I_{event(r)} - I_{static(r)}\right)}}{\boldsymbol{r^2_{term} I_{static(r)}}} \quad \text{(4.6)}$$

- $\boldsymbol{\sigma_{event}}$: OCS of the event.
- $\boldsymbol{\sigma_{term}}$: OCS of termination echo.
- $\boldsymbol{I_{event(r)}}$: scattering from atmospheric fauna.
- $\boldsymbol{I_{static(r)}}$: scattering from pure air.
- $\boldsymbol{r^2_{event}}$: Distance where the insect event is detected.
- $\boldsymbol{r^2_{term}}$:Distance where the laser is terminated on.

The LIDAR experiment generates range-time files. Each file covers 5s time window inboth the LUMBO and Stellenbosch LIDAR experiment setup, see Fig 42. In the experiment shown in Fig.42, we ran the system for about 4:00 hours (00:30 to 04:30am). Every range-time file contains various event parameters such as OCS, velocity and wing-beat frequency. The parametrization algorithm enables us to subtract the background and calibrate the arbitrary intensity of a back scattered event signal into OCS (mm^2, cm^2) using the reflectance from the termination.

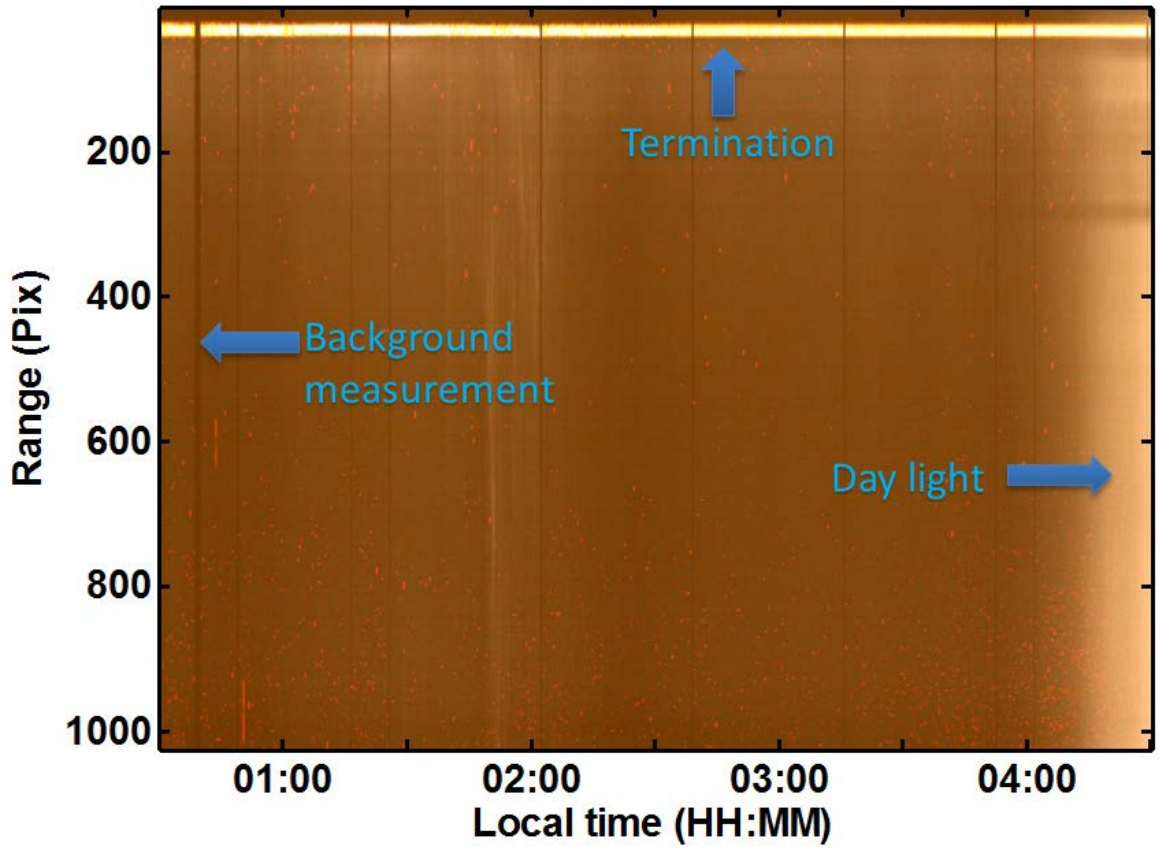

***Figure 42**: Panoramic false colour composition range-time map. During the four hours measurement from mid night until about 4:30am in the morning we detected more than 6000 events (red dots in the range-time map. Every line comprises 10^4LIDAR samples. The black lines are background data when the laser is switched off torecord a 5 second background. This Range-time map is produced from 40 million LIDAR sample during the whole experiment.*

NEO LIDAR experimental setup was also usedin Brunslov, Sweden. Every range-time map in this experiment coversa 10s time window. A synchronization signal from the camera in this setup alternates the laser between dark and bright state to subtract the radiation from the sun and pixel specific dark current dynamically. This is done by subtracting between add and even exposure. After interpolating and subtracting the background the effective sampling rate in this case becomes half of the total.This setup canbe used for day time experiment. The panoramic false colour composition of 24 hours of measurement gives the general picture of the insect activities on 17 July, 2014, see Fig.43. The effective sampling rate of this setup is 100Hz, which makes it difficultto resolve wing-beat frequencyof high wing-beat frequency insects considering the Nyquistcriterion [192,193]. It is slow as compared to the LUMBO and Stellenbosch LIDAR setups, where the sampling rate is in the order of kHz. However, this setup has the advantage in terms of sensitivity since the camera has bigger pixels (8x200µm)compared to the other two setups where the pixel size is smaller (14x14µm).

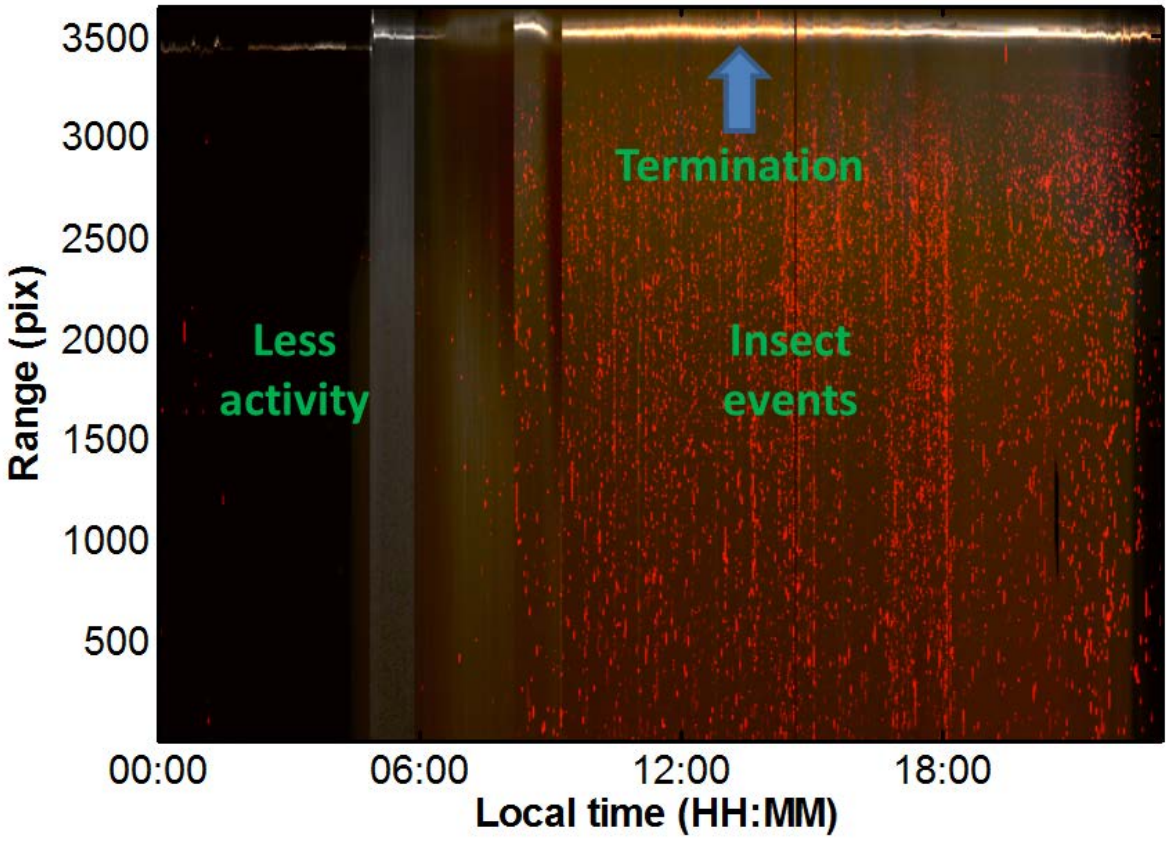

Figure 43:*Panoramic false colour composition range-time map. This is a 24hours measurement on 17 July, 2014. Around 1600 events/hour m^3 was detected.The high intensity static line around 3500 pixel comes from the termination of the laser beam. The red dots are scattering from atmospheric fauna. The detector is operated at 200Hz, but the effective sampling rate is 100Hz since the camera captures background every second acquisition. The activity of insect is minimal during the time between 00:00 to 06:00am. The number of insect dramatically increases starting from 06:00am until about around 11:00pm.*

The range-time map generated from the LIDAR data enables us to make three statistical measurements (minimum intensity (blue curve), median intensity (green curve) and maximum intensity (red curve)), see Fig 44. The median intensity is the static intensity with the background subtracted.The background data is generated from the data set where the laser was turned off. In our first LIDAR experiments, the laser was turned off every 10minutes in order to get a single 5s background file as discussed earlier. The interpolation between those files gives the background file for every file. Now, the setup isimproved in such a way thata synchronization signal from the camera alternates the laser between dark and bright state to subtract the radiation from the sun and pixel specific dark current dynamically [55]. This enables us to use the LIDAR system during day and night time and there will be no need to do post-processing of background subtraction in this case. The difference between the minimum and the static curve gives the noise level. The reason why the median was chosen to define the static signal is because it is insensitive to outlier, which in thiscase means insect event.This can be seen in Fig. 44, where the insect event is manifested in the maximum intensity, but not in the median and minimum intensity.

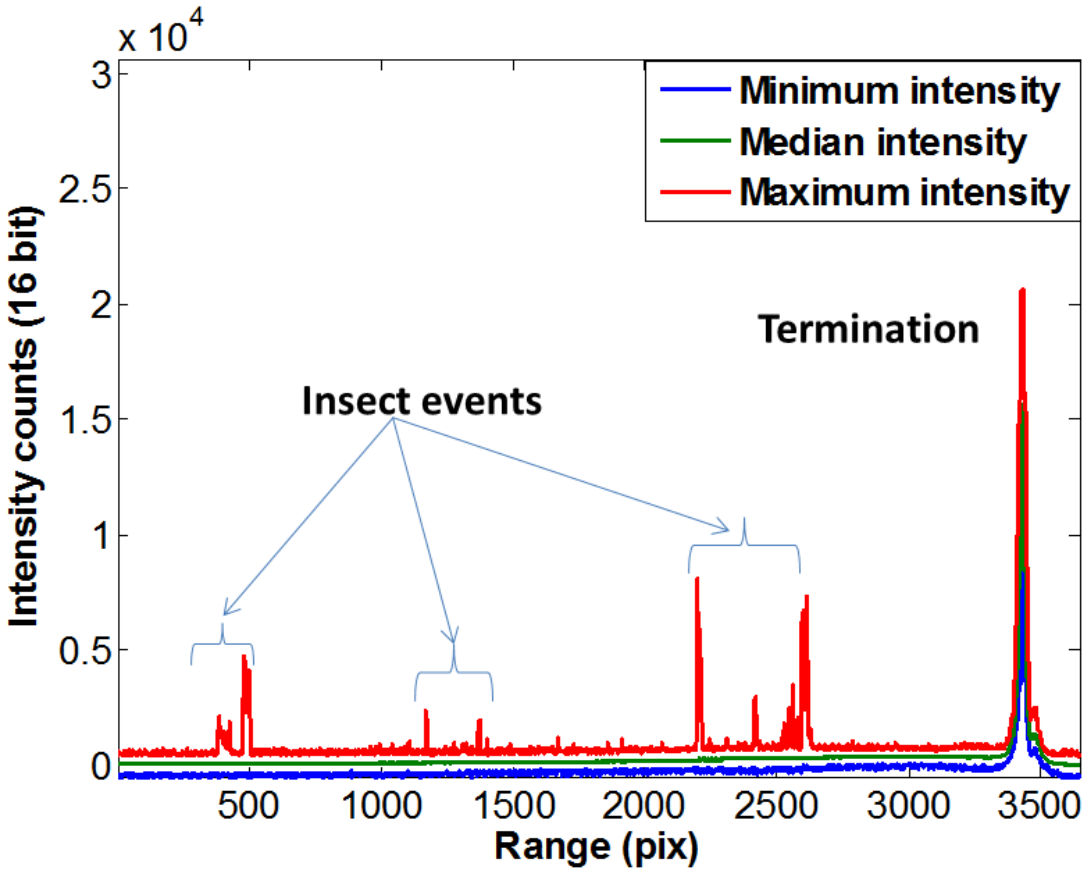

***Figure 44**: Intensity (count) versus range (pix).Temporal minimum, median and maximum intensity distribution. The strong peak around 3500pix is the termination echo. The smaller and sharp peaks around 500pix, between 1000-1500pix, and around 2500 are all insect events. The insect event manifested itself in the maximum intensity, but not in the median since median is insensitive to outliers (atmospheric fauna in our case).*

In the process of insect identification, it is important to set a threshold in order to distinguish event from static intensity. In principle, a certain intensity level can be considered as an event if it is one noise level greater than the static signal, but this introduces some uncertainty. To minimize uncertainties, the threshold was set to be twice the noise level, which mean that the signal-to-noise ratio is two (SNR=2).A histogram of an example event showinghow we set the threshold is given inFig.45. In a situation where there is no insect event, the histogram will show a symmetric distribution since noise behaves like a normal distribution. The width of the symmetric intensity distribution determines the system noise. However, the histogram will be skewed towards the higher intensities if insect event exist, which confirms that event signals aren't evenly distributed like noise[194]. This is exactly what happens in Fig.45.

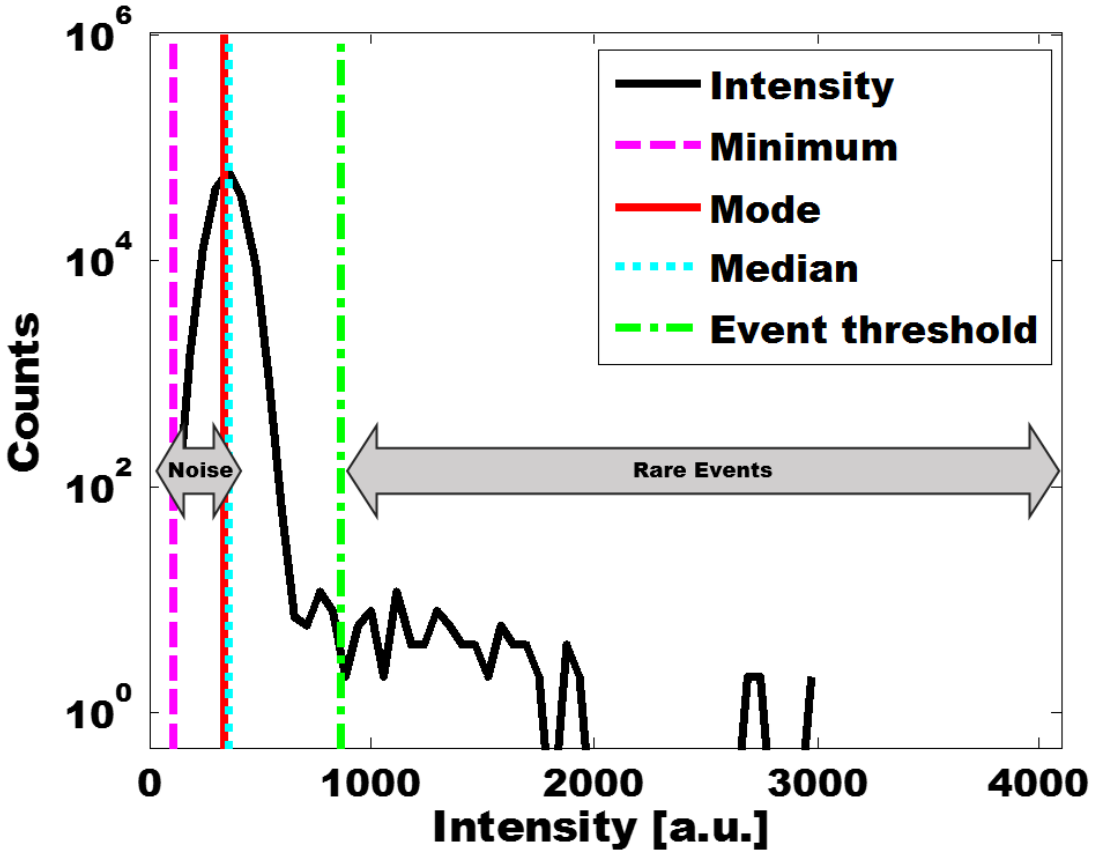

Figure 45: *Histogram of the intensity distribution for rare events. The pink line indicates the minimum intensity, the blue line indicates the median intensity and the green line is event threshold, which is twice the noise limit. The noise is evenly distributed around the median value at that range. The region above 10^3a.u intensity is where we expect rare events. Adopted from [194].*

4.2.2 OCS Calibration using white diffuse sphere –dark field spectroscopy

Calibration of OCS is done using white diffuse spheres in the dark field spectroscopyexperiment. This was implemented by dropping white diffuse sphere in front of the dark termination boxclose to the object plane, where the spheres are infocus. The detector dark current and static atmospheric contribution is subtracted first and then the absolute OCS was calibrated using diffuse white spheres. The sphere is assumed to have 100% lambertian reflectance.The backscattered signal strength from the sphere is differentin the three bands (VIS, NIR and SWIR), see Fig.46. This has to do with the sensitivity of each detector in the different wavelength ranges and the calibration hasbeen done accordingly.

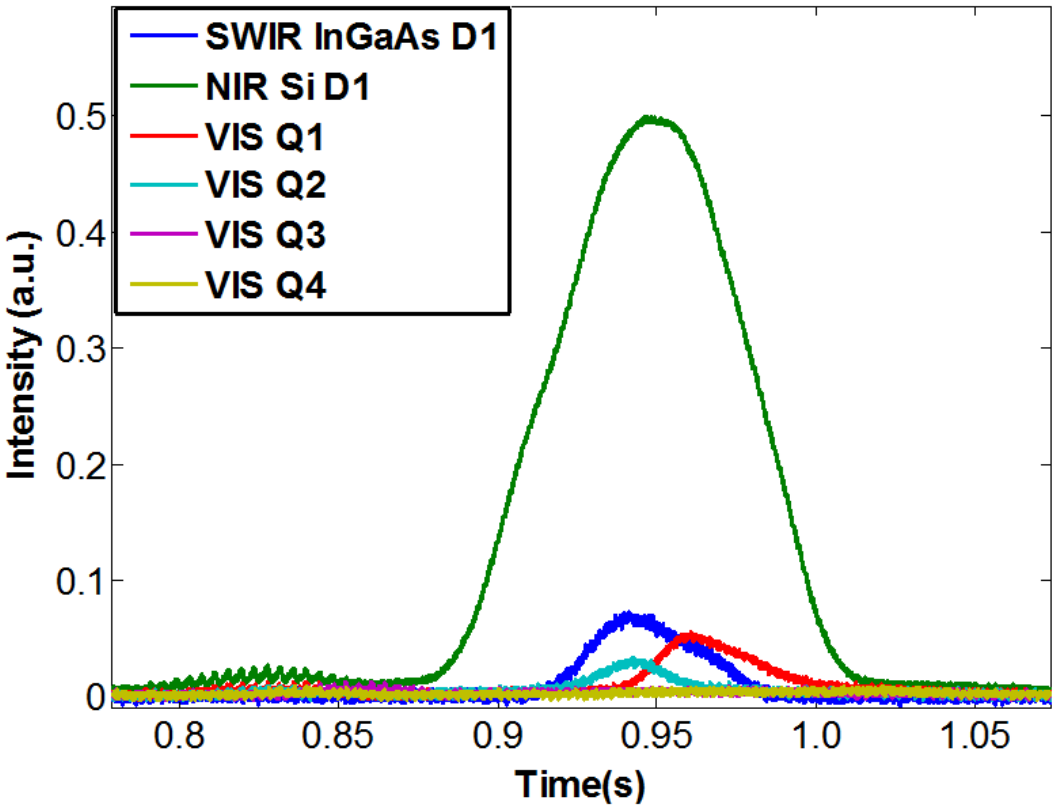

***Figure 46**: Signal from white diffuse sphere in three bands (VIS, NIR and SWIR). The three bands were calibrated according to the strength of the signal. The NIR and SWIR signal comes from single integrated sensors, where the Si sensor is on top of the InGaAs sensor, see Fig.24. The visible signals (VIS Q_1, VIS Q_2,VIS Q_3,and VIS Q_4) are from the quadrant detector.*

If the sphere was in focus, the signal would have been sharp with a flattop. Assuming a sphere event in focus, we can calculate its full width at half maximum (FWHM). The ratio of the integrated sphere event and its FWHM gives us equivalent strength of the sharp sphere event in volts. The intensity in (volts) of a sharp sphere event (rectangular height) together with the known projected area of the sphere is used as calibration factor from volt to cm^2.We implement this to describe the size of each sphere (diameters 25mm, 18mm, and 12mm) in different bands,

which was originally in volts in to square centimetres, see Fig.47. We define OCS as the product of surface area and reflectance of the sphere, see Eq.4.7.

$$OCS = \pi r^2 R \quad \text{(4.7)}$$

- $\boldsymbol{\pi r^2}$- surface area of the sphere
- $\boldsymbol{R}$-reflectance of the sphere

The calibration result was used to estimate the sizes of different insects. Because of the range dependent sensitivity of the form factor, the absolute OCS calculation using this technique is only accurate close to the object plane were the calibration and controlled release was made.

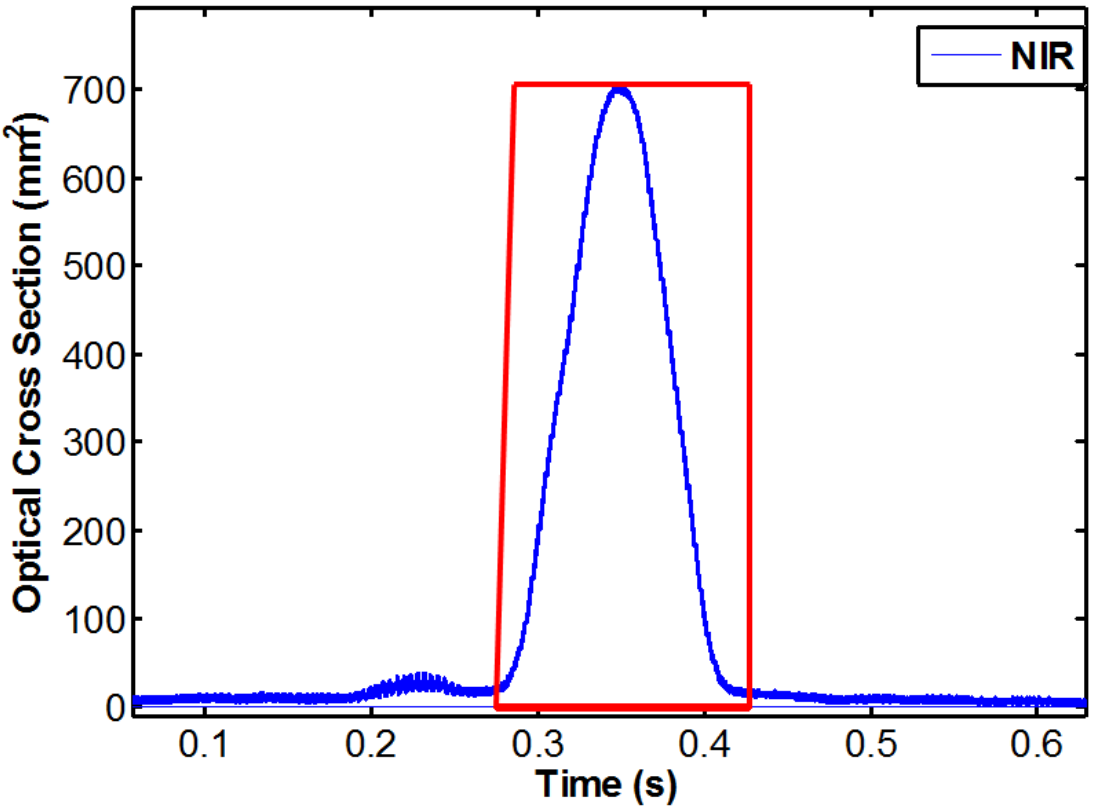

Figure 47:*Signal from white diffuse spherein the NIR range (blue). If the sphere was in focus, it would have been sharp with a flat top (red box).*

4.3 Flight direction – dark field spectroscopy

Insect are symmetrical especially in the SWIR and one can use quadrant detectors to break symmetry. Flight direction of insects can be determined using a quadrant photodiode. This Photodiode has four equally divided sections with the same quantum efficiency. A pendulum with known oscillation direction was used to determine the orientation of the quadrant and also to quantify the amount of light impinging during the day while we do long term recordings to estimate the amount of radiation from the sun. This can be used to determine insect flight direction. This calibration was done by oscillating the pendulum through the FOV from East to West or vice versa for about 10s every 30minutes throughout the measurement session. The backscattered signal from the pendulum is a periodicsignal, see Fig 48.

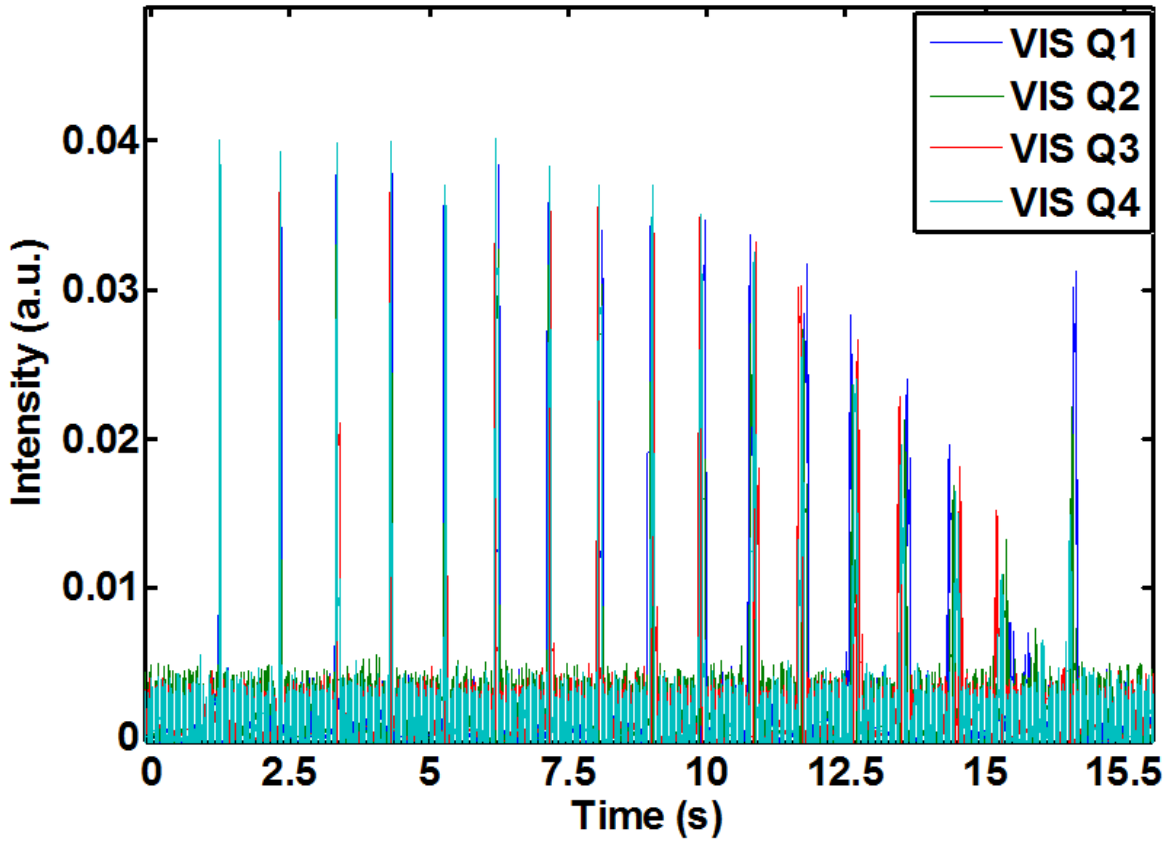

***Figure 48*:** *Scattering from pendulum measurement. The periodic pattern of the signal shows that the pendulum was sweeping West-East in the FOV for about 12seconds. VIS Q_1, VIS Q_2 , VIS Q_3, and VIS Q_4show the different section of the quadrant detector.*

A closer look to the signal of a half period of the oscillation shows the sequence where the pendulum enters each section of the quadrant, see Fig. 49. Knowing the initial position of the pendulum, we can determine the orientation of the quadrant, which leads us to determine the flight direction of insect events. In this specific example, the pendulum was released from West to East in the FOV. From the temporal sequence of the quadrant signal, we can see that the pendulum first enters Q_1 (West) and exists at Q_3 (East). The most likely orientation of the quadrantis shown in Fig.50. This result is from a specific experiment in Stellenbosch. One could also choose to release the pendulum West-East as far as the dark termination cavity faces the sun or the sun is behind the receiving telescope in order to get backscattering signal. This will improve the signal strength as compare to front scattering when the receiver faces the sun. In general, the receiving telescope was setto look southwards in Stellenbosch (Southern hemisphere) and towards the north in Sweden (Northern hemisphere), which enabled us to collect a backscattered signal.

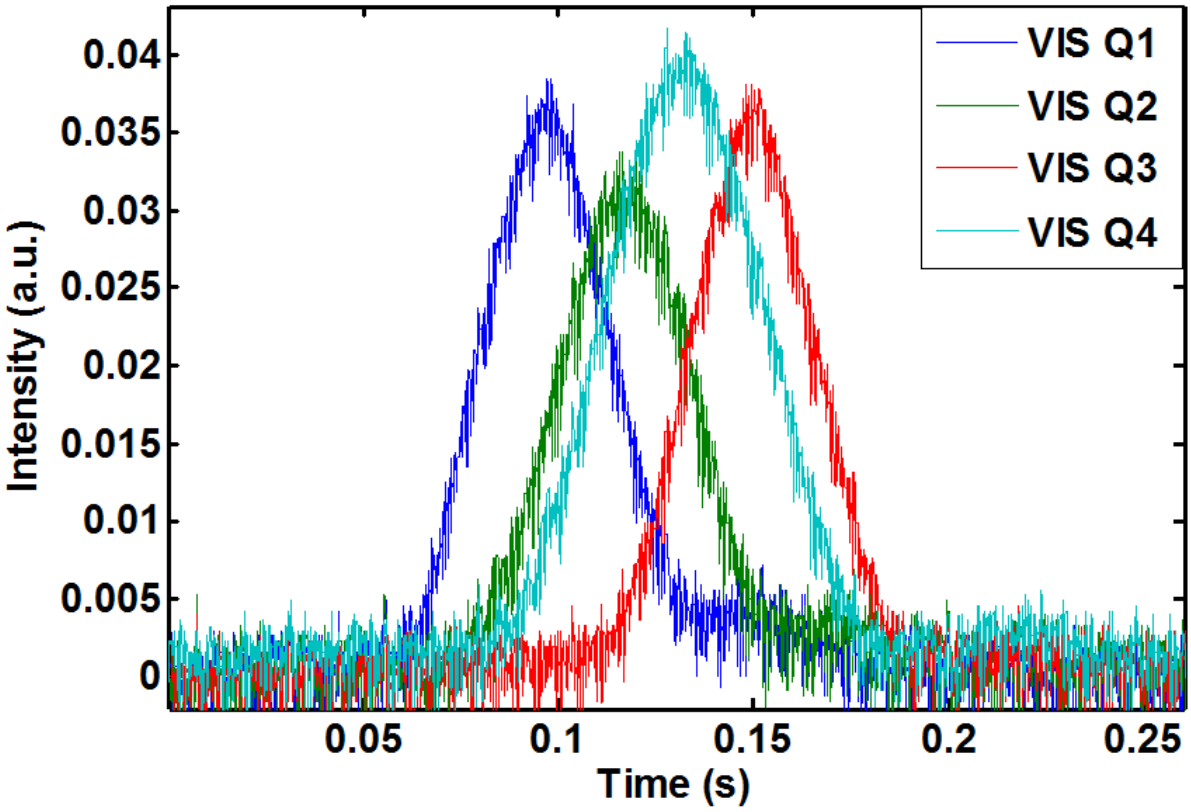

Figure 49: *Zoomed temporal sequence ofthe pendulum signal for a half oscillation. Signal recorded by the Si quadrants (Q1, Q2, Q3, and Q4) from pendulum oscillation (east to west). The time sequence of the signal shows that the pendulum first enters Q1 (East) and exists at Q3 (West). The quadrant orientation suggestion in this case is: Q1-East, Q2-Down, Q3- West, and Q4-Up relative to each other.*

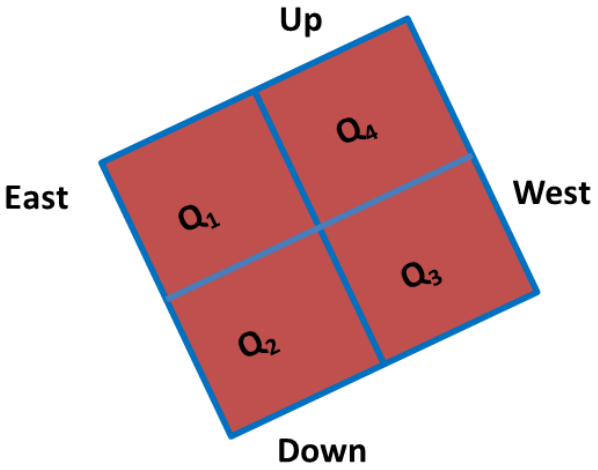

***Figure 50**: Quadrant orientation based on the signal in Fig.31.*

An Example of an insect event recorded in Brunslov, Swedenwhen the insect happens to fly from east-west in the same direction as the wind is shown in Fig.51. In this experiment the pendulum was oscillating from west-east, which is in the same direction as the direction of the wind.

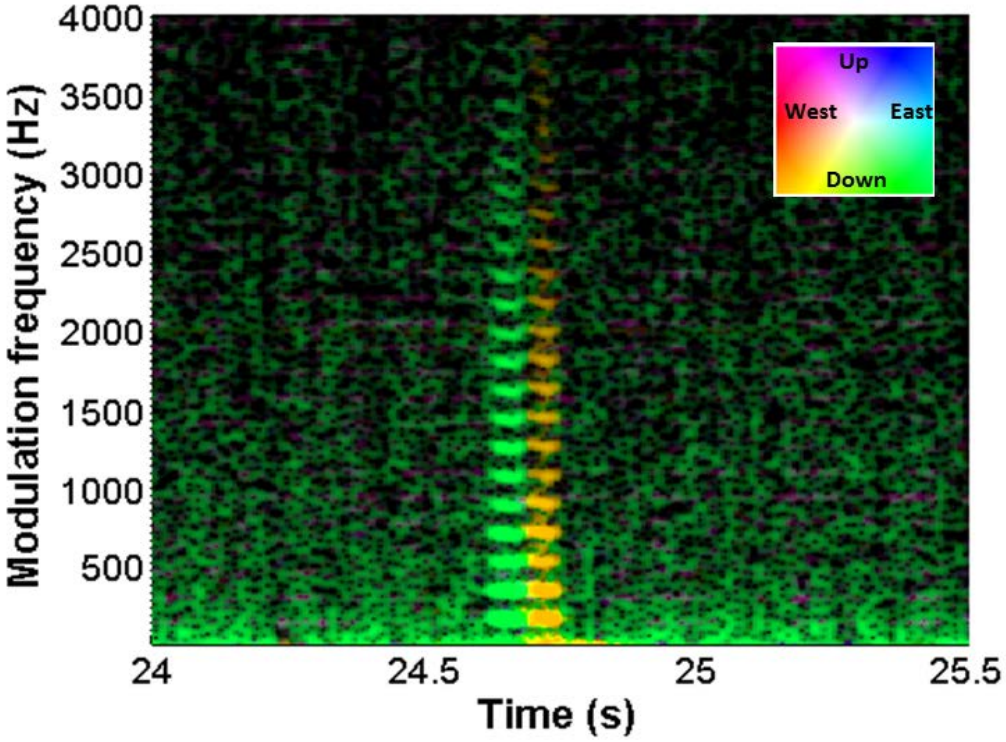

***Figure 51:**Flight direction of the same insect event from the quadrant detector. The insect at 24.7s flies from East (E) to West (W) similar to the direction of the wind. The speed and direction of the wind during the day was between 2.4-3.2ms^{-1}west.*

4.4 Spectral information – dark field spectroscopy

Calibration of the spectral information retrieved by the spectrometer is done in a similar way asfor the Si and InGaAs sensors (Section 4.2.2). We have used white diffuse sphere to estimate the amount of sun light impinging into the FOV. The white sphere was released in front of the dark termination cavity whereit is in focus (close to the object plane). By retrieving the spectra during the time when the sphere was in the FOV, one can see the reflection from the sphere, see Fig.52. At this stage the spectra has arbitrary intensity value.

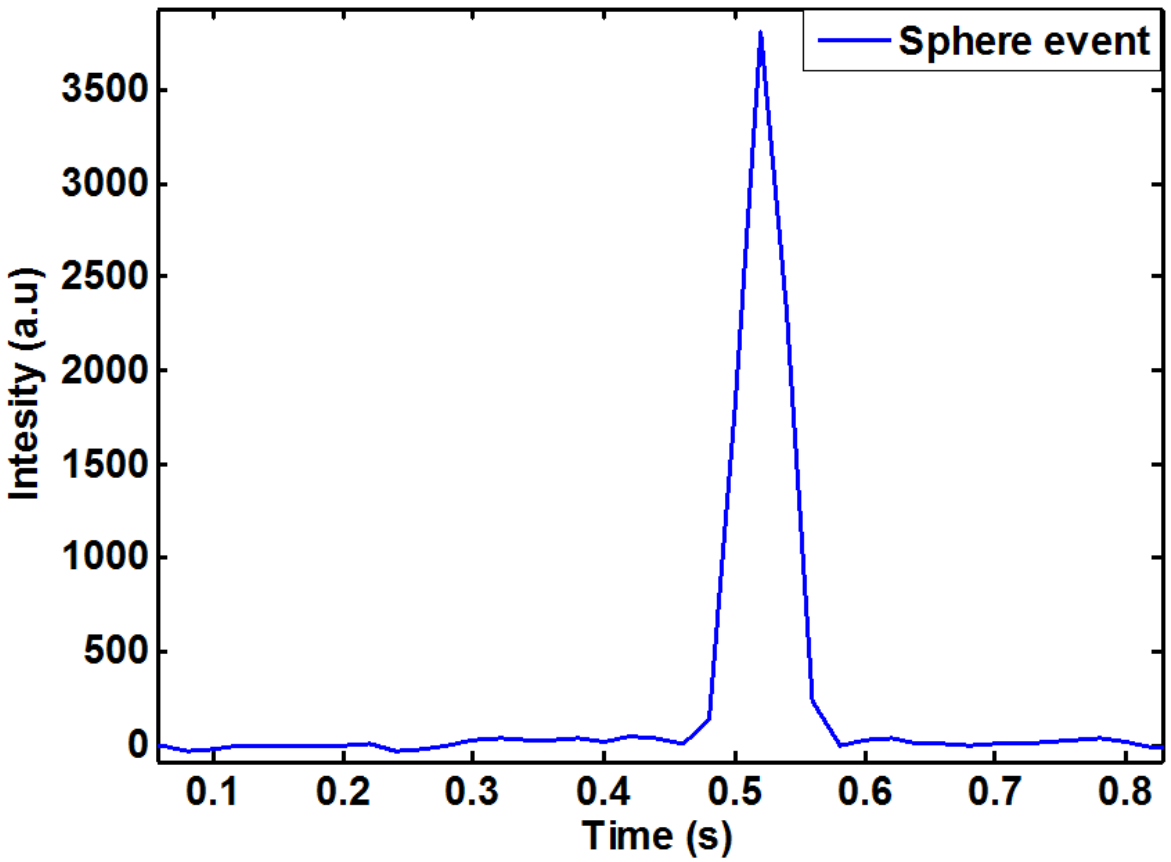

Figure 52: *Reflectance from sphere eventaround 0.5s and arbitrary intensity value.The sphere is ø12mm andassumed 100% reflectance.*

The next step will then be to convert the arbitrary intensity into OCS in units of square millimetre. In this specific example, we used a **ø24mm** sphere to calculate the amount of signal per square millimetre and the area of sphere is 452mm^2. Assuming the sphere has 100% reflectance and applying Eq. 4.7, the OCS of sphere will be 452mm^2. Finally, we can plot the spectrum of the sun, which is reflected by thewhite diffuse sphere, see Fig.53. Once we have the spectrum from the sun reflected from the sphere of known area, we can now use this spectrum to determine the OCS of insect events of arbitrary intensity. The signal from an insect is much sharper spike compared to the signal from sphere, which shows a slow increase, see Fig.54.

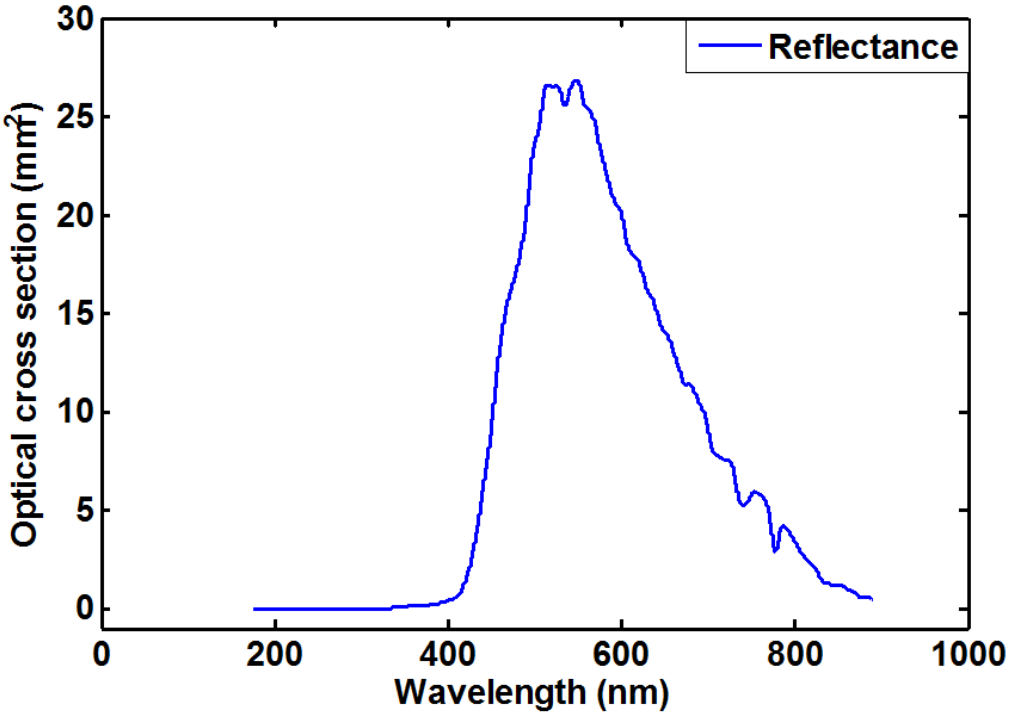

Figure 53: *Spectrum reflected by a white sphere.We use this spectrum to determine the size of an insect.*

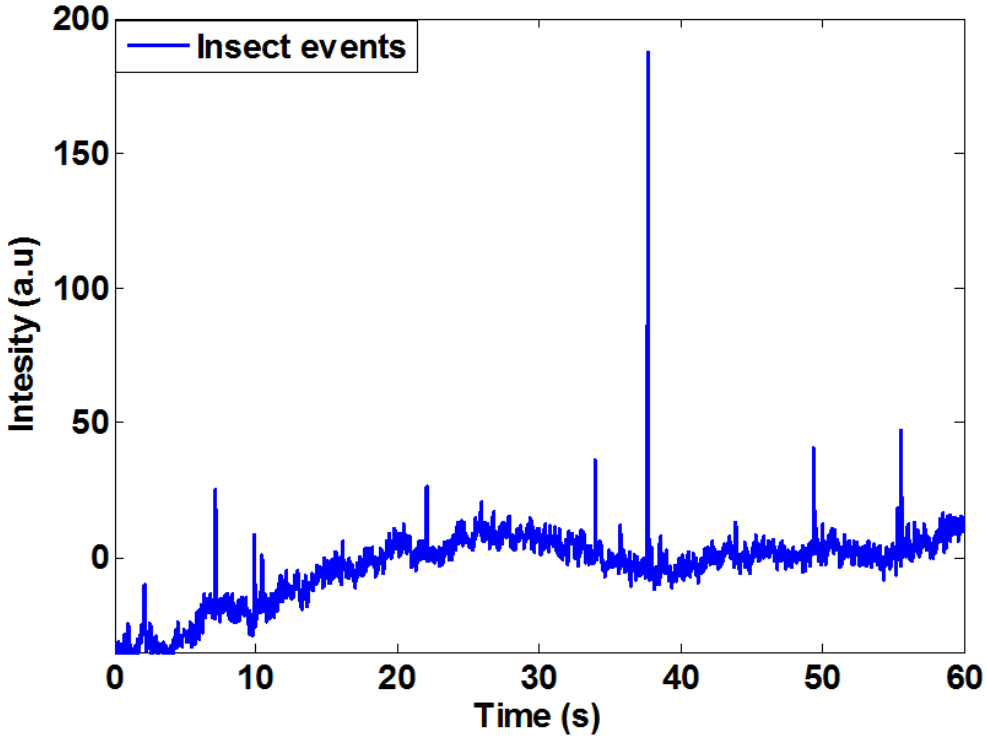

Figure 54: *Insect events recorded by a spectrometer. The sampling frequency in this case is 50Hz, which is too slow to resolve wing-beat information, butcolour information can be obtained as can be seen in Fig.32 (green powder marked dragonfly)*

Chapter V

5. Result and Computational methods

5.1 Intensity calibration

Intensity calibration was done in this dissertation to determine the size of insects. The general trend of intensity calibration is to subtract the background signal (dark reference) from the event intensity and white reference. The ratio of both terms would then give a calibrated intensity value, see Eq, 5.1. This could be in units of cm^2 or mm^2, which is realistic size for insects inour context. The procedure of OCS calibration is discussed in chapter IV.

$$R = \frac{I_0 - I_{dark}}{I_{White} - I_{dark}} \quad \text{..... (5.1)}$$

where: $I_0$is the intensity recorded from the insect event, I_{dark} is intensity recorded with no light (it means when the laser is off for LIDAR experiments and during the time where no insect crosses the FOV in the dark field experiment). I_{White} is the intensity from white diffuse sphere, see Fig.55.The use of Eq. 5.1 in this case assumes detection linearity of a first order polynomial. In some cases, there is a possibility that the photon could escape from the FOV even though the commercial white spheres are certified for the visible and infrared wavelength ranges. This means that the instrument measurement geometry determines the accuracy of reflectance experiments. In reflectance experiments, the absolute value of R is determined by the spot size, numerical aperture, and angle of incidence of both illumination and detection [191]. The bright spot in such cases is due to specular reflection, which is observed at aspecific viewing angle. This means that the incoming photon remembers its original phase, polarization and propagation direction. In some applications, the specular reflection is rejected because of the fact that it creates some kind of disturbance. Rejection of specular reflection is commonin the study of surface properties or of speciesclassification [195,196]. In this experiment, the specular reflection is the reason why the higher order harmonics appears and it can also be used to estimate wing membrane thickness of insects.

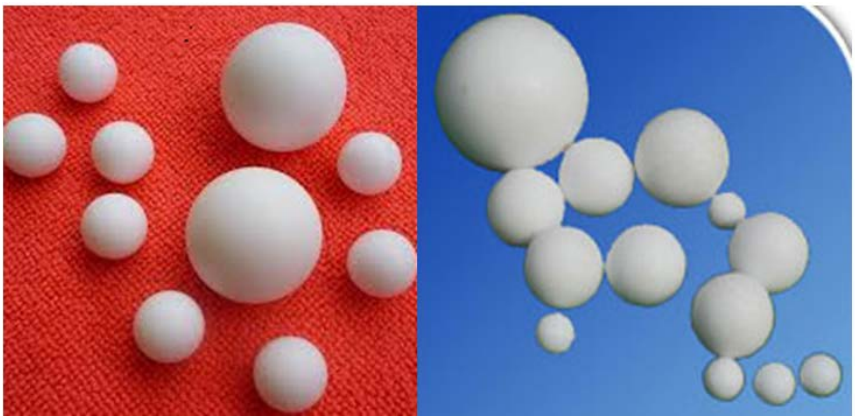

Figure 55: *Different size Teflon spheres used to collect white reference spectrum. They are certified white references for the wavelength range between 300nm to 2µm.*

5.2 Trajectory in colour space

The trajectory in colour space is mostly known as (Red-Green-Blue) RGB colour space, which is common in applications such as computer graphics [197-200]. This additive colour space has intensity on the three axis. Considering a cube of an additive RGB colour space, each corner on the space refers to specific colours: white, black, blue green, red, yellow, magenta and cyan. Those 8 different colours which are represented by the colour space are the possible colours that can be produced by mixing the three main colours (RGB). The three basic colours belongs to a specific peak wavelength (λ_{Peak}) in the visible electromagnetic spectrum (λ_{Peak}~560nm for Red, λ_{Peak}~ 530nm for green, λ_{Peak}~ 430nm for blue).Example: The colours in a certain mixed fruit image can be plotted in 3D RGB colour space, see Fig. 56. The RGB values correspond to real values of the original image. Human beings have a three band (RGB) visual system, which is similar to the colour model in computer graphics. Horses have only two bands [201-204] while birds have 4 bands [205-207].

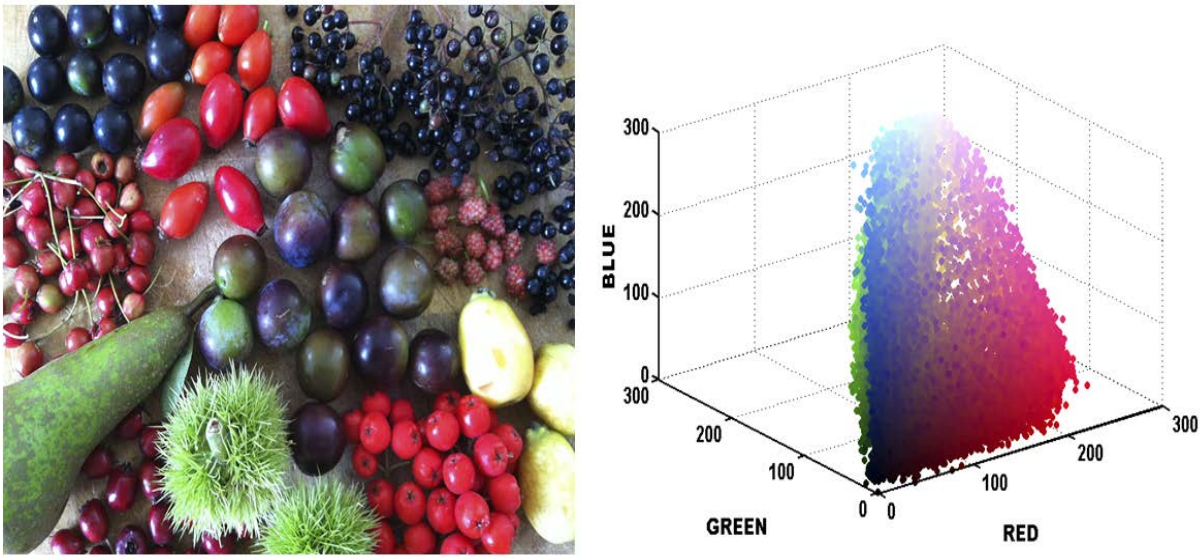

***Figure 56: Left**: real image of mixed fruits of different colours. **Right**: RGB value corresponding to real values in the left image.*

In the context of this dissertation, trajectory in colour spaceis not the same as the well-known RGB colour space discussed aboverather it is an extension of the concept. This refers tothe wave-form of a wing-beat cycle, see Fig 57. This example insect wing-beat waveform has 9 wing-beat cycles and each temporal waveform of an insect event has a different amplitude, harmonic content and phase [208]. One can exploit this specific feature of the trajectory in 2D-color plane in order to useit as indicators of insect differences, which is similar to fingerprints of human beings. The trajectories for different insect species are different because of the difference in terms of position, phase, modulation size and direction of temporal waveform, see Fig.58.

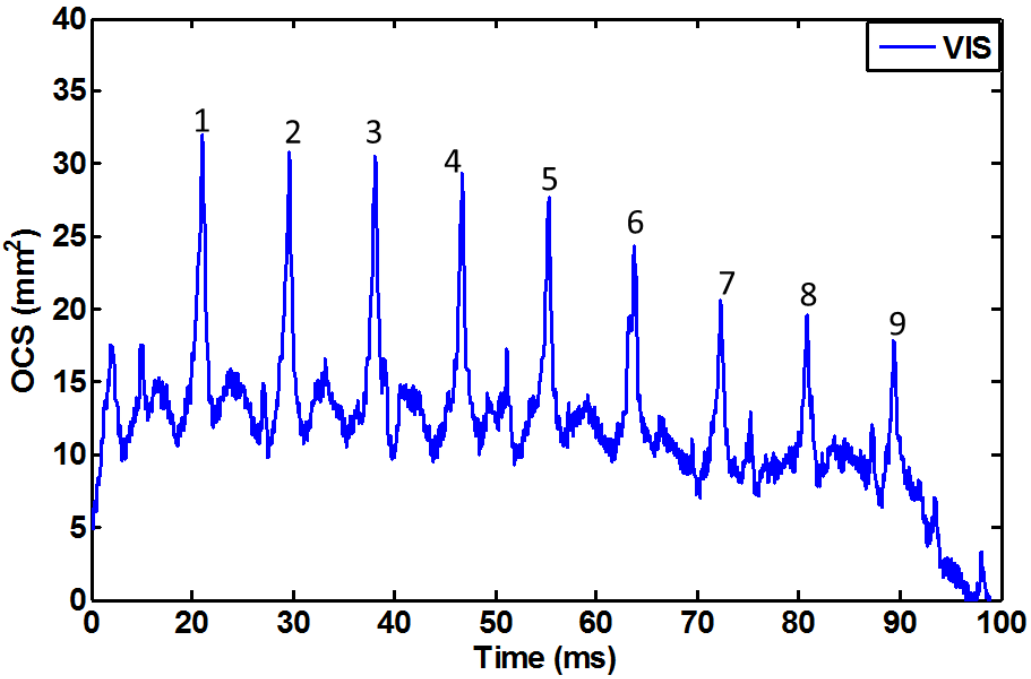

Figure 57: *Temporal waveform of insect wing-beat with 9 cycles. This wing-beat cycle has specific amplitude, harmonics content and phase.*

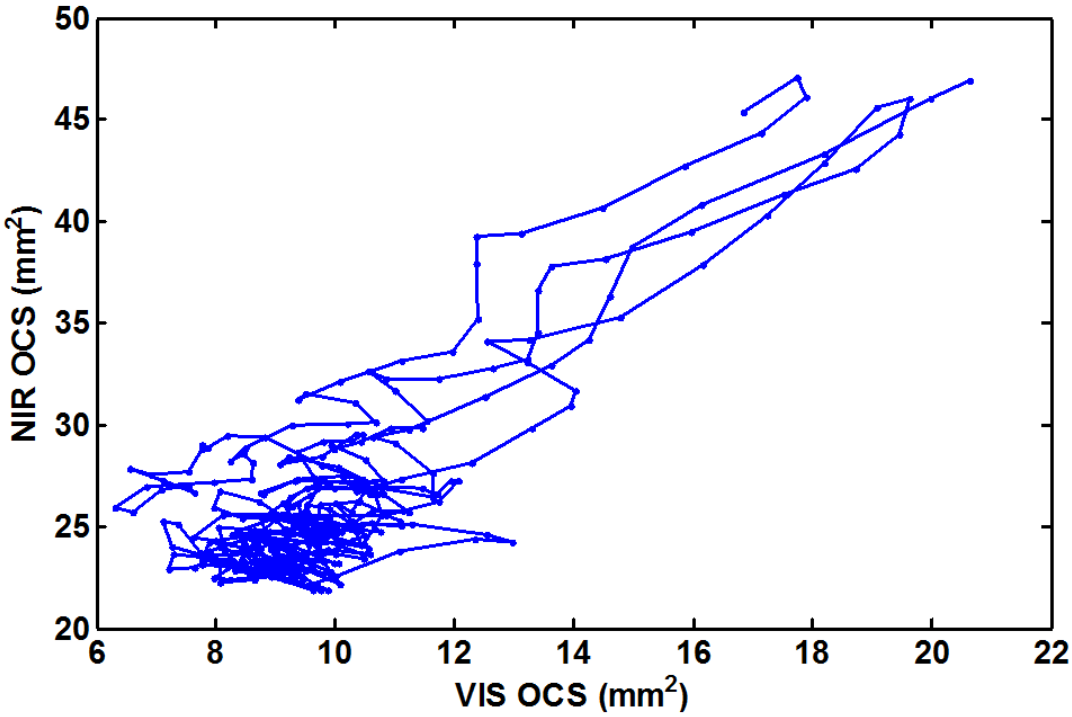

Figure 58: *Wing-beat trajectory of insect event for the last 3 wing-beat cycles (7 to 9) of the event in Fig.55. This comes from the OCS in two bands (VIS and NIR)*

In the passive remote sensing experiment, we have evaluated the significance of melanization in the VIS and omnidirectional sub-illumination in the NIR to the shape of the wing-beat waveform. It is found that these two effects could be used as a tool to see changes between insect wing and body melanization among different insect species, see Fig.59. The degree of wing-melanization is correlated to the slope of the trajectory in colour plane, which means that the bigger the angle the higher the melanization. On the other hand, the degree of body melanization is determined by the off-set. For instance, insect 2 has a more melanized body as compared to the other two. In other words, this insect has a black body and white wings. Melanization is the reason why some people have darker skin as compared others.

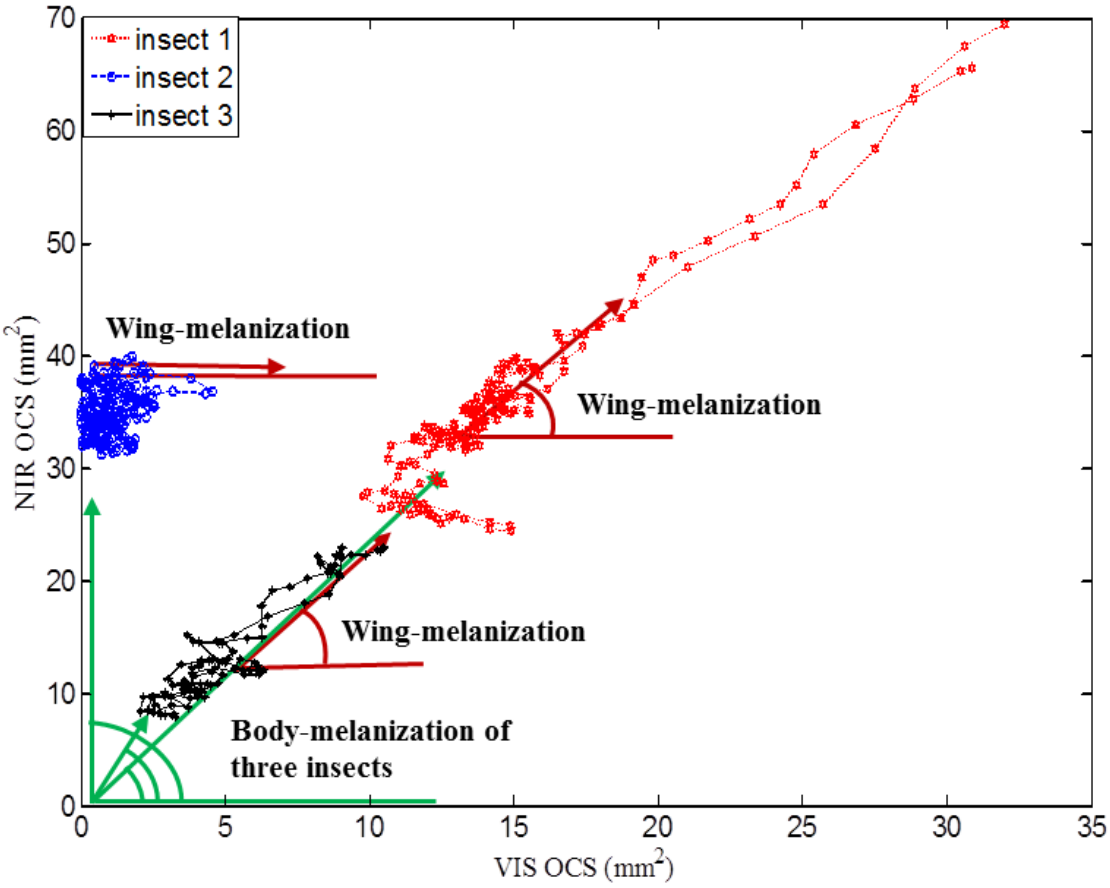

***Figure 59**: Trajectory in two-dimensional (2-D) VIS-NIR colour plane for three insects with sizes and wing-beat frequencies. NIR OCS: near-infrared optical cross-section and VIS OCS: visible optical cross-section. Wing melanization is related to the slope of oscillation and body melanization is related to the off-set. Melanin is the most common chromophore in all insects, which is responsible for colours.*

5.3 Parametrization

In this context parameterization is the process of quantifying different properties of backscattering objects in the laser radar experiment. The parametrization algorithm used in this dissertation selects the oscillating property in the range-time map as an event. An algorithm was used to determine size, wing-beat frequency and its harmonics, range and velocity of an insect event.

5.3.1 Range-time map

The input to the parameterization algorithm is the range-time file. Every file in this specific experimentcomes from8000 LIDAR samples at a 2 kHz sampling frequency. This file is then stored as12-bit TIFF image (1024x8000pixels). The vertical and horizontal axis of the file represents the range and time respectively. A flow chart of the main process steps and input parameters to the algorithm is shown in[194]. The main process are: File statistics, where the algorithm does three statistical measures (minimum, median and maximum) as describedin chapter IV, background and OCS calibration, event identification and fit of the harmonics functions. Apart from the range-time file, this main process has inputs like geometrical parameters, threshold of the intensity and time steps of the oscillating signal (the minimum time step the insect should have to be considered as insect. A threshold of 3 time steps was used in this dissertation). The parametrization algorithm stores every event, which is above the threshold while discarding the others and it loops over the rest of range-time files until the last event. An insect event with certain wing-beat frequency produces oscillating signal on the time axis, see Fig 60.The wing-beat frequency of this specific example insect is 285Hz, which is close to what one could expect of Mosquito wing-beat.

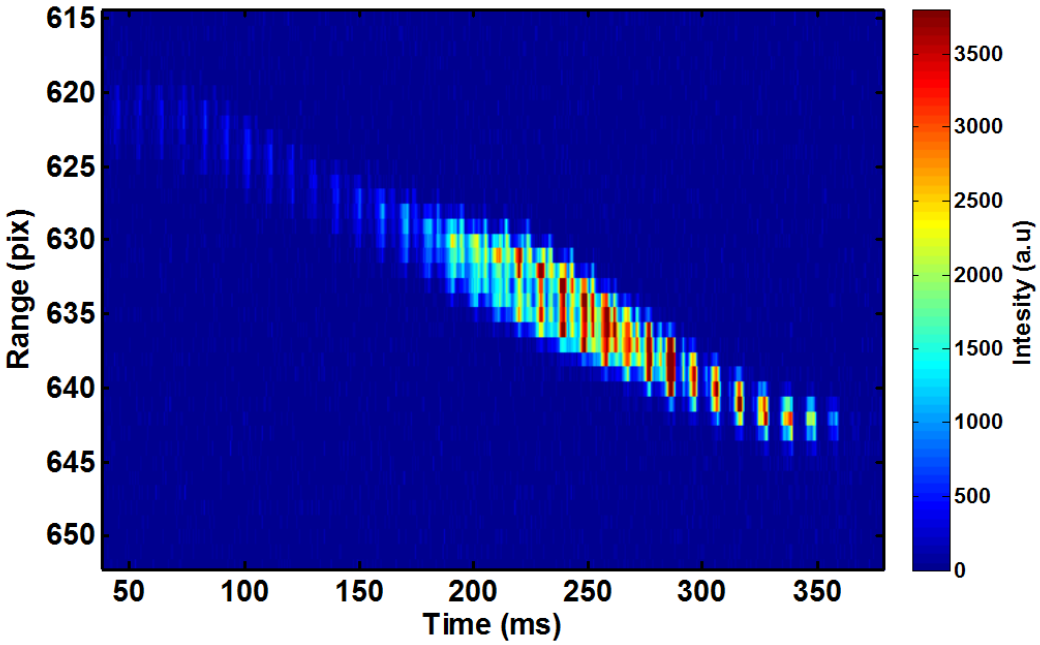

Figure 60: *Range-time map of 285Hz insect event.The change in colour of the oscillation shows the difference in signal strength.*

Looking a bit more in detail at the event described above, we can see that the range in which the event was detected is around 60.5m from the receiving telescope, see Fig 61. This size of the insect varies depending on itsorientation as was discussed in the previous sections. In the upper panel, we can see that the OCS is higher between 40ms and 50ms compared to the OCS between 30ms and 40ms. It is also shown in the lower subplot that every peak corresponds to different OCS of the event and Δt corresponds to the time that the insect spends in the probe volume.

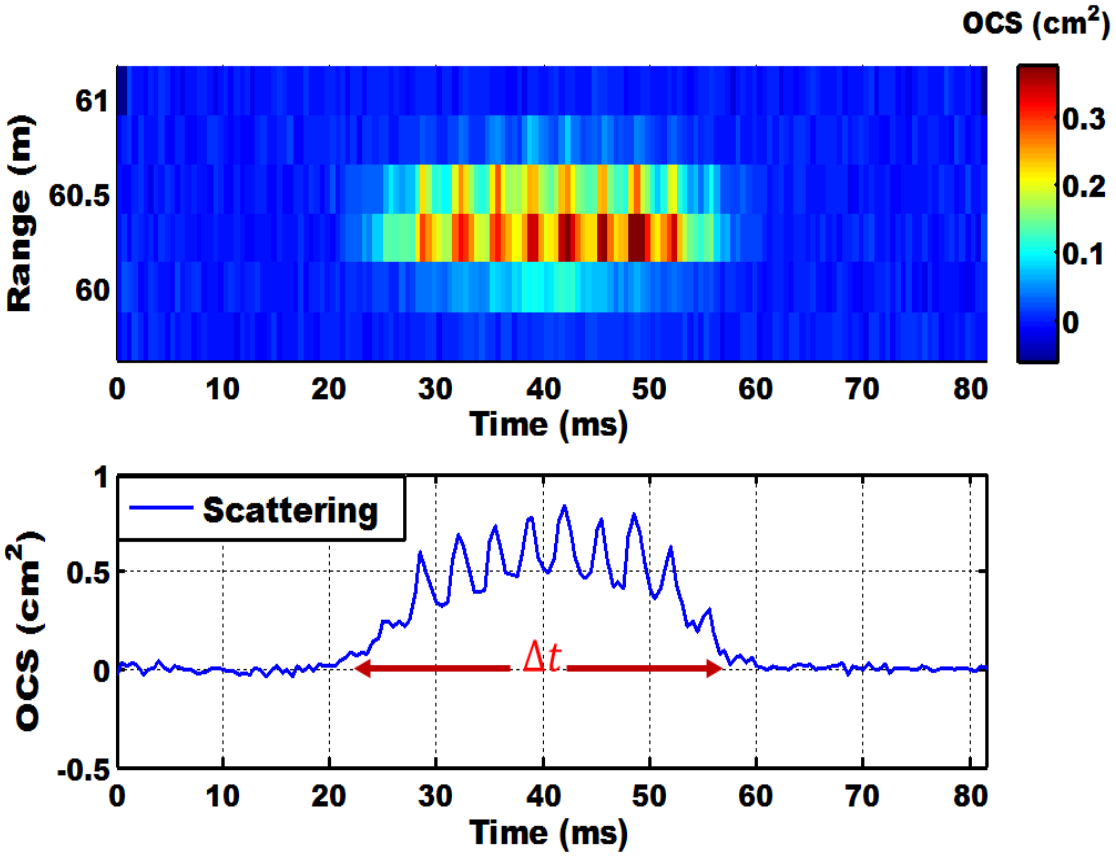

Figure 61: *The upper and lower subplot indicates the extracted insect event in the range-time map and back scattering time series of the same event respectively.*

5.3.2 Analysis of modulation spectra

The parametrization algorithm discussed in section 5.2.1comprisesfast Fourier transforms (FFT)to determine the frequency content of an event and its associated harmonics. FFT is an algorithm which calculates the discrete Fourier transform. It is usually called “fast computational algorism for discrete Fourier transform” (DFT). This algorithm is one of the most important tools in the fields like signal processing. It enables to convert data from the time to frequency domain and vice versa [209]. The reason why we chose FFT over simple DFT is because the later is computationally expensive. To understand this, one can see a simple DFT equation:

$X(k) = \sum_{n=0}^{N-1} x(n).\ e^{\frac{-j2\pi kn}{N}}$ ..... (5.2)

Where the "n" is the sample number and "." is complex multiplication.

The term $e^{\frac{-j2\pi}{N}}$ is a constant number and the above equation can be rewritten as:

$X(k) = \sum_{n=0}^{N-1} x(n)\ .W_N^{nk}$ ..... (5.3)

Where W_N^{nk} is equivalent to $e^{\frac{-j2\pi kn}{N}}$

In this case, the complex multiplication is executed every time the sum runs from n=0 to N-1. This involves (N.N)N^2complex multiplications while FFT only involves $NlogN$ complex multiplications. The method used in FFT algorithm to improve the computational issue isdividing the $x(n)$in Eq. (5.3) in to odd and even sequences, see Eq.5.4.

$X(k) = \sum_{m=0}^{\frac{N}{2}-1} x(2m)\ W_N^{2mk} + \sum_{m=0}^{\frac{N}{2}-1} x(2m+1)\ W_N^{(2m+1)k}$ ..... (5.4)

Even Sequence$\left(\frac{N}{2}\right)^2$+ odd sequence$\left(\frac{N}{2}\right)^2$

By executing Eq. (5.4) once, we can simplify the number of complex multiplications to$\frac{N^2}{2}$, which comes from the sum of the even and odd sequences. By performing division of even and odd sequence multiple timesone can arrive at $NlogN$ complex multiplication, which is faster compared to N^2.

When converting an array of time-domain datato an array of frequency-domaindata, the maximum frequency that can represent back in the time domain is half the sampling frequency, which is called the Nyquist frequency. ForN number of samples running from n=0 to N-1 and duration of the impute array in the time domain (T_d) in seconds (s),the span in the frequency domain after the FFT will have N samples and bandwidth (B_b) in hertz (Hz). In this case, the inputs are real valued samples while the outputs arecomplex valued samples, which mean that in the frequency domain there will be magnitude and phase representation of the complex values. The sampling interval will be the ratio of the duration input array (T_d) and sampling frequency (N) and it can be represented as: $\Delta t = \frac{T_d}{N}$. The inverse of sampling interval gives the sampling frequency in units of Hz. The first value in the time domain will be zero, the second value is Δt, the next value $2\Delta t$ and the last value of the array is$(N-1)\Delta t$. Similarly, the sampling frequency in the frequency domain is given by$f_s = \frac{1}{\Delta t} = \frac{N}{T_d}$, and the first frequency value of the array will be zero, which is usually called direct current (DC) to indicate zero frequency. In other words, DC is the average value of the time-domain waveform on which the FFT is applied. In this dissertation, this term is used to estimate the body contribution of an insect to the total OCS. The second frequency value will be $2\Delta f$, where $\Delta f = \frac{f_s}{N} = \frac{B_b}{N}$(sampling frequency and bidirectional bandwidth are the same) and the last frequency value will be the product of the last term and the (N-1) Δf, see Fig.62. Here, it should be noted that the bandwidth in this case is bidirectional, which means that the actual frequency that can be represented in the time domain will be half of the bidirectional bandwidth. This is called the

Nyquist frequency. See Eq.5.5. This implies that sampling frequency at least twice the frequencyof an event is required. The sampling frequency implemented in this dissertation is on the order of kHz, which is fast enough to resolve fast the wing-beat of an insect and its harmonics. Generally, the FFT works as it was described above and we use the Matlab built-in FFT function to generate the power spectrum of the rare events.

$$f_{max} = \frac{B_b}{2} = \frac{f_s}{2} \quad \text{(5.5)}$$

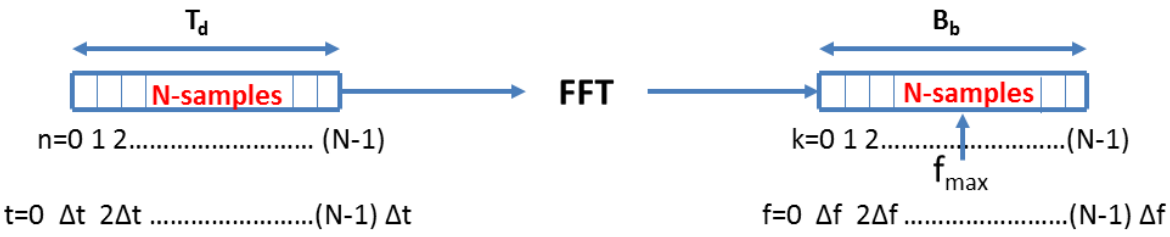

Figure 62: *Working principle of FFT to convert array of time-domain data to an array of frequency-domain data. Where:* ***n****: time index.* ***N****: total number of samples.* $\boldsymbol{f_{max}}$*: maximum frequency that we can represent back in the time domain (Nyquist frequency).* ***k****: is frequency index or bin number.* $\boldsymbol{B_b}$*: is bidirectional bandwidth.* $\boldsymbol{T_d}$***:*** *duration of the input array.*

5.3.3 Power spectral density (PSD)

Power spectral density (PSD)describes how the contributions to the power are distributed in the frequency domain. This can also be described as a stationary random process in the frequency domain [210]. The power spectrum is the discrete time Fourier transform (DTFT) of thecorrelation sequence ($S(\omega) \overset{DTFT}{\Longleftrightarrow} r[k]$). Mathematically, one can describe this as:

$$S(\omega) = \sum_{-\infty}^{\infty} r[k]e^{-jk\omega} \leftrightarrow r[k] = \int_{-\pi}^{\pi} S(\omega)e^{-jk\omega}d\omega \quad \text{(5.4)}$$

Considering two points in the frequency domain (ω_1 and ω_2), the area between the two points indicates the power this portion contribute to the process, see Fig 63. One can calculate the average contribution to the total power (variance) due to the components of the random process between the two points, see Eq. 5.5.

$$S_{1\to2} = \frac{1}{2\pi}\int_{\omega_1}^{\omega_2} S(\omega)d\omega \quad \text{(5.5)}$$

The PSD was used to evaluate the strength of the variation as a function of frequency. It is useful if one wants to identify an oscillatory signal in a time series data and want to know its amplitude. In ourcase, the power spectrum is obtained using the FFT discussed in section 5.2.2 and it contains contributions from the insect body (envelope)[194],the fundamental frequency and harmonics as shown inthe next section.

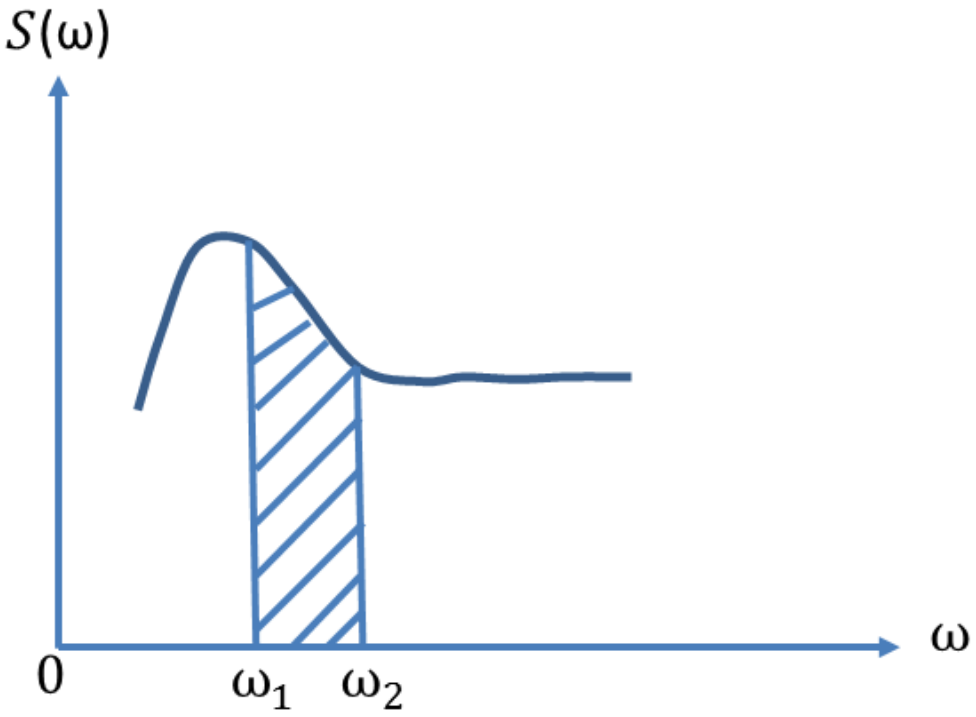

Figure 63: *Power spectral density (PSD) of a random process in frequency domain. The area between* $\boldsymbol{\omega_1}$ ***and*** $\boldsymbol{\omega_2}$ *indicates the average contribution of the components in between the two points to the total power.*

5.3.4 Wing-beat frequency and harmonics

A number of studies have been done to estimate the fundamental frequency (pitch)using different pitch recognition algorithms ineither frequency or time domain. One application of this is in speech recognition, which is as unique to an individual like fingerprints or an iris scan and is related to the length of a speaker vocal tract, missing teeth and behavioural elements [211,212]. One of the privacy issues in this case is the fact that individuals can be identified without their consent like other biometrics [212,213].

In this project, the fundamental wing-beat frequency and its harmonics is calculated from the power spectrum, which is obtained using a FFT from the time dependent back scatter signal of an insect event. In this process, the noise component of the power spectrum is identified while the envelope is assumed Gaussian. The power spectrum is represented in the new basis function, which enablesone to remove the envelope and noise components so that the only component left in the power spectrum is the wing-beat frequency with known allowed values (minimum and maximum).The maximum power within the allowed frequency range is taken as initial guess for the fundamental frequency of the wing-beat ($\omega_{initial}$). The final fundamental frequency will then be calculated by performing a best least square fit to the wing-beat signal in a frequency interval within 30% of the initial guess frequency ($\omega_{initial}$). To reproduce the original OCS of the wing-beat, a combination of the fundamental frequency is used to first describe the harmonics. This is done by first subtracting the contribution of the body from the

total OCS and the value that only describes the contribution from the Wing-beat is then used to describe the absolute strength and phase of the different Harmonics. Generally speaking, a linear combination of Harmonic basis functions (H) is used to represent fundamental frequencies and Harmonics in the OCS [194] . Mathematically, the linear combination of harmonic basis functions used to represent the fundamental frequency and harmonics in the OCS can be described as:

$$H = \{\sin(2\pi\omega nt) \mid n \in \mathbb{N}\} \cup \{\cos(2\pi\omega nt) \mid n \in \mathbb{N}\} \cup \{1\} \quad (5.6)$$

The time dependent OCS shows how to parametrizeinsect as a discrete set of harmonicsusing Eq.5.7. This is also discussed in chapter II.

$$OCS(t) = \beta(t) \sum_{h=0}^{h<1/2 f_s} \left(C_{1,h} \sin(2\pi f_0 ht) + 2\, C_{2,h} \cos(2\pi f_0 ht)\right) \quad (5.7)$$

To visualize howthis is related to insects in reality, it is important to see how the basic insect model explainsthe harmonic content of a certain insect's wing-beat, see Fig.64. We can see that the insect become large twice only from the side, but not in the anterior or dorsal view. It is shown that insect have three physiological planes and four different phases according this specific model.

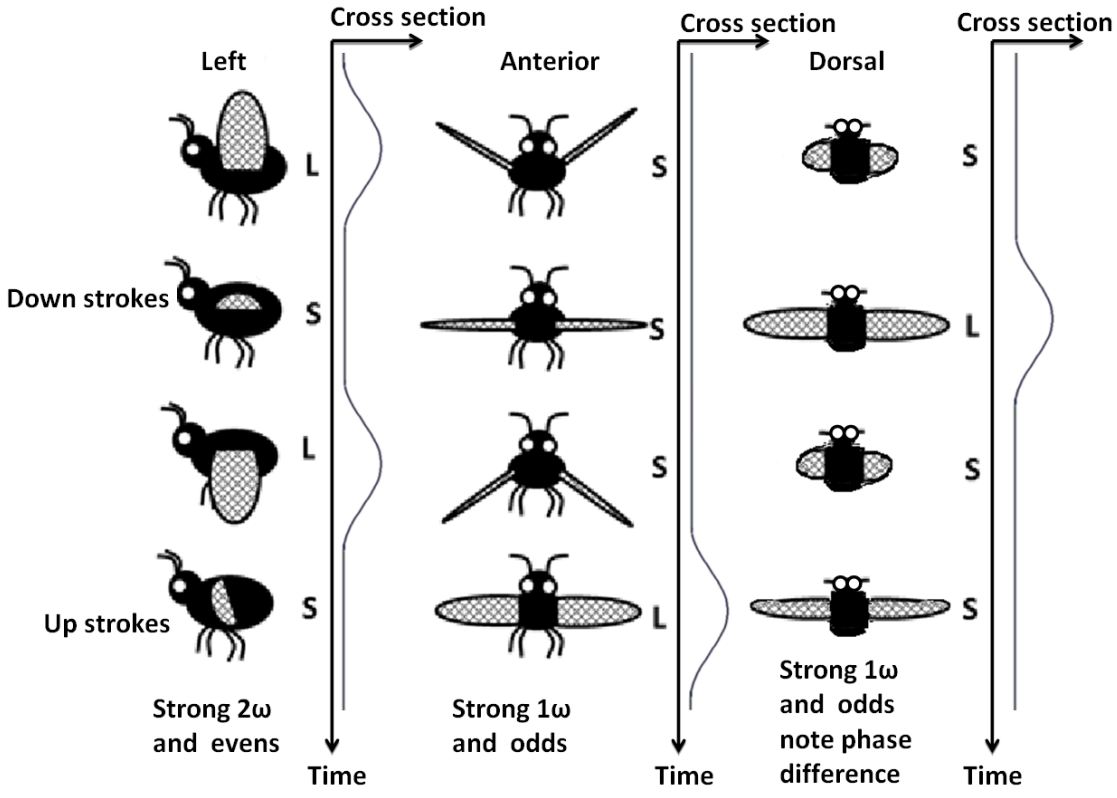

Figure 64: *Basic insect model to visualize harmonic content in respect to insect physiology. From the side the insect appears large twice (strong 2ω). Anterior and dorsal view only produces strong 1ω. Adopted from[137].*

Chapter VI

6. Conclusion and Outlook

6.1 Optics and Bio-Photonics

The general aim of this projectwas to develop and implementapplied optical remote sensing methods to help solve entomological questions like interaction strength on a millisecond time scale, biomass distribution and overall activities of insects over a several kilometres agricultural landscape. The passive and active remote sensing techniques that we have developed during the course of thisPhD project revealedgreat potential in solving basic environmental questions. It helps to bridge the gap between the two broad disciplines (physics and biology). It is understood that some ofthe conceptsfrom physics such as fundamental tone estimation and harmonicovertones could essentiallyanswer very important ecological question. Considering the species specific nature of those parameters, it is interesting to track activities of a number of insect species over different ecosystems in time and space.

Considering the passive remote sensing techniques, it is shown that one can determine flight direction, colour information, wing-beat frequency and its harmonics and iridescence features of fast insect events [158]. Insects are symmetric in many ways, especially in SWIR since this wavelength range is insensitive to melanization. One can use quadrant detector to break symmetry in order to determine the flight direction.It is also possible to compare the relative strength of odd and even harmonics for the determination of instant flight dynamics. When it comes to size determination, the limit with the passive techniques is the fact that we are so far not able to retrieve range information. Considering the range dependent sensitivity or form factor, it is challenging to precisely determine absolute OCS using this technique without having range information. Because of this reason, the OCS determination is only accurate close the object plane and the termination where the calibration and controlled release were performed. However, limited range information could be retrieved by looking at the flank rise and fall time of an insect event, which could be associated with the event distance from the object plan.

With regards to active remotes sensing, a number of important range resolved quantitative assessments of insects can be done. We have shown that the CW-LIDAR based on the Scheimpflug principle improves the range resolution beyond the diffraction limit. The reason for this is because of the fact that the sampling frequency is in the order of kHz and insects behave like blinking particles [44]. Unlike the conventional LIDAR techniques, this method is not limited by the round trip time of the laser pulse, which enables us to resolve the wing-beat frequency and its harmonics. This technique hasthe additionaladvantage over the passive remote sensingwhen it comes to retrieving range information and having stable (fixed) illumination intensity. One cantherefore perform accurate analysis of OCS, speed and other important quantitative parameters by day and night. This could enable one to manage a sustainable and healthy environment. We have recently shown that 24hours assessment and evaluation of atmospheric fauna can be done using this technique. From this experiment, we have seen 1700event/m^3hour on average, which indicates how impossible it would be to evaluate such huge numbers using manual techniques.

From physics point of view, we consider insects to be symmetrical objects especially in the SWIR wavelength range as discussed above and we use quadrants to break the symmetry. They generate oscillating OCS depending on their orientation in space. Theirorientations in space can be divided in to three physiological planes and four different phases as it was discussed in chapter V. The contribution of the body (DC) and fundamental frequency (1ω) to the total OCS happens in two planes while the contribution to the second harmonic (2ω) is only in one plane.

Generally, this dissertation highlights the potential of applied optical remote sensing techniques to remotely identify insects andtheirimpactto ecology. Considering the massive experience of the LIDAR community in environmental monitoring,it is important to recognize some of the aspects that one can take as a basis for this application and it will also help to understand similarities and differences between the different techniques. One can consider insects as a living aerosol with a certain wing-beat frequency.

6.2 Developing realistic instrumentation

Development of less costly and realistic instrumentation is usefulfor advanced research projects in developing countries. As it was discussed in section 6.1, part of this project aim was to develop such an instrument platform for ecological studies. This enables the development of skills and helps to understand the physics behind such experiments. I had an opportunity to participate in the African spectral imaging network (AFSIN) 4th international workshop on optical system design and computerized acquisition.My responsibilities were to assemble the instrumentation platform and demonstrate active and passive remote sensing experiments to the workshop participants at Yamoussoukro, Ivory Coast, 4-14 November 2013.

In the beginning of this project, we had a ø25cm and 120cm focal length Newtonian reflecting telescopewith a dobsonian mount, which was used for passive remote sensing experiments, see Fig.65. The same telescope together with ø105mm and 500 focal length refracting telescope was also used for the active remotes sensing experiments. Using this setup, we have organized a workshop at Jan Marias nature reserve in February 2013 and also tested the first CW-LIDAR setup based on Scheimpflug principle. During the course of the project the instrumentation platform was modified and the refracting telescope we had in the beginning is now replaced by a new ø90mm and 500mm focal length refractor. All the other mechanical parts of the setup are built in Stellenbosch University, Physics department workshop. The instruments purchased are: the 808nm laser source, reflecting and refracting telescopes, filters and detectors. The current setup is motorized and computer controlled. Both the refractor and reflecting telescope are placed on a metal mount. The distance between the midpoints of the two telescopes is 120cm, which is equal to the focal length of the receiving telescope to fulfil the Scheimpflug condition, see Fig.66. With regards to detectors, Si S4349 and InGaAs G6849, Hamamatsu quadrant detectors, dual detector (Si/InGaAs) sitting on top of each other and a low resolution spectrometer with sensitivity from 300nm to 1100nm were used. Comparingthe detector costs, the spectrometer (**Ocean Optics: USB4000**) is the most expensive equipment.

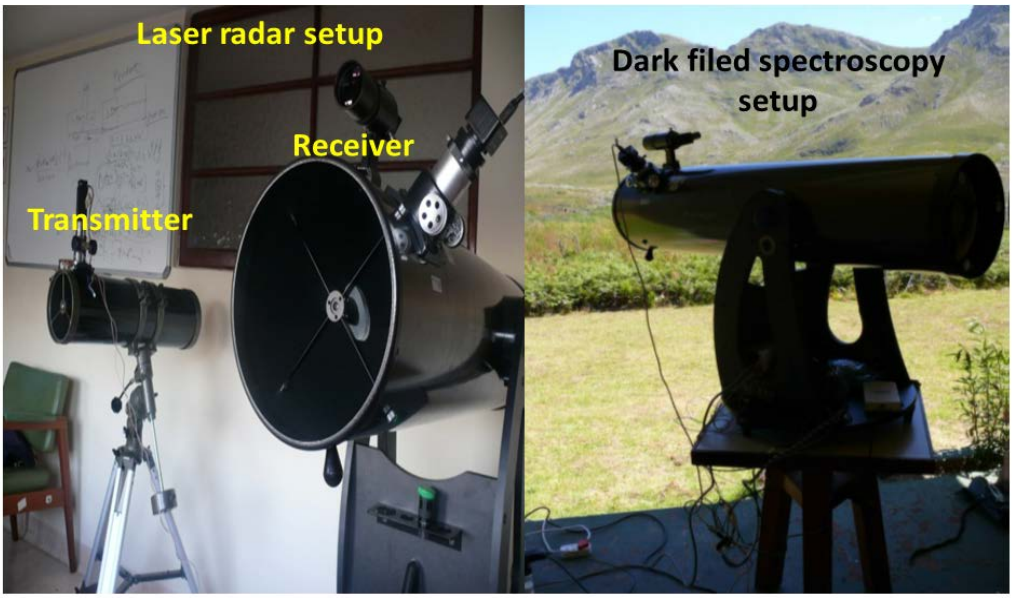

Figure 65: *The first setup we used for laser radar in Stellenbosch and dark field spectroscopy experiment at Kogelberg and Jan Marias nature reserve.*

Figure 66: *The newly built passive and active remote sensing setup. The white smaller telescope (left) is the refractor we used to transmit the laser. The black larger telescope (right) is used to collect backscattered signal.*

6.3 Ecology and Biosphere monitoring

The existence of life on earth depends on the proper functioning of the ecosystem. This includes the interaction of organisms with their environment and their response towards drastic changes. It means that proper monitoring of the environment is important forhuman existence. That is whydeveloping a more accurate ecological monitoring technique will have a big impact.

Considering the fact that about 80% of the animal population on earth are insects and their contributionfor pollinating more than 80% of flowering plants on earth, it is understood that they can be used asindicators to assess the wellbeing of our ecosystem. Needless to say, they have also a negative impact in terms of destroying forest and agriculture and disease transmission to humans and animals as it was discussed in Chapter I. The system developed in the course of this PhD project showed potential for monitoring pollinators in agricultural fields, the analysis of vector spreading disease to humans and animals and agricultural pest monitoring.

Several techniques have been used to study insect activities over the years and they have made significant contributions to understand insect behaviour. However, there is still room for improvement considering the instrument biases with regards to age and gender difference and life stages caught using the most commonly used manual techniques like traps and sweep nets. In this dissertation, it is shown that the accuracy of environmental monitoring can be improved significantly when it comes to the determination of flight direction, investigating distributions and biodiversity, improving sampling frequency, and identification of colour differences beyond human vision. Additionally, the techniques presented in this dissertation are non-intrusive, which enable the study of insect activities without affecting their normal life unlike the manual techniques like traps.

Some of the important features one could investigate using these optical techniques are melanization [214-218] and warning colours of different insects [219-223]. As it was discussed above, melanin is an important chromophore in the wings of insects, which enables them to increase heat uptake. This feature can be used to identify species by comparing the spectral content of a certain insect in the NIR and SWIR [137]. The warning colours of insects enable them to frighten their predator by telling the predatorthat they are poisonous orthey are unpalatable. However, some insect species show those colours even though they are neither poisonous nor unpalatable. They use colour to imitate warning or attract mates. The three warning colours in insects are: red, yellow and orange with black patches, see Fig.67.

With regards assessment of biodiversity, we have recently shown that evaluation of the insect biomass spectrum can be done using laser CW-LIDAR techniques. We have related insect observations to relevant ecological landscape features in Brunslove, Sweden. This technique shows a potential to identify aerial insect fauna and study the effect of insecticide on pollinators [55].

Figure 67: *Warning colours:* ***Left:*** *Yellow with black patches of a bee.* ***Middle:*** *Orange with black patches of a butterfly.* ***Right:*** *Red with black patches of a beetle.*

Acknowledgements

First and foremost I would like to thank the Almighty God for reasons too numerous to mention and beyond words to describe. You give me the power to stay motivated all the time and pursue my dreams. I could never have done this without the faith I have in you, the Almighty.

I would like thank Mikkel Brydegaard for his invaluable support throughout the PhD work. Thank you so much for giving me huge opportunity and made me believe that I can have a successfulresearch carrier. Thank you for being exceptionallygenerousin sharing your knowledge and skills to everyone who needs it.

I would like to thank Erich Rohwer and Pieter Neethling for extraordinary support and guidance. Thank you so much for allowing me to work on a project, which is new to the department and for believing in me that I could succeed. It demands so much courage to make such a decision and I am extremely grateful for the effort you put in.

I would like thank my beloved mother and all family for their exceptional support. Thank you so much Mam for being the best role model. Thank you for helping me tomake the right choices in life. Thank you, for being so patient and sympathetic with my teenage growing pains. It would be very difficult to be successful without your words of encouragement regardless of very long distance between us. I am extremely happy to be part of such a loving, understanding and supportive family.

I would like to thank my sweetheart for all the sleepless nights and scarifies. Thank you for appearing in my life and made it glorious. You mean a lot to me and I look forward to an exciting life together.

Finally, I am so grateful to all staffs of Stellenbosch and Lund University for welcoming me. It helped my early days in the department to be productive. I offer my regards to all of those who supported me in any respect during the completion of the project. I believe that I have defined my life pathway.

Publication

1. **A. Gebru**, E. Rohwer, P. Neethling, and M. Brydegaard, "Investigation of atmospheric insect wing-beat frequencies and iridescence features using a multispectral kHz remote detection system," *Journal of Applied Remote Sensing*, vol. 8, pp. 083503, 2014.
2. M. Brydegaard, **A. Gebru**, and S. Svanberg, "Super Resolution Laser Radar with Blinking Atmospheric Particles - Application to Interacting Flying Insects," *Progress in Electromagnetics Research*, vol. 147, pp. 141-151, 2014.
3. Mikkel Brydegaard, Aboma Merdasa, **Alem Gebru**, Hiran Jayaweera, Sune Svanberg," Realistic instrumentation platform for active and passive optical remote sensing", Journal of applied spectroscopy,2015.
4. Mikkel Brydegaard, **Alem Gebru**, Carsten Kirkeby, Susanne Åkesson, Henrik Smith, "Daily evaluation of the insect biomass spectrum in an agricultural landscape accessed with LIDAR", conference Proceedings,27th International Laser Radar Conference, New York, 2015.
5. **A. Gebru**, E. Rohwer, P. Neethling, and M. Brydegaard, "Applied kHz optical remote sensing for determination of insect flight direction and relative size", Frontiers in Optics/Laser Sience 2015, San Jose, California, USA, OSA Publishing JTu4A.54-2, 2015
6. **A. Gebru**, E. Rohwer, P. Neethling, and M. Brydegaard, "Probing insect flight direction and diffuse scatter cross section using kHz optical remote detection system", manuscript in preparation.

Conference and workshop participation

1. **"8th African laser centre student workshop"**, laser research institute, Stellenbosch University 2-6 December 2015
2. **"ALC Laser workshop on laser spectroscopy",**laser research institute, Stellenbosch University, 30 Nov - 2 Dec 2015.
3. **"Frontier in Optics/Laser Science (FiO/LS) Conference"** Fairmont San Jose in San Jose, California, USA from October 18 – 22.
4. **"Laser and Optics in Atmospheric Remote Sensing"**, Kwazulu-Natal University, Durban, 09-11 September, 2015
5. **"2015 South African institute of Physics conference annual conference"**, Nelson Mandela Metropolitan University and Rhodes University, Port Elizabeth, 29 June- 3 July 2015
6. **"Work shop onFemto-second lasers and application in Physics and chemistry"**, laser research institute, Stellenbosch University, 18-20 November 2014.
7. **"New trends and faces II Spectroscopy of organic materials",** PhD and post doc symposium, Stellenbosch University, South Africa, 20-24 October 2014.
8. **"SPIE Optical Engineering and applications, part of Optics and Photonics symposium",** invited talk, San Diego, California, 17-21 August 2014.
9. **"African spectral imaging network (AFSIN) 4th international work shop on optical system design and computerized accusation",** invited talk and demonstrate active

and passive remote sensing experiment, Yamoussoukro, Ivory Coast, 4-14 November 2013.

Reference

[1] Á Fernández-Llamazares, M. E. Méndez-López, I. Díaz-Reviriego, M. F. McBride, A. Pyhälä, A. Rosell-Melé, and V. Reyes-García, "Links between media communication and local perceptions of climate change in an indigenous society," *Climatic Change*, 2015.

[2] B. Mayer, "Conceiving the rationale for international climate law," *Climatic Change*, vol. 130, no. 3, pp. 371-382, 2015.

[3] J. Painter and N. T. Gavin, "Climate Skepticism in British Newspapers, 2007–2011," *Environmental Communication*, 2015.

[4] M. Previdi and L. M. Polvani, "Climate system response to stratospheric ozone depletion and recovery," *Quarterly Journal of the Royal Meteorological Society*, vol. 140, no. 685, pp. 2401-2419, 2014.

[5] V. Srinivasan, S. Thompson, K. Madhyastha, G. Penny, K. Jeremiah, and S. Lele, "Why is the Arkavathy River drying? A multiple-hypothesis approach in a data-scarce region," *Hydrology and Earth System Sciences*, vol. 19, no. 4, pp. 1905-1917, 2015.

[6] R. Costanza, R. dArge, R. deGroot, S. Farber, M. Grasso, B. Hannon, K. Limburg, S. Naeem, R. V. ONeill, J. Paruelo, R. G. Raskin, P. Sutton, and M. vandenBelt, "The value of the world's ecosystem services and natural capital," *Nature*, vol. 387, no. 6630, pp. 253-260, 1997.

[7] S. M. Aly and J. Wen, "Molecular identification of forensically relevant Diptera inferred from short mitochondrial genetic marker." *The Libyan Journal of Medicine*, vol. 8, pp. 20954, 2013.

[8] P. Boehme, P. Spahn, J. Amendt, and R. Zehner, "The analysis of temporal gene expression to estimate the age of forensically important blow fly pupae: Results from three blind studies," *International Journal of Legal Medicine*, vol. 128, no. 3, pp. 565-573, 2014.

[9] J. G. Fiene, G. A. Sword, S. L. Vanlaerhoven, and A. M. Tarone, "The role of spatial aggregation in forensic entomology," *Journal of Medical Entomology*, vol. 51, no. 1, pp. 1-9, 2014.

[10] E. Rosier, E. Cuypers, M. Dekens, R. Verplaetse, W. Develter, W. Van De Voorde, D. Maes, and J. Tytgat, "Development and validation of a new TD-GC/MS method and its applicability in the search for human and animal decomposition products Forensic Toxicology," *Analytical and Bioanalytical Chemistry*, vol. 406, no. 15, pp. 3611-3619, 2014.

[11] R. Costanza, "Introduction - Special section: Forum on valuation of ecosystem services - The value of ecosystem services," *Ecological Economics*, vol. 25, no. 1, pp. 1-2, 1998.

[12] R. Costanza, R. d'Arge, R. de Groot, S. Farber, M. Grasso, B. Hannon, K. Limburg, S. Naeem, R. V. O'Neill, J. Paruelo, R. G. Raskin, P. Sutton, and M. van den Belt, "The value of the world's ecosystem services and natural capital (Reprinted from Nature, vol 387, pg 253, 1997)," *Ecological Economics*, vol. 25, no. 1, pp. 3-15, 1998.

[13] R. Hickling, D. B. Roy, J. K. Hill, and C. D. Thomas, "A northward shift of range margins in British Odonata," *Global Change Biology*, vol. 11, no. 3, pp. 502-506, 2005.

[14] C. M. Oliveira, A. M. Auad, S. M. Mendes, and M. R. Frizzas, "Crop losses and the economic impact of insect pests on Brazilian agriculture," *Crop Protection*, vol. 56, pp. 50-54, 2014.

[15] P. D. Coley and T. A. Kursar, "On Tropical Forests and Their Pests," *Science*, vol. 343, no. 6166, pp. 35-36, 2014.

[16] P. Azambuja, E. S. Garcia, and N. A. Ratcliffe, "Gut microbiota and parasite transmission by insect vectors," *Trends in Parasitology*, vol. 21, no. 12, pp. 568-572, 2005.

[17] J. Wang, Y. Zhang, Y. O. Zhao, M. W. M. Li, L. Zhang, S. Dragovic, N. M. Abraham, and E. Fikrig, "Anopheles gambiae Circumsporozoite Protein-Binding Protein Facilitates Plasmodium Infection of Mosquito Salivary Glands," *Journal of Infectious Diseases*, vol. 208, no. 7, pp. 1161-1174, 2013.

[18] C. -. Chu and T. J. Henneberry, "Development of a new whitefly trap," *Journal of Cotton Science*, vol. 2, no. 3, pp. 104-109, 1998.

[19] G. Kriska, G. Horváth, and S. Andrikovics, "Why do mayflies lay their eggs en masse on dry asphalt roads? Water-imitating polarized light reflected from asphalt attracts ephemeroptera," *Journal of Experimental Biology*, vol. 201, no. 15, pp. 2273-2286, 1998.

[20] U. Bauer and W. Federle, "The insect-trapping rim of Nepenthes pitchers: surface structure and function." *Plant Signaling & Behavior*, vol. 4, no. 11, pp. 1019-1023, 2009.

[21] F. Nchu, N. K. Maniania, A. Hassanali, and J. N. Eloff, "Performance of a Metarhizium anisopliae-treated semiochemical-baited trap in reducing Amblyomma variegatum populations in the field," *Veterinary Parasitology*, vol. 169, no. 3-4, pp. 367-372, 2010.

[22] R. A. De Clerck-Floate, P. Saunders, and K. D. Floate, "Release and recapture of three insect species test the efficacy of trap method and air flow in insect containment," *Canadian Entomologist*, vol. 144, no. 4, pp. 609-616, 2012.

[23] "Water pan trap," *Retrived 2015, http://www.Fondriest.Com*.

[24] "Light trap," *Retrived 2015, http://Entomology.Unl.Edu*.

[25] "Sweep nets," *Retrived 2015, http://Entomology.Org.Uk*.

[26] G. E. A. P. A. Batista, Y. Hao, E. Keogh, and A. Mafra-Neto, "Towards automatic classification on flying insects using inexpensive sensors," *Proceedings - 10th International Conference on Machine Learning and Applications, ICMLA 2011*, vol. 1, pp. 364-369, 2011.

[27] M. Brydegaard, Z. Guan, M. Wellenreuther, and S. Svanberg, "Insect monitoring with fluorescence lidar techniques: feasibility study," *Applied Optics*, vol. 48, no. 30, pp. 5668-5677, 2009.

[28] Z. Guan, M. Brydegaard, P. Lundin, M. Wellenreuther, A. Runemark, E. I. Svensson, and S. Svanberg, "Insect monitoring with fluorescence lidar techniques: Field experiments," *Applied Optics*, vol. 49, no. 27, pp. 5133-5142, 2010.

[29] J. A. Shaw, N. L. Seldomridge, D. L. Dunkle, P. W. Nugent, L. H. Spangler, J. J. Bromenshenk, C. B. Henderson, J. H. Churnside, and J. J. Wilson, "Polarization lidar measurements of honey bees in flight for locating land mines," *Optics Express*, vol. 13, no. 15, pp. 5853-5863, 2005.

[30] D. S. Hoffman, A. R. Nehrir, K. S. Repasky, J. A. Shaw, and J. L. Carlsten, "Range-resolved optical detection of honeybees by use of wing-beat modulation of scattered light for locating land mines," *Applied Optics*, vol. 46, no. 15, pp. 3007-3012, 2007.

[31] K. S. Repasky, J. A. Shaw, R. Scheppele, C. Melton, J. L. Carsten, and L. H. Spangler, "Optical detection of honeybees by use of wing-beat modulation of scattered laser light for locating explosives and land mines," *Applied Optics*, vol. 45, no. 8, pp. 1839-1843, 2006.

[32] F. De Lussy, D. Greslou, C. Dechoz, V. Amberg, J. M. Delvit, L. Lebegue, G. Blanchet, and S. Fourest, "Pleiades HR in flight geometrical calibration: Location and mapping of the focal plane," *International Archives of the Photogrammetry, Remote Sensing and Spatial Information Sciences - ISPRS Archives*, vol. 39, pp. 519-523, 2012.

[33] K. E. Dungan, C. Austin, J. Nehrbass, and L. C. Potter, "Civilian vehicle radar data domes," *Proceedings of SPIE - the International Society for Optical Engineering*, vol. 7699, 2010.

[34] T. Karthick and S. Aravind, "Unmanned Air Vehicle collision avoidance system and method for safety flying in civilian airspace," *Proceedings - 3rd International Conference on Emerging Trends in Engineering and Technology, ICETET 2010*, , pp. 116-119, 2010.

[35] I. Balajti, G. Kende, and E. Sinner, "Increased importance of VHF radars in ground-based air defense," *IEEE Aerospace and Electronic Systems Magazine*, vol. 27, no. 1, pp. 4-18, 2012.

[36] R. Gente, C. Jansen, R. Geise, O. Peters, M. Gente, N. Krumbholz, C. Möller, S. Busch, and M. Koch, "Scaled bistatic radar cross section measurements of aircraft with a fiber-coupled THz time-domain spectrometer," *IEEE Transactions on Terahertz Science and Technology*, vol. 2, no. 4, pp. 424-431, 2012.

[37] Y. Shi, Y. Li, and J. Wang, "Effectiveness evaluation about self-screening jamming of assaulting aircraft in complex em environment," *Communications in Computer and Information Science*, vol. 159 CCIS, no. PART 2, pp. 360-365, 2011.

[38] V. A. Drake and D. R. Reynolds, "Radar entomology: Observing insect flight and migration," *Radar Entomology: Observing Insect Flight and Migration*, , pp. 1-489, 2012.

[39] "2010 Earth Guide at Scripps Institute of Oceanography," *Retrived,2015, Www.Commons.Wikimedia.Org*, .

[40] J. W. Chapman, D. R. Reynolds, and A. D. Smith, "Migratory and foraging movements in beneficial insects: A review of radar monitoring and tracking methods," *International Journal of Pest Management*, vol. 50, no. 3, pp. 225-232, 2004.

[41] J. W. Chapman, V. A. Drake, and D. R. Reynolds, "Recent insights from radar studies of insect flight," *Annual Review of Entomology*, vol. 56, pp. 337-356, 2011.

[42] G. L. Pilkay, F. P. F. Reay-Jones, and J. K. Greene, "Harmonic radar tagging for tracking movement of Nezara viridula (Hemiptera: Pentatomidae)," *Environmental Entomology*, vol. 42, no. 5, pp. 1020-1026, 2013.

[43] N. Tahir and G. Brooker, "Recent developments and recommendations for improving harmonic radar tracking systems," *Proceedings of the 5th European Conference on Antennas and Propagation, EUCAP 2011,* , pp. 1531-1535, 2011.

[44] M. Brydegaard, A. Gebru, and S. Svanberg, "Super Resolution Laser Radar with Blinking Atmospheric Particles - Application to Interacting Flying Insects," *Progress in Electromagnetics Research,* vol. 147, pp. 141-151, 2014.

[45] M. Dorman, T. Svoray, and A. Perevolotsky, "Homogenization in forest performance across an environmental gradient - The interplay between rainfall and topographic aspect," *Forest Ecology and Management,* vol. 310, pp. 256-266, 2013.

[46] T. Luong, K. Jang, H. Lim, W. Choi, and K. Lee, "Correlation of tree ring growths of four major species with climate changes in South Korea," *Forest Science and Technology,* vol. 9, no. 4, pp. 180-186, 2013.

[47] R. Penttilä, K. Junninen, P. Punttila, and J. Siitonen, "Effects of forest restoration by fire on polypores depend strongly on time since disturbance - A case study from Finland based on a 23-year monitoring period," *Forest Ecology and Management,* vol. 310, pp. 508-516, 2013.

[48] G. Wang, D. Guan, M. R. Peart, Y. Chen, and Y. Peng, "Ecosystem carbon stocks of mangrove forest in Yingluo Bay, Guangdong Province of South China," *Forest Ecology and Management,* vol. 310, pp. 539-546, 2013.

[49] D. Zhou, S. Liu, J. Oeding, and S. Zhao, "Forest cutting and impacts on carbon in the eastern United States," *Scientific Reports,* vol. 3, 2013.

[50] C. Bone, J. C. White, M. A. Wulder, C. Robertson, and T. A. Nelson, "Impact of forest fragmentation on patterns of mountain pine beetle-caused tree mortality," *Forests,* vol. 4, no. 2, pp. 279-295, 2013.

[51] T. B. Chapman, T. T. Veblen, and T. Schoennagel, "Spatiotemporal patterns of mountain pine beetle activity in the southern Rocky Mountains," *Ecology,* vol. 93, no. 10, pp. 2175-2185, 2012.

[52] M. J. Jenkins, J. B. Runyon, C. J. Fettig, W. G. Page, and B. J. Bentz, "Interactions among the mountain pine beetle, fires, and fuels," *Forest Science,* vol. 60, no. 3, pp. 489-501, 2014.

[53] B. Petersen and D. Stuart, "Explanations of a changing landscape: A critical examination of the British Columbia bark beetle epidemic," *Environment and Planning A,* vol. 46, no. 3, pp. 598-613, 2014.

[54] Y. Wang, L. Lim, S. Diguistini, G. Robertson, J. Bohlmann, and C. Breuil, "A specialized ABC efflux transporter GcABC-G1 confers monoterpene resistance to Grosmannia clavigera, a bark beetle-associated fungal pathogen of pine trees," *New Phytologist,* vol. 197, no. 3, pp. 886-898, 2013.

[55] M. Brydegaard, Gebru,Alem, Kirkeby,Carsten, S. Åkesson, and H. Smith, "Daily evaluation of the insect biomass spectrum in an agricultural landscape accessed with LIDAR," *Submitted to ILRC27, 2015.*

[56] S. Kärvemo, T. P. Van Boeckel, M. Gilbert, J. Grégoire, and M. Schroeder, "Large-scale risk mapping of an eruptive bark beetle - Importance of forest susceptibility and beetle pressure," *Forest Ecology and Management,* vol. 318, pp. 158-166, 2014.

[57] K. N. Nelson, M. E. Rocca, M. Diskin, C. F. Aoki, and W. H. Romme, "Predictors of bark beetle activity and scale-dependent spatial heterogeneity change during the course of an outbreak in a subalpine forest," *Landscape Ecology*, vol. 29, no. 1, pp. 97-109, 2014.

[58] "Evergreen lawn and tree care," *Retrived 2015, Http://www.Treecarecheyenne.Com*.

[59] "Infested pine tree," *Retrived 2015, Http://www.Backyardchickens.Com*.

[60] B. C. O'Neill, "Population scenarios based on probabilistic projections: An application for the Millennium Ecosystem Assessment," *Population and Environment*, vol. 26, no. 3, pp. 229-254, 2005.

[61] P. D. Raskin, "Global scenarios: Background review for the Millennium Ecosystem Assessment," *Ecosystems*, vol. 8, no. 2, pp. 133-142, 2005.

[62] A. S. Van Jaarsveld, R. Biggs, R. J. Scholes, E. Bohensky, B. Reyers, T. Lynam, C. Musvoto, and C. Fabricius, "Measuring conditions and trends in ecosystem services at multiple scales: The Southern African Millennium Ecosystem Assessment (SAfMA) experience," *Philosophical Transactions of the Royal Society B: Biological Sciences*, vol. 360, no. 1454, pp. 425-441, 2005.

[63] J. E. Losey and M. Vaughan, "The economic value of ecological services provided by insects," *Bioscience*, vol. 56, no. 4, pp. 311-323, 2006.

[64] M. Brydegaard, ""Aspects of Optical Broad Band Spectroscopy and Information Extraction - Applications in Medicine and Ecology."*978-91-7473-353-2, 2012. Doktoral Thesis, Lund University*.

[65] K. Asenso-Okyere, F. A. Asante, J. Tarekegn, and K. S. Andam, "A review of the economic impact of malaria in agricultural development," *Agricultural Economics*, vol. 42, no. 3, pp. 293-304, 2011.

[66] A. Egbendewe-Mondzozo, M. Musumba, B. A. McCarl, and X. Wu, "Climate change and vector-borne diseases: An economic impact analysis of malaria in Africa," *International Journal of Environmental Research and Public Health*, vol. 8, no. 3, pp. 913-930, 2011.

[67] M. S. Mia, R. A. Begum, A. -. Er, R. D. Z. R. Z. Abidin, and J. J. Pereira, "Malaria and climate change: Discussion on economic impacts," *American Journal of Environmental Sciences*, vol. 7, no. 1, pp. 73-82, 2011.

[68] E. E. Brouwer, J. J. Van Hellemond, P. J. Van Genderen, E. Slot, L. Van Lieshout, L. G. Visser, and P. J. Wismans, "A case report of transfusion-transmitted Plasmodium malariae from an asymptomatic non-immune traveller," *Malaria Journal*, vol. 12, no. 1, 2013.

[69] K. Kast, N. Berens-Riha, A. Zeynudin, N. Abduselam, T. Eshetu, T. Löscher, A. Wieser, J. Shock, and M. Pritsch, "Evaluation of Plasmodium falciparum gametocyte detection in different patient material," *Malaria Journal*, , pp. 438, 2013.

[70] M. T. Tchioffo, A. Boissière, T. S. Churcher, L. Abate, G. Gimonneau, S. E. Nsango, P. H. Awono-Ambéné, R. Christen, A. Berry, and I. Morlais, "Modulation of malaria infection in Anopheles gambiae mosquitoes exposed to natural midgut bacteria," *PLoS ONE*, vol. 8, no. 12, 2013.

[71] E. H. Nardin and R. S. Nussenzweig, "T cell responses to pre-erythrocytic stages of malaria: Role in protection and vaccine development against pre-erythrocytic stages," *Annual Review of Immunology*, vol. 11, pp. 687-727, 1993.

[72] A. M. Vaughan, M. T. O'Neill, A. S. Tarun, N. Camargo, T. M. Phuong, A. S. I. Aly, A. F. Cowman, and S. H. I. Kappe, "Type II fatty acid synthesis is essential only for malaria parasite late liver stage development," *Cellular Microbiology*, vol. 11, no. 3, pp. 506-520, 2009.

[73] M. Clark, N. C. Fisher, R. Kasthuri, and C. Cerami Hand, "Parasite maturation and host serum iron influence the labile iron pool of erythrocyte stage Plasmodium falciparum," *British Journal of Haematology*, vol. 161, no. 2, pp. 262-269, 2013.

[74] C. Currà, T. Pace, B. M. D. Franke-Fayard, L. Picci, L. Bertuccini, and M. Ponzi, "Erythrocyte Remodeling in Plasmodium berghei Infection: The Contribution of SEP Family Members," *Traffic*, vol. 13, no. 3, pp. 388-399, 2012.

[75] E. J. Dawes, S. Zhuang, R. E. Sinden, and M. -. Basáñez, "The temporal dynamics of Plasmodium density through the sporogonic cycle within Anopheles mosquitoes," *Transactions of the Royal Society of Tropical Medicine and Hygiene*, vol. 103, no. 12, pp. 1197-1198, 2009.

[76] G. Margos, I. Sidén-Kiamos, R. E. Fowler, T. R. Gillman, R. Spaccapelo, G. Lycett, D. Vlachou, G. Papagiannakis, W. M. Eling, G. H. Mitchell, and C. Louis, "Myosin A expressions in sporogonic stages of Plasmodium," *Molecular and Biochemical Parasitology*, vol. 111, no. 2, pp. 465-469, 2000.

[77] S. Cho, S. Kim, Y. Kim, and Y. Park, "Optical imaging techniques for the study of malaria," *Trends in Biotechnology*, vol. 30, no. 2, pp. 71-79, 2012.

[78] M. Ferrer, L. Martin-Jaular, M. De Niz, S. M. Khan, C. J. Janse, M. Calvo, V. Heussler, and H. A. Del Portillo, "Imaging of the spleen in malaria," *Parasitology International*, vol. 63, no. 1, pp. 195-205, 2014.

[79] C. Yuen and Q. Liu, "Magnetic field enriched surface enhanced resonance Raman spectroscopy for early malaria diagnosis," *Journal of Biomedical Optics*, vol. 17, no. 1, 2012.

[80] B. R. Wood, A. Hermelink, P. Lasch, K. R. Bambery, G. T. Webster, M. A. Khiavi, B. M. Cooke, S. Deed, D. Naumann, and D. McNaughton, "Resonance Raman microscopy in combination with partial dark-field microscopy lights up a new path in malaria diagnostics," *Analyst*, vol. 134, no. 6, pp. 1119-1125, 2009.

[81] J. M. Bélisle, S. Costantino, M. L. Leimanis, M. Bellemare, D. S. Bohle, E. Georges, and P. W. Wiseman, "Sensitive detection of malaria infection by third harmonic generation imaging," *Biophysical Journal*, vol. 94, no. 4, pp. L26-L28, 2008.

[82] M. Brydegaard, A. Merdasa, H. Jayaweera, J. Ålebring, and S. Svanberg, "Versatile multispectral microscope based on light emitting diodes," *Review of Scientific Instruments*, vol. 82, no. 12, 2011.

[83] A. Merdasa, M. Brydegaard, S. Svanberg, and J. T. Zoueu, "Staining-free malaria diagnostics by multispectral and multimodality light-emitting-diode microscopy," *Journal of Biomedical Optics*, vol. 18, no. 3, 2013.

[84] A. Dao, A. S. Yaro, M. Diallo, S. Timbine, D. L. Huestis, Y. Kassogue, A. I. Traore, Z. L. Sanogo, D. Samake, and T. Lehmann, "Signatures of aestivation and migration in Sahelian malaria mosquito populations," *Nature*, vol. 516, no. 7531, pp. 387-390, 2014.

[85] B. S. Grandey and P. Stier, "A critical look at spatial scale choices in satellite-based aerosol indirect effect studies," *Atmospheric Chemistry and Physics*, vol. 10, no. 23, pp. 11459-11470, 2010.

[86] K. H. Lee and Y. J. Kim, "Satellite remote sensing of Asian aerosols: A case study of clean, polluted, and Asian dust storm days," *Atmospheric Measurement Techniques*, vol. 3, no. 6, pp. 1771-1784, 2010.

[87] K. Millard and M. Richardson, "Wetland mapping with LiDAR derivatives, SAR polarimetric decompositions, and LiDAR-SAR fusion using a random forest classifier," *Canadian Journal of Remote Sensing*, vol. 39, no. 4, pp. 290-307, 2013.

[88] J. Praks, O. Antropov, and M. T. Hallikainen, "LIDAR-aided SAR interferometry studies in boreal forest: Scattering phase center and extinction coefficient at X-and L-band," *IEEE Transactions on Geoscience and Remote Sensing*, vol. 50, no. 10 PART1, pp. 3831-3843, 2012.

[89] K. Calders, J. Armston, G. Newnham, M. Herold, and N. Goodwin, "Implications of sensor configuration and topography on vertical plant profiles derived from terrestrial LiDAR," *Agricultural and Forest Meteorology*, vol. 194, pp. 104-117, 2014.

[90] X. T. Chen, M. I. Disney, P. Lewis, J. Armston, J. T. Han, and J. C. Li, "Sensitivity of direct canopy gap fraction retrieval from airborne waveform lidar to topography and survey characteristics," *Remote Sensing of Environment*, vol. 143, pp. 15-25, 2014.

[91] H. Kariminezhad, P. Parvin, F. Borna, and A. Bavali, "SF6 leak detection of high-voltage installations using TEA-CO_2 laser-based DIAL," *Optics and Lasers in Engineering*, vol. 48, no. 4, pp. 491-499, 2010.

[92] A. R. Nehrir, K. S. Repasky, J. L. Carlsten, M. D. Obland, and J. A. Shaw, "Water vapor profiling using a widely tunable, amplified diode-laser-based differential absorption lidar (DIAL)," *Journal of Atmospheric and Oceanic Technology*, vol. 26, no. 4, pp. 733-745, 2009.

[93] M. Brydegaard, A. Merdasa, A. Gebru, H. Jayaweera, and S. Svanberg, "Realistic instrumentation platform for active and passive optical remote sensing, Accepted, Journal of Applied Spectroscopy, 2015," .

[94] A. Runemark, M. Wellenreuther, H. H. E. Jayaweera, S. Svanberg, and M. Brydegaard, "Rare events in remote dark-field spectroscopy: An ecological case study of insects," *IEEE Journal on Selected Topics in Quantum Electronics*, vol. 18, no. 5, pp. 1573-1582, 2012.

[95] A. Gebru, E. Rohwer, P. Neethling, and M. Brydegaard, "Investigation of atmospheric insect wing-beat frequencies and iridescence features using a multispectral kHz remote detection system," *Journal of Applied Remote Sensing*, vol. 8, pp. 083503, 2014.

[96] D. Ehlert, R. Adamek, and H. -. Horn, "Assessment of laser rangefinder principles for measuring crop biomass," *Precision Agriculture 2007 - Papers Presented at the 6th European Conference on Precision Agriculture, ECPA 2007*, pp. 317-324, 2007.

[97] L. Wang, J. Gao, X. Wang, J. Eckstein, and P. Ott, "Error factors in the rotational symmetric triangulation sensor," *Yi Qi Yi Biao Xue Bao/Chinese Journal of Scientific Instrument*, vol. 28, no. SUPPL. 3, pp. 9-13, 2007.

[98] F. Blais, "Review of 20 years of range sensor development," *Journal of Electronic Imaging*, vol. 13, no. 1, pp. 231-243, 2004.

[99] "Focusing normal and Tilt/ Swing lenses,"*Retrived 2015, https://www.waldonell.com*.

[100] G. C. Hulley, C. G. Hughes, and S. J. Hook, "Quantifying uncertainties in land surface temperature and emissivity retrievals from ASTER and MODIS thermal infrared data," *Journal of Geophysical Research: Atmospheres*, vol. 117, no. 23, 2012.

[101] C. J. Merchant, O. Embury, N. A. Rayner, D. I. Berry, G. K. Corlett, K. Lean, K. L. Veal, E. C. Kent, D. T. Llewellyn-Jones, J. J. Remedios, and R. Saunders, "A 20year independent record of sea surface temperature for climate from Along-Track Scanning Radiometers," *Journal of Geophysical Research: Oceans*, vol. 117, no. 12, 2012.

[102] L. Mereni, D. Pepe, and D. Zito, "Analyses and design of 95-GHz SoC CMOS radiometers for passive body imaging," *Analog Integrated Circuits and Signal Processing*, vol. 77, no. 3, pp. 373-383, 2013.

[103] K. Rausch, S. Houchin, J. Cardema, G. Moy, E. Haas, and F. J. De Luccia, "Automated calibration of the Suomi National Polar-Orbiting Partnership (S-NPP) Visible Infrared Imaging Radiometer Suite (VIIRS) reflective solar bands," *Journal of Geophysical Research: Atmospheres*, vol. 118, no. 24, pp. 13434-13442, 2013.

[104] V. Kopacková, S. Chevrel, A. Bourguignon, and P. Rojík, "Application of high altitude and ground-based spectroradiometry to mapping hazardous low-pH material derived from the Sokolov open-pit mine," *Journal of Maps*, vol. 8, no. 3, pp. 220-230, 2012.

[105] J. T. Randerson, Y. Chen, G. R. Van Der Werf, B. M. Rogers, and D. C. Morton, "Global burned area and biomass burning emissions from small fires," *Journal of Geophysical Research: Biogeosciences*, vol. 117, no. 4, 2012.

[106] J. I. Glaser, "BISTATIC RCS OF COMPLEX OBJECTS NEAR FORWARD SCATTER." *IEEE Transactions on Aerospace and Electronic Systems*, vol. AES-21, no. 1, pp. 70-78, 1985.

[107] Y. Toduka, T. Toyooka, and Y. Ibuki, "Flow cytometric evaluation of nanoparticles using side-scattered light and reactive oxygen species-mediated fluorescence-correlation with genotoxicity," *Environmental Science and Technology*, vol. 46, no. 14, pp. 7629-7636, 2012.

[108] M. W. Sigrist, "Laser photoacoustic spectrometry for trace gas monitoring," *The Analyst*, vol. 119, no. 4, pp. 525-531, 1994.

[109] P. W. Werle, "High frequency modulation spectroscopy: a sensitive detection technique for atmospheric pollutants," *Proceedings of SPIE - the International Society for Optical Engineering*, vol. 2092, pp. 4-15, 1994.

[110] A. Bohlin and C. J. Kliewer, "Diagnostic imaging in flames with instantaneous planar coherent Raman spectroscopy," *Journal of Physical Chemistry Letters*, vol. 5, no. 7, pp. 1243-1248, 2014.

[111] C. Di Napoli, I. Pope, F. Masia, P. Watson, W. Langbein, and P. Borri, "Hyperspectral and differential CARS microscopy for quantitative chemical imaging in human adipocytes," *Biomedical Optics Express*, vol. 5, no. 5, pp. 1378-1390, 2014.

[112] R. Galli, O. Uckermann, E. Koch, G. Schackert, M. Kirsch, and G. Steiner, "Effects of tissue fixation on coherent anti-Stokes Raman scattering images of brain," *Journal of Biomedical Optics*, vol. 19, no. 7, 2014.

[113] J. M. Levitt, O. Katz, and Y. Silberberg, "Frequency-encoded multiplexed CARS microscopy by rapid pulse shaping," *Journal of Modern Optics*, vol. 61, no. 10, pp. 872-876, 2014.

[114] Y. Zhang, Y. -. Zhen, O. Neumann, J. K. Day, P. Nordlander, and N. J. Halas, "Coherent anti-Stokes Raman scattering with single-molecule sensitivity using a plasmonic Fano resonance," *Nature Communications*, vol. 5, 2014.

[115] M. Georganopoulos, E. S. Perlman, D. Kazanas, and J. Mcenery, "Quasar X-ray jets: Gamma-ray diagnostics of the synchrotron and inverse compton hypotheses: The case of 3C 273," *Astrophysical Journal*, vol. 653, no. 1 II, pp. L5-L8, 2006.

[116] S. Miyamoto, Y. Asano, S. Amano, D. Li, K. Imasaki, H. Kinugasa, Y. Shoji, T. Takagi, and T. Mochizuki, "Laser Compton back-scattering gamma-ray beamline on NewSUBARU," *Radiation Measurements*, vol. 41, no. SUPPL. 2, pp. S179-S185, 2006.

[117] J. N. Stenzler, J. G. Lee, D. A. Santavicca, and W. Lee, "Penetration of liquid jets in a cross-flow," *Atomization and Sprays*, vol. 16, no. 8, pp. 887-906, 2006.

[118] X. M. Sun, Y. P. Han, and H. H. Wang, "Near-infrared light scattering by ice-water mixed clouds," *Progress in Electromagnetics Research*, vol. 61, pp. 133-142, 2006.

[119] X. Jian, S. Dixon, N. Guo, R. S. Edwards, and M. Potter, "Pulsed Rayleigh wave scattered at a surface crack," *Ultrasonics*, vol. 44, no. SUPPL., pp. e1131-e1134, 2006.

[120] P. Polyakov, J. Luettmer-Strathmann, and S. Wiegand, "Study of the thermal diffusion behavior of alkane/benzene mixtures by thermal diffusion forced rayleigh scattering experiments and lattice model calculations," *Journal of Physical Chemistry B*, vol. 110, no. 51, pp. 26215-26224, 2006.

[121] Q. -. Yang, Z. -. Liu, Q. -. Lu, and S. -. Liu, "Resonance Rayleigh scattering method for determination of some anionic surfactants with chlorpromazine hydrochloride as probe," *Gaodeng Xuexiao Huaxue Xuebao/Chemical Journal of Chinese Universities*, vol. 27, no. 12, pp. 2281-2284, 2006.

[122] G. Adler, T. Koop, C. Haspel, I. Taraniuk, T. Moise, I. Koren, R. H. Heiblum, and Y. Rudich, "Formation of highly porous aerosol particles by atmospheric freeze-drying in ice clouds," *Proceedings of the National Academy of Sciences of the United States of America*, vol. 110, no. 51, pp. 20414-20419, 2013.

[123] V. N. Lukashin and A. N. Novigatsky, "Chemical composition of aerosols in the near-water surface atmospheric layer of the central Caspian Sea in the winter and autumn of 2005," *Oceanology*, vol. 53, no. 6, pp. 727-738, 2013.

[124] E. S. Robinson, R. Saleh, and N. M. Donahue, "Organic aerosol mixing observed by single-particle mass spectrometry," *Journal of Physical Chemistry A*, vol. 117, no. 51, pp. 13935-13945, 2013.

[125] G. Jin, P. I. Widenborg, P. Campbell, and S. Varlamov, "Lambertian matched absorption enhancement in PECVD poly-Si thin film on aluminum induced textured glass superstrates for solar cell applications," *Progress in Photovoltaics: Research and Applications*, vol. 18, no. 8, pp. 582-589, 2010.

[126] T. Roch, E. Beyer, and A. Lasagni, "Surface modification of thin tetrahedral amorphous carbon films by means of UV direct laser interference patterning," *Diamond and Related Materials*, vol. 19, no. 12, pp. 1472-1477, 2010.

[127] H. Yamane, T. Narisawa, T. Hasegawa, and S. Ishio, "Structural characterization for L 10 - ordered FePt films with (001) texture by x-ray diffraction," *Journal of Applied Physics*, vol. 108, no. 11, 2010.

[128] Y. -. Dai, H. -. Chang, K. -. Lai, C. -. Lin, R. -. Chung, G. -. Lin, and J. -. He, "Subwavelength Si nanowire arrays for self-cleaning antireflection coatings," *Journal of Materials Chemistry*, vol. 20, no. 48, pp. 10924-10930, 2010.

[129] C. -. Wu, C. -. Lin, C. Cheng, C. -. Wu, H. -. Ting, F. -. Chang, and F. -. Ko, "Design of artificial hollow moth-eye structures using anodic nanocones for high-performance optics," *Chemistry of Materials*, vol. 22, no. 24, pp. 6583-6589, 2010.

[130] J. Gjessing, E. S. Marstein, and A. Sudbø, "2D back-side diffraction grating for improved light trapping in thin silicon solar cells," *Optics Express*, vol. 18, no. 6, pp. 5481-5495, 2010.

[131] S. P. Huber, R. W. E. Van De Kruijs, A. E. Yakshin, E. Zoethout, K. -. Boller, and F. Bijkerk, "Subwavelength single layer absorption resonance antireflection coatings," *Optics Express*, vol. 22, no. 1, pp. 490-497, 2014.

[132] G. Kedawat, S. Srivastava, V. K. Jain, P. Kumar, V. Kataria, Y. Agrawal, B. K. Gupta, and Y. K. Vijay, "Fabrication of artificially stacked ultrathin ZnS/MgF2 multilayer dielectric optical filters," *ACS Applied Materials and Interfaces*, vol. 5, no. 11, pp. 4872-4877, 2013.

[133] R. Rungsawang, N. Jukam, J. Maysonnave, P. Cavalí, J. Mad´o, D. Oustinov, S. S. Dhillon, J. Tignon, P. Gellie, C. Sirtori, S. Barbieri, H. E. Beere, and D. A. Ritchie, "Gain enhancement in a terahertz quantum cascade laser with parylene antireflection coatings," *Applied Physics Letters*, vol. 98, no. 10, 2011.

[134] "Iridescence," *Retrived 2015, Https://En.Wikipedia.Org*, .

[135] "Rain bow oil," *Retrived, 2015, Http://Www.Suggestkeyword.Com*, .

[136] "Betterflies at home," *Retrived 2015, Http://Www.Butterfliesathome.Com*, .

[137] M. Brydegaard, "Towards Quantitative Optical Cross Sections in Entomological Laser Radar–Potential of Temporal and Spherical Parameterizations for Identifying Atmospheric Fauna," *PloS One*, vol. 10, no. 8, pp. e0135231, 2015.

[138] J. T. Kiehl and K. E. Trenberth, "Earth's Annual Global Mean Energy Budget," *Bulletin of the American Meteorological Society*, vol. 78, no. 2, pp. 197-208, 1997.

[139] K. Y. Kondratyev, P. P. Fedchenko, A. I. Ivanenko, J. Lacasa, and K. P. Fedchenko, "On the biological role of Fraunhofer lines of the Sun," *Nuovo Cimento Della Societa Italiana Di Fisica C*, vol. 28, no. 6, pp. 913-923, 2005.

[140] J. A. Rust, J. A. Nóbrega, C. P. Calloway Jr., and B. T. Jones, "Fraunhofer effect atomic absorption spectrometry," *Analytical Chemistry*, vol. 77, no. 4, pp. 1060-1067, 2005.

[141] W. Silfvast, "Population inversions in lightning discharges?" *Optics and Photonics News*, vol. 21, no. 9, pp. 32-37, 2010.

[142] D. Braunstein and R. Shuker, "Absorption with inversion and amplification without inversion in a coherently prepared V system: A dressed-state approach," *Physical Review A.Atomic, Molecular, and Optical Physics*, vol. 64, no. 5, pp. 538121-5381212, 2001.

[143] F. Koyama, "Recent advances of VCSEL photonics," *Journal of Lightwave Technology*, vol. 24, no. 12, pp. 4502-4513, 2006.

[144] C. J. Chang-Hasnain, Y. Zhou, M. C. Y. Huang, and C. Chase, "High-contrast grating VCSELs," *IEEE Journal on Selected Topics in Quantum Electronics*, vol. 15, no. 3, pp. 869-878, 2009.

[145] E. I. Moses, "Ignition on the National Ignition Facility: A path towards inertial fusion energy," *Nuclear Fusion*, vol. 49, no. 10, 2009.

[146] C. A. Haynam, P. J. Wegner, J. M. Auerbach, M. W. Bowers, S. N. Dixit, G. V. Erbert, G. M. Heestand, M. A. Henesian, M. R. Hermann, K. S. Jancaitis, K. R. Manes, C. D. Marshall, N. C. Mehta, J. Menapace, E. Moses, J. R. Murray, M. C. Nostrand, C. D. Orth, R. Patterson, R. A. Sacks, M. J. Shaw, M. Spaeth, S. B. Sutton, W. H. Williams, C. C. Widmayer, R. K. White, S. T. Yang, and B. M. Van Wonterghem, "National ignition facility laser performance status," *Applied Optics*, vol. 46, no. 16, pp. 3276-3303, 2007.

[147] M. Cornacchia, S. Di Mitri, G. Penco, and A. A. Zholents, "Formation of electron bunches for harmonic cascade x-ray free electron lasers," *Physical Review Special Topics - Accelerators and Beams*, vol. 9, no. 12, 2006.

[148] G. L. Chen, K. T. Chang, and T. C. Fan, "A wave approach to hollow cylindrical electron cyclotron masers," *International Journal of Infrared and Millimeter Waves*, vol. 1, no. 2, pp. 247-254, 1980.

[149] R. F. C. Vessot, M. W. Levine, E. M. Mattison, E. L. Blomberg, T. E. Hoffman, G. U. Nystrom, B. F. Farrel, R. Decher, P. B. Eby, C. R. Baugher, J. W. Watts, D. L. Teuber, and F. D. Wills, "Test of relativistic gravitation with a space-borne hydrogen maser," *Physical Review Letters*, vol. 45, no. 26, pp. 2081-2084, 1980.

[150] S. S. Charschan, "EVOLUTION OF LASER MACHINING AND WELDING, WITH SAFETY." *Proceedings of the Society of Photo-Optical Instrumentation Engineers*, vol. 229, pp. 144-153, 1980.

[151] W. M. Steen, "Arc augmented laser processing of materials," *Journal of Applied Physics*, vol. 51, no. 11, pp. 5636-5641, 1980.

[152] S. R. Gallagher, "The battle of the blue laser DVDs: The significance of corporate strategy in standards battles," *Technovation*, vol. 32, no. 2, pp. 90-98, 2012.

[153] K. F. Reim, J. Nunn, X. -. Jin, P. S. Michelberger, T. F. M. Champion, D. G. England, K. C. Lee, W. S. Kolthammer, N. K. Langford, and I. A. Walmsley, "Multipulse addressing of a Raman quantum memory: Configurable beam splitting and efficient readout," *Physical Review Letters*, vol. 108, no. 26, 2012.

[154] D. F. Gordon, M. H. Helle, and J. R. Penano, "Fully explicit nonlinear optics model in a particle-in-cell framework," *Journal of Computational Physics*, vol. 250, pp. 388-402, 2013.

[155] B. Shen, "Extreme Light Field Generation I: Quasi-Single-Cycle Relativistic Laser Pulse," *Ion Acceleration and Extreme Light Field Generation Based on Ultra-Short and Ultra-Intense Lasers*, , pp. 57-64, 2014.

[156] A. Bohlin, A. Kindeya, E. Nordstrom, and P. Bengtsson, "Validation of a rotational coherent anti-Stokes Raman scattering model for N2O at temperatures from 295K to 796K," *Journal of Raman Spectroscopy*, vol. 43, no. 5, pp. 604-610, 2012.

[157] E. Nordstrom, A. Bohlin, and P. Bengtsson, "Pure rotational Coherent anti-Stokes Raman spectroscopy of water vapor and its relevance for combustion diagnostics," *Journal of Raman Spectroscopy*, vol. 44, no. 10, pp. 1322-1325, 2013.

[158] A. Gebru, E. Rohwer, P. Neethling, and M. Brydegaard, "Investigation of atmospheric insect wing-beat frequencies and iridescence features using a multispectral kHz remote detection system," *Journal of Applied Remote Sensing*, vol. 8, no. 1, 2014.

[159] H. Kuze, H. Kinjo, Y. Sakurada, and N. Takeuchi, "Field-of-view dependence of lidar signals by use of Newtonian and Cassegrainian telescopes," *Applied Optics*, vol. 37, no. 15, pp. 3128-3132, 1998.

[160] R. Bardet, F. Roussel, S. Coindeau, N. Belgacem, and J. Bras, "Engineered pigments based on iridescent cellulose nanocrystal films," *Carbohydrate Polymers*, vol. 122, pp. 367-375, 2015.

[161] S. Niu, B. Li, Z. Mu, M. Yang, J. Zhang, Z. Han, and L. Ren, "Excellent structure-based multifunction of morpho butterfly wings: A review," *Journal of Bionic Engineering*, vol. 12, no. 2, pp. 170-189, 2015.

[162] E. Nakamura, S. Yoshioka, and S. Kinoshita, "The origin of two-color iridescence in the neck feathers of the Rock Dove," *Journal of Ornithology*, vol. 147, no. 5, pp. 217-217, 2006.

[163] H. Yin, L. Shi, J. Sha, Y. Li, Y. Qin, B. Dong, S. Meyer, X. Liu, L. Zhao, and J. Zi, "Iridescence in the neck feathers of domestic pigeons," *Physical Review E*, vol. 74, no. 5, pp. 051916, 2006.

[164] K. J. McGraw, "Multiple UV reflectance peaks in the iridescent neck feathers of pigeons," *Naturwissenschaften*, vol. 91, no. 3, pp. 125-129, 2004.

[165] E. Lee, M. Aoyama, and S. Sugita, "Microstructure of the feather in Japanese Jungle Crows (Corvus macrorhynchos) with distinguishing gender differences," *Anatomical Science International*, vol. 84, no. 3, pp. 141-147, 2009.

[166] S. M. Doucet, M. D. Shawkey, M. K. Rathburn, H. L. Mays, and R. Montgomerie, "Concordant evolution of plumage colour, feather microstructure and a melanocortin receptor gene between mainland and island populations of a fairy-wren," *Proceedings of the Royal Society B-Biological Sciences*, vol. 271, no. 1549, pp. 1663-1670, 2004.

[167] I. Galvan, "Feather microstructure predicts size and colour intensity of a melanin-based plumage signal," *Journal of Avian Biology*, vol. 42, no. 6, pp. 473-479, 2011.

[168] E. Lee, H. Lee, J. Kimura, and S. Sugita, "Feather Microstructure of the Black-Billed Magpie (Pica pica sericea) and Jungle Crow (Corvus macrorhynchos)," *Journal of Veterinary Medical Science*, vol. 72, no. 8, pp. 1047-1050, 2010.

[169] F. M. Lei, Y. H. Qu, Y. L. Gan, A. Gebauer, and M. Kaiser, "The feather microstructure of Passerine sparrows in China," *Journal Fur Ornithologie*, vol. 143, no. 2, pp. 205-212, 2002.

[170] T. Seki, K. Isono, M. Ito, and Y. Katsuta, "Flies in the Group Cyclorrhapha use (3s)-3-Hydroxyretinal as a Unique Visual Pigment Chromophore," *European Journal of Biochemistry*, vol. 226, no. 2, pp. 691-696, 1994.

[171] S. N. Fry, R. Sayaman, and M. H. Dickinson, "The aerodynamics of hovering flight in Drosophila," *Journal of Experimental Biology*, vol. 208, no. 12, pp. 2303-2318, 2005.

[172] R. J. Bomphrey, "Insects in flight: Direct visualization and flow measurements," *Bioinspiration and Biomimetics*, vol. 1, no. 4, 2006.

[173] L. C. Johansson, S. Engel, E. Baird, M. Dacke, F. T. Muijres, and A. Hedenström, "Elytra boost lift, but reduce aerodynamic efficiency in flying beetles," *Journal of the Royal Society Interface*, vol. 9, no. 75, pp. 2745-2748, 2012.

[174] C. Hou, P. Wang, W. Li, H. Guo, L. Fu, Z. Qiao, M. Lu, W. Wei, and B. Peng, "Preparation of the oxyfluoride glass with high 3ω laser induced damage threshold," *Optics & Laser Technology*, vol. 56, no. 0, pp. 88-91, 2014.

[175] R. M. Wood, R. T. Taylor, and R. L. Rouse, "Laser damage in optical materials at 1.06 μm," *Optics & Laser Technology*, vol. 7, no. 3, pp. 105-111, 1975.

[176] "Point Of Focus And Depth Of Field," *Retrived 2015, Www.Steves-Digicams.Com*, .

[177] "Shallow depth of filed," *Retrived 2014, Https://Steamcommunity.Com*, .

[178] "depth of field," *Retrived 2014, Https://Steamcommunity.Com*, .

[179] N. Brimhall, T. L. Andrews, R. Manthena, and R. Menon, "On breaking the Abbé diffraction limit in optical nanopatterning," *Optics InfoBase Conference Papers*, , 2010.

[180] M. J. Rust, M. Bates, and X. Zhuang, "Sub-diffraction-limit imaging by stochastic optical reconstruction microscopy (STORM)," *Nature Methods*, vol. 3, no. 10, pp. 793-795, 2006.

[181] J. S. Verdaasdonk, A. D. Stephens, J. Haase, and K. Bloom, "Bending the Rules: Widefield Microscopy and the Abbe Limit of Resolution," *Journal of Cellular Physiology*, vol. 229, no. 2, pp. 132-138, 2014.

[182] D. R. Whelan, T. Holm, M. Sauer, and T. D. M. Bell, "Focus on super-resolution imaging with direct stochastic optical reconstruction microscopy (dSTORM)," *Australian Journal of Chemistry*, vol. 67, no. 2, pp. 179-183, 2014.

[183] J. Fischer and M. Wegener, "Three-dimensional direct laser writing inspired by stimulated-emission-depletion microscopy [Invited]," *Optical Materials Express*, vol. 1, no. 4, pp. 614-624, 2011.

[184] J. Fischer and M. Wegener, "Three-dimensional optical laser lithography beyond the diffraction limit," *Laser and Photonics Reviews*, vol. 7, no. 1, pp. 22-44, 2013.

[185] P. Sengupta, S. B. Van Engelenburg, and J. Lippincott-Schwartz, "Superresolution imaging of biological systems using photoactivated localization microscopy," *Chemical Reviews*, vol. 114, no. 6, pp. 3189-3202, 2014.

[186] T. Klein, S. Proppert, and M. Sauer, "Eight years of single-molecule localization microscopy," *Histochemistry and Cell Biology*, vol. 141, no. 6, pp. 561-575, 2014.

[187] A. Nickerson, T. Huang, L. -. Lin, and X. Nan, "Photoactivated localization microscopy with Bimolecular Fluorescence Complementation (BiFC-PALM) for nanoscale imaging of protein-protein interactions in cells," *PLoS ONE*, vol. 9, no. 6, 2014.

[188] L. Mei and M. Brydegaard, "Contineous-wave differential absorption lidar,"*Submitted to LPR*, 2014.

[189] D. N. Whiteman, S. H. Melfi, and R. A. Ferrare, "Raman Lidar System for the Measurement of Water-Vapor and Aerosols in the Earths Atmosphere," *Applied Optics*, vol. 31, no. 16, pp. 3068-3082, 1992.

[190] H. Kuze, H. Kinjo, Y. Sakurada, and N. Takeuchi, "Field-of-view dependence of lidar signals by use of Newtonian and Cassegrainian telescopes," *Applied Optics*, vol. 37, no. 15, pp. 3128-3132, 1998.

[191] M. Brydegaard, "Aspects of Optical Broad Band Spectroscopy and Information Extraction - Applications in Medicine and Ecology." *978-91-7473-353-2, Doktoral Thesis, Lund University, ,* 2012.

[192] M. Mishali and Y. C. Eldar, "Expected RIP: Conditioning of the modulated wideband converter," *2009 IEEE Information Theory Workshop, ITW 2009*, pp. 343-347, 2009.

[193] U. Münz, A. Papachristodoulou, and F. Allgöwer, "Generalized Nyquist consensus condition for high-order linear multi-agent systems with communication delays," *Proceedings of the IEEE Conference on Decision and Control, ,* pp. 4765-4771, 2009.

[194] E. Malmqvist and M. Brydegaard, "Effective parameterization of laser radar observations of atmospheric fauna," *Accepted, JSTQE-IEEE, 2015, .*

[195] P. Lundin, P. Samuelsson, S. Svanberg, A. Runemark, S. Akesson, and M. Brydegaard, "Remote nocturnal bird classification by spectroscopy in extended wavelength ranges," *Applied Optics*, vol. 50, no. 20, pp. 3396-3411, 2011.

[196] M. Brydegaard, A. Runemark, and R. Bro, "Chemometric approach to chromatic spatial variance. Case study: Patchiness of the Skyros wall lizard," *Journal of Chemometrics*, vol. 26, no. 6, pp. 246-255, 2012.

[197] J. P. Dandois and E. C. Ellis, "High spatial resolution three-dimensional mapping of vegetation spectral dynamics using computer vision," *Remote Sensing of Environment*, vol. 136, pp. 259-276, 2013.

[198] K. P. Pyun, C. Choi, A. V. Morozov, S. Kim, and J. An, "Compact holographic printer using RGB waveguide holographic optical elements," *Proceedings of SPIE - the International Society for Optical Engineering*, vol. 8616, 2013.

[199] J. Shen, P. Su, S. Cheung, and J. Zhao, "Virtual mirror rendering with stationary RGB-D cameras and stored 3-D background," *IEEE Transactions on Image Processing*, vol. 22, no. 9, pp. 3433-3448, 2013.

[200] M. Zollhöfer, M. Nießner, S. Izadi, C. Rehmann, C. Zach, M. Fisher, C. Wu, A. Fitzgibbon, C. Loop, C. Theobalt, and M. Stamminger, "Real-time non-rigid reconstruction using an RGB-D camera," *ACM Transactions on Computer Systems*, vol. 33, no. 4, 2014.

[201] E. Kaplan and R. M. Shapley, "The primate retina contains two types of ganglion cells, with high and low contrast sensitivity," *Proceedings of the National Academy of Sciences of the United States of America*, vol. 83, no. 8, pp. 2755-2757, 1986.

[202] T. Macuda and B. Timney, "Luminance and chromatic discrimination in the horse (Equus caballus)," *Behavioural Processes*, vol. 44, no. 3, pp. 301-307, 1999.

[203] C. A. Saslow, "Understanding the perceptual world of horses," *Applied Animal Behaviour Science*, vol. 78, no. 2-4, pp. 209-224, 2002.

[204] J. Caroll, C. J. Murphy, M. Neitz, J. N. Ver Hoeve, and J. Neitz, "Photopigment basis for dichromatic color vision in the horse," *Journal of Vision*, vol. 1, no. 2, pp. 80-87, 2001.

[205] J. K. Bowmaker and A. Knowles, "The visual pigments and oil droplets of the chicken retina," *Vision Research*, vol. 17, no. 7, pp. 755-764, 1977.

[206] N. S. Hart, "Microspectrophotometry of visual pigments and oil droplets in a marine bird, the wedge-tailed shearwater Puffinus pacificus: Topographic variations in photoreceptor spectral characteristics," *Journal of Experimental Biology*, vol. 207, no. 7, pp. 1229-1240, 2004.

[207] T. H. Goldsmith, "What birds see," *Scientific American*, vol. 295, no. 1, pp. 68-75, 2006.

[208] M. Brydegaard, P. Samuelsson, M. W. Kudenov, and S. Svanberg, "On the Exploitation of Mid-infrared Iridescence of Plumage for Remote Classification of Nocturnal Migrating Birds," *Applied Spectroscopy*, vol. 67, no. 5, pp. 477-490, 2013.

[209] ""FFT,"*Retrived 2015, http://www.dspguide.com*" .

[210] ""Power spectral density,"*Retrived 2015, http://allsignalprocessing.com*" .

[211] B. D. Barkana and J. Zhou, "A new pitch-range based feature set for a speaker's age and gender classification," *Applied Acoustics*, vol. 98, pp. 52-61, 2015.

[212] D. Shultz, "When your voice betrays you," *Science*, vol. 347, no. 6221, pp. 494, 2015.

[213] J. Xu, J. S. Bradley, and B. N. Gover, "An artificial neural network approach for predicting architectural speech security (L)," *Journal of the Acoustical Society of America*, vol. 117, no. 4 I, pp. 1709-1712, 2005.

[214] C. An, S. Lovell, M. R. Kanost, K. P. Battaile, and K. Michel, "Crystal structure of native Anopheles gambiae serpin-2, a negative regulator of melanization in mosquitoes," *Proteins: Structure, Function and Bioinformatics*, vol. 79, no. 6, pp. 1999-2003, 2011.

[215] K. M. Fedorka, E. K. Copeland, and W. E. Winterhalter, "Seasonality influences cuticle melanization and immune defense in a cricket: Support for a temperature-dependent immune

investment hypothesis in insects," *Journal of Experimental Biology*, vol. 216, no. 21, pp. 4005-4010, 2013.

[216] D. A. Roff and D. J. Fairbairn, "The costs of being dark: The genetic basis of melanism and its association with fitness-related traits in the sand cricket," *Journal of Evolutionary Biology*, vol. 26, no. 7, pp. 1406-1416, 2013.

[217] H. Yassine, L. Kamareddine, and M. A. Osta, "The Mosquito Melanization Response Is Implicated in Defense against the Entomopathogenic Fungus Beauveria bassiana," *PLoS Pathogens*, vol. 8, no. 11, 2012.

[218] Y. H. Ye, M. Woolfit, E. Rancès, S. L. O'Neill, and E. A. McGraw, "Wolbachia-Associated Bacterial Protection in the Mosquito Aedes aegypti," *PLoS Neglected Tropical Diseases*, vol. 7, no. 8, 2013.

[219] M. Borer, T. Van Noort, M. Rahier, and R. E. Naisbit, "Positive frequency-dependent selection on warning color in alpine leaf beetles," *Evolution*, vol. 64, no. 12, pp. 3629-3633, 2010.

[220] C. Kang, S. -. Lee, and P. G. Jablonski, "Effect of sex and bright coloration on survival and predator-induced wing damage in an aposematic lantern fly with startle display," *Ecological Entomology*, vol. 36, no. 6, pp. 709-716, 2011.

[221] T. Keasar, M. Kishinevsky, A. Shmida, Y. Gerchman, N. Chinkov, A. Koplovich, and G. Katzir, "Plant-derived visual signals may protect beetle herbivores from bird predators," *Behavioral Ecology and Sociobiology*, vol. 67, no. 10, pp. 1613-1622, 2013.

[222] R. M. Merrill, Z. Gompert, L. M. Dembeck, M. R. Kronforst, W. O. McMillan, and C. D. Jiggins, "Mate preference across the speciation continuum in a clade of mimetic butterflies," *Evolution*, vol. 65, no. 5, pp. 1489-1500, 2011.

[223] R. D. Reed, R. Papa, A. Martin, H. M. Hines, B. A. Counterman, C. Pardo-Diaz, C. D. Jiggins, N. L. Chamberlain, M. R. Kronforst, R. Chen, G. Halder, H. F. Nijhout, and W. O. McMillan, "Optix drives the repeated convergent evolution of butterfly wing pattern mimicry," *Science*, vol. 333, no. 6046, pp. 1137-1141, 2011.